The University of Nottingham

UNITED KINGDOM · CHINA · MALAYSIA

Fatigue life assessment of thermal cracked dies and moulds for remanufacturing

by

Changrong Chen, BSc, MSc

Thesis submitted to the University of Nottingham

for the degree of Doctor of Philosophy

July 2016

Dedicated to my family, my father Yushui, my mother Xiujin, my brother Guocai, my sister Guozhu and my wife Wanzhu.

Declaration

I hereby declare that except where specific reference is made to the work of others, the contents of this dissertation are original and have not been submitted in whole or in part for consideration for any other degree or qualification in this, or any other university. This dissertation is the result of my own work and includes nothing which is the outcome of work done in collaboration, except where specifically indicated in the text. This dissertation contains fewer than 65,000 words including appendices, bibliography, footnotes, tables and equations and has fewer than 150 figures.

Changrong Chen

July 2016

Publications

- **Changrong Chen**, Yan Wang, Hengan Ou, Nabil Gindy. 2011. "Remanufacture of Die Casting Dies." Applied Mechanics and Materials 121-126: 3482-3486.
- **Changrong Chen**, Yan Wang, Hengan Ou, Yan He, Xianzhi Tang. 2014. "A review on remanufacture of dies and moulds." Journal of Cleaner Production 64(0): 13-23.
- **Changrong Chen**, Yan Wang, Hengan Ou. 2014. "Comparison of thermal fatigue test methods for die casting process: a finite element study." 5th International Conference on Mechanical, Industrial and Manufacturing Technologies.
- **Changrong Chen**, Yan Wang, Hengan Ou. 2015."Study of weld characteristics for repair using sequential experimental design and artificial neural networks." International Journal of Advanced Manufacturing Technology(Accepted).
- **Changrong Chen**, Yan Wang, Hengan Ou, Y.J. Lin. 2015. "An energy life approach to thermal fatigue life of tool steels for die casting dies." International Journal of Fatigue (To be Submitted).

Abstract

The conventional life cycle of dies and moulds is not eco-efficient, which shows great potential for the application of remanufacturing. The essence of remanufacturing activity is to ensure sufficient service life of remanufactured products. Therefore, it is of great importance to establish life evaluation technology for remanufacturing dies and moulds in order for remanufacturers to predict the remaining service life. The main contribution of this thesis is the development of key technologies for life evaluation of dies and moulds after remanufacturing through a thorough review of remanufacture related activities within the die and mould industry.

It is proposed that evaluation of remaining service life of dies and moulds after remanufacturing is carried out using finite element modelling. It involves determination of residual stresses induced by repair welding, working conditions for the future operation and fatigue life model of die material.

Specifically, the thesis is firstly focused on the design of representative die geometry. Dies and moulds are normally designed for specific products. Therefore, it is impossible to take individual die and mould into consideration in research. A reasonable approach is to develop representative die geometry. Real dies and moulds are then simplified by using a cylindrical cavity. The geometry is optimized based on the effect of thermal loading and the effect of residual stress due to laser welding.

Secondly, fatigue life model was established by conducting thermal fatigue tests and finite element modelling as well. Induction heating based thermal fatigue test method was adopted for its capacity of achieving similar thermal shock effects as dies and moulds experience in operation. Finite element modelling provided the stress-strain information of test samples during thermal fatigue tests. An energy based fatigue life model was derived by taking into account the test period.

Using laser welding as the remanufacturing process, the weld characteristics are studied based on which laser welding process is selected. A sequential experimental design combining Orthogonal method and Uniform Design was adopted for experiments. Radial Basis Function neutral networks were used to obtain regression models of weld performances for enabling process optimization.

Then, the finite element modelling methodology was established for laser welding process. Heat source models were calibrated by achieving sufficient agreement between the finite element calculated weld profile and the experimental one. Structural analysis of laser welding was also established for the case of laser surfacing. Therefore, all key technologies required for life evaluation were established.

Lastly, the effect due to residual stress on the fatigue life model should also be identified and the life model should be updated accordingly. Another set of thermal experiments were run to show the influence. Fitting of data from welded samples demonstrates a linear effect caused by the residual stresses after laser welding. Another fitting was conducted to verify the corrected life model. With close agreement between corresponding coefficients from the

two curve fittings, the corrected model is proved to be reliable for evaluating remaining useful life of remanufactured dies/moulds.

Acknowledgements

I would like to express my gratitude to Dr. Yan Wang, my former supervisor, for giving me the opportunity to pursue my degree here at the University of Nottingham Ningbo China. I am extremely grateful for her dedication towards cultivating academic thinking and providing support and encouragement that allow me to explore my research ideas through the course of my study. I am particularly thankful for intellectual discussions we had during these years.

I would like to thank my co-supervisor Dr. Hengan Ou for his unconditional support and guidance throughout these years. I am grateful for the countless intellectual exchanges we had in discussing the moulding processes, thermal fatigue tests, and heat source calibration. Much of the success in my research is owing to him. I am thankful for his dedication towards culturing good career development and plan. I am particularly grateful for his supporting the research exchange to Huazhong University of Science and Technology where broadens my horizontal in repair/remanufacture of dies and moulds.

I am grateful to Professor Y.J. Lin for his involvement in supervision at the final stage of my study. I particularly appreciate the discussions we had on my thesis and research. I also appreciate his constructive suggestions and elaborate comments on the thesis writing up. His sagacious perception is extremely beneficial to my

current research and future work. I am also thankful to Professor Lin for his encouragement in developing my academic career.

I would like to thank the following people for helping with the experimental work during various stages of this project. I am grateful to Professor Lijun Liu for allowing me to use the Han's laser welder and thermal fatigue test machine for my experiments at the Ningbo Institute of Technology, Zhejiang University. I aslo appreciate the discussions we had towards the experimental plan and preparation. Many gratitudes to Mr Hualiang Shi and Ms Yaqing Jiang for instructing me on how to operate the Han's laser and the thermal fatigue test machine. I am particularly thankful for their help with sample preparation and crack observation.

Table of contents

List of figures

List of tables

Nomenclature

Roman Symbols

A the lost area due to damage

A_0 the original area

c specific heat

D Damage variable

D_c the critical damage

$\dot{U}_I$ the internal energy rate

$\dot{U}_K$ the kinetic energy rate

$\dot{U}_V$ the rate of increase of energy in V

$\dot{W}$ the rate of work done by external forces across S

E the modulus of elasticity

h the convection coefficient

L the characteristic length associated with the material point

N_0 the number of cycles to damage initiation

$\dot{q}$ the rate of heat generated or consumed within the volume, V

S a closed surface of study

T temperature

T_0 a radiative exchange temperature

T_e a convective exchange temperature

T_s temperature of an unknown surface

V an arbitrary fixed volume

Greek Symbols

α the coefficient of thermal expansion

Δw the accumulated inelastic hysteresis energy per cycle

ε'_f the fatigue ductility coefficient

ε strain

ε_{sec} the surface emission coefficient

ρ the density of a medium

σ'_f the fatigue strength coefficient

σ_{sb} the Stefan–Boltzmann constant

Acronyms / Abbreviations

AI Artificial Intelligence

ANN Artificial Neural Network

AR Aspect Ratio

ARMA Autoregressive moving average

BW Bead Width

CDM Continuum Damage Mechanics

CM condition monitoring

CO carbon monoxide

CWM computational welding mechanics

DMD Direct Metal Deposition

DoF Depth of Focus

DP Depth of Penetration

EDM Electrical Discharge Machining

ELV End-of-life Vehicles

EOL End-of-Life

FEA Finite Element Analysis

FEM Finite Element Modelling

FVM Finite Volume Method

GTAW Gas Tungsten Arc Welding

HAZ Heat affected zone

LB the Larger the Better

LCA Life cycle assessment

LEFM Linear Elastic Fracture Mechanics

NB the Nominal the Better

NDE non-destructive evaluation

NOx nitrogen oxide

OEM Original Equiment Manufacturer

OFAT one-factor-at-a-time

PAW Plasma arc welding

RBF Radial basis function

RUL Remaining Useful Life

SB the Smaller the Better

SOx sulfur oxide

SS Scanning Speed

TIG Tungsten Inert Gas Welding

WA Weld Area (of molten zone)

Chapter 1

Introduction

1.1 Background

In recent decades, increased economy has become the principal contributor to the increase in waste production. From the 1950s onwards, the world's waste has grown exponentially each year, which drives disposal methods such as landfills becoming increasingly expensive as they are being exhausted (Ijomah et al., 2007). It is reported that the environmental pressure from increase in waste generation has been threefold (King et al., 2006). Additionally, the issue of climate change, energy security and scarcity of raw materials faced by governments all over the world has become increasingly severe. The governments over the world and international organizations have been prompt to link the economic growth to the ecological concerns and thus policy and legislation solutions were originally resolved to obtain sustainable development. Hitherto, numerous policies and directives were implemented over the last two decades (Sakai et al., 2014). For example, the EU Landfill of Waste Directive entered into force on 16th July 1999 and the legislation of ELV (End-of-life Vehicles) Directive was officially published by the European

Parliament and Council on 21st October 2000. Similar measures were taken place in other countries like China, Japan and South Korea. China enforced the End-of-Life Vehicle Recycling Regulation in 2001. The Japanese Automobile Recycling Law was promulgated in July 2002 and put into effect in April 2005. The Act for Recycling of Electrical and Electronic Equipment and Automobiles, Bill Number 176319 came into force in South Korea on 1st January 2008.

Manufacturers are driven by both the legislation pressure and environmental challenges to implement sustainable measures in order to achieve a step change in practice. From doing this, product manufacturers need to consider the entire life cycle of a product from extraction of raw materials, through manufacturing, product use and final disposal(King et al., 2006). And the key to being truly sustainable is to divert the disposal streams of end-of-life products to become new raw materials, components or products, as shown in Figure 1.1.

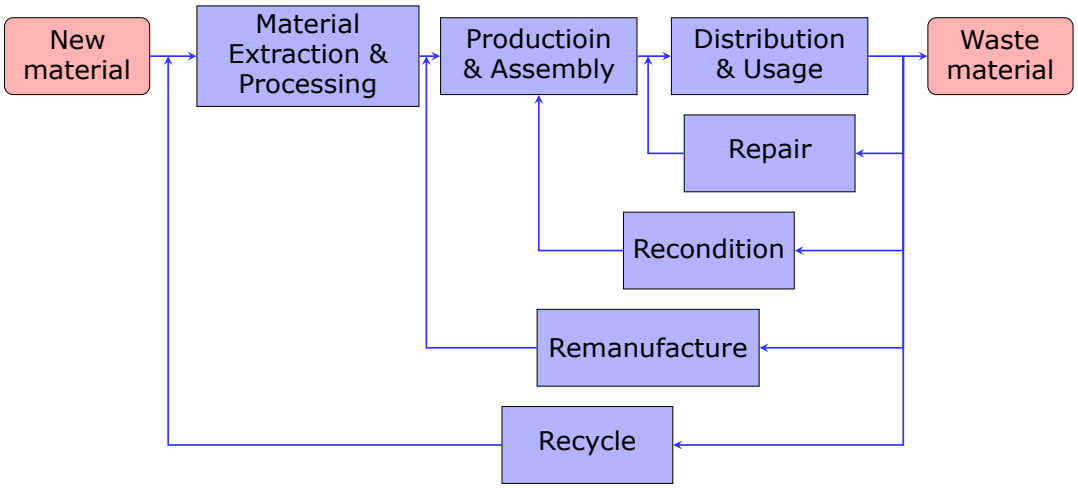

Figure. 1.1 Closed loop design through repair, remanufacturing or recycling

Both in industry and academia, a great deal of attention have been paid to material recycling. It is evident that material recycling is more environmentally friendly than landfill of end-of-life products.

And it has become the most mature strategy to avoid waste, with recycle rates as high as 80% for certain products (ICER, 2000). However, many designers are reluctant to use recycled materials due to uncertainty of quality or supply standards. In addition, the geometry of end-of-life products and the associated value are destroyed, which indicates that additional energy is still required to reform them into newly manufactured products.

Repair is another logical approach to closing the loop on product use. Repair extends products' life simply by the correction of specific faults in products. Consequently, a warranty on a repaired product may only apply to the specific part (or area) repaired, but not the whole product.

Comparably, a more efficient way to reduce environmental impacts can be made through the reuse and remanufacture of used or obsolete products, in which case the product retains its geometry and is reused for the same purpose as during its original life cycle. Remanufacture is the only process to return products back to Original Equipment Manufacturer (OEM) performance specification. This is greatly preferable to material recycling and repair because it adds value to waste products by returning them to working order, rather than simply reducing a used product to its raw materials value (Ijomah et al., 2007). Also, remanufactured products are usually given warranties equal to those of newly manufactured (Ijomah, 2002).

Recently, remanufacture has attracted much attention due to its economic and ecological advantages over the manufacture of new products, since it has the potential to provide solutions that satisfy all requirements of the 'triple bottom line' of people, planet and profit (Giuntini and Gaudette, 2003). In purely financial terms,

remanufacturing can provide between 20% and 80% production cost saving in comparison to conventional manufacturing and it is reported that a 20% increment of die life could result in annual savings of over US$200 million in the United States alone (Zhu et al., 2004). Numerous investigations have also concluded that remanufacturing is profitable for Original Equipment Manufacturers (OEMs)(Subramoniam et al., 2009). Ecologically speaking, remanufactured products also outperform new manufactured products in reducing environmental impacts. According to Lund (1984), 85% of the weight of a remanufactured product may come from used components, but require 50% less energy. Smith and Keoleian (2004) found that the remanufactured engines could be produced with 26% to 90% less raw material, 68% to 83% less energy, 65% to 88% less solid waste generation and 73% to 87% fewer carbon dioxide emissions. They also observed significant savings of other air emissions including 48% to 88% carbon monoxide (CO) reductions, 72% to 85% nitrogen oxide (NOx) reductions, 71% to 84% sulfur oxide (SOx) reductions, and 50% to 61% nonmethane hydrocarbon reductions. The investigation by Amaya et al. (2010) observed that environmental impacts can be reduced by 8.64% with 25% of the truck injectors remanufactured. The benefit increases with the rate of remanufactured products, for a maximum of 46.10% improvement when 100% of injectors recovered.

Remanufacturing activities have been increasingly adopted in various industries, such as automobile, household appliance and industrial machinery, etc. Fortune Magazine recently reported that the top ten companies (Honda, Goldman Sachs, Continental Airlines to name a few) across a variety of industries were going beyond what is required by law to operate in an environmentally responsible

way. Automotive components are typically reused and remanufactured for part replacement purposes by many automotive companies (Amelia et al., 2009; Hammond et al., 1998). Even in the wind power industry, perceived as a sector of low environmental impact energy generation, attention has been paid to updating conventional sustainable technologies with remanufacturing (Ortegon et al., 2013).

With respect to customer satisfaction, environmental impacts and the society, a variety of advantages over other waste avoidance strategies may be resulted through remanufacturing, as shown in Table 1.1. Specifically, products of the same quality as new ones are accessible to customers with lower cost because of savings in reuse of built values. The society is then not burdened with high pressure for waste handling and extraction of new materials. Also, this new industry section will need more people for operation. And for the environment, the benefits are quite apparent due to savings in material, energy and manufacturing.

Table 1.1 Benefits of Remanufacture Process

Customer	Society	Environment
• High quality • Lower cost	• Job creation • Less pressure on waste handling • Less dependence on raw material markets	• Energy conservation • Material saving • Waste prevention • CO_2 emission prevention

1.2 Motivation

Dies and moulds are one of the typical manufacturing facilities as machine tools, and one of the tools necessary for mass-production.

Nearly all mass produced discrete parts are manufactured by dies and moulds that are used in production processes such as forging, stamping, casting, and injection moulding (Altan et al., 2001).

Apparently, the geometry and surface quality of the final parts formed by moulding processes are directly determined by mould halves. The production of die halves is commonly time consuming, technically difficult and expensive for the required specialized materials, labour and manufacturing techniques. Meanwhile, manufacture operations release a great deal of greenhouse gases and consume large amounts of limited natural resources, which result in severe environmental impacts.

Eco-efficiency (both economically and ecologically) demands that dies and moulds are maintained in good working order, with their useful life being extended beyond the limits that are normally imposed by wear, accidental damage or obsolescence.

When in use, dies and moulds are exposed to severe conditions: regular wear, impact, corrosion, thermal cycling and high stresses causing deterioration. Die wear and failure significantly affects the service life of dies and moulds resulting in the need for new ones. This thereby usually leads to an unexpected high production cost. For instance, according to Lavtar et al. (2011), the expenses for hot forging dies account for 8%-15% of the product's cost while unexpected die failure causes an increase of 30% in production costs. Moreover, dies and moulds may require frequent modifications during product development as a result of design changes. According to Pecas et al. (2006), around 80% of the moulds used to produce automotive components undergo a repair/remanufacture process.

Traditionally, when dies and moulds do not function properly, they are often recycled to recover the materials, during which the

geometry of the dies and moulds and their associated value are destroyed and only the constituent materials are introduced into a new cycle of usage. However, this traditional life cycle of dies and moulds is neither environmentally sustainable nor economically efficient. Though recycling by melting offers a less energy intensive alternative to making products from ore, it still consumes more energy than reusing without melting (Allwood and Cullen, 2011). The success of remanufacturing activities in other industries holds great attraction for the die and mould industry.

1.3 Problem

The conventional life cycle of dies and moulds is not eco-efficient, which shows great potential for the application of remanufacturing. While repair processing of dies and moulds has been regular in the industry because of mould modification or deterioration, remanufacturing is rarely considered due to the shortfall of currently utilized techniques such as welding to restore microstructures of failed tools to 'like-new' condition. Until recently, scientific and engineering advances in laser-based fabrication technology have made dies and moulds remanufacturing technologically accessible and feasible (Morrow et al., 2007).

Remanufacture is a manufacturing process that normally includes a number of steps including disassembly, cleaning, repairability analysis, repair or replacement, and reassembly at the part level. The repair or replacement of worn out or obsolete components and modules is one key step involved in remanufacturing. Parts subjected to degradation are replaced if the performance of next life cyle is affected. Otherwise, parts may be repaired and put back into operation. Remanufacture differs from repair in its completeness: a

remanufactured product should match the same customer expectation as new ones (BS 8887-220:2010). Therefore, remanfuactured products are generally superior to the repaired ones.

The essence of remanufacture is to retain parts of value in a new life cycle. It is necessary for remanufacturers to assure the quality of remanufactured products before returning them to the market. Life evaluation technology is frequently used to predict the remaining useful life (RUL) of a structure or system from the current time to the end of life. Therefore, the central point of reliability assessment becomes to evaluate the RUL of remanufactured products. Unlike common products, dies and moulds are generally product specific and one-off design, which stresses the importance of long service life and accurate prediction.

Although recently repair of damaged dies and moulds has been regularly performed in the industry, remaining useful life prediction is scarcely conducted after that. Both academia and industry are still concentrated on the optimization of repair processes. These researches normally correlate process parameters to material properties such as micro-hardness rather than the resistance of specific failure mode. For more accurate prediction, it is necessary to directly correlate remanufacturing process to specific failure modes. Remaining useful life evaluation technology needs to be well developed to understand the effect of remanufacturing process on the service life. Not only does this offer remanufacturers quantitative life information but also enable optimization of remanufacturing process. It is a significant measure for a remanufacturer to make a decision on whether collected cores should be used for next life cycle or whether they can be remanufactured. Therefore, it is the

first and foremost task to establish remaining useful life technique for remanufacturing dies and moulds.

1.4 Aims and objectives

The aim of this study is to develop the methodology of remaining useful life evaluation for dies and moulds, specifically thermal cracked die casting dies, after remanufacturing. In order to achieve this, the specific research objectives are:

- To establish the life prediction model for thermal fatigue cracking of die casting dies;
- To correlate process parameters of laser beam welding applied for mould remanufacture to post welding residual stress;
- To study the influences of welding residual stresses on the thermal fatigue behaviour of repaired die casting dies;
- And to test and validate the life prediction model with thermal fatigue testing of specimens made of die material.

1.5 Organization of thesis

The thesis is organised as follows: the literature review (Chapter TWO) that follows this introduction (Chapter ONE), is mainly concerned with principal technologies in remanufacture of dies and moulds, in terms of remaining useful life evaluation, reconditioning technology such as welding, and reliability analysis. Based on the detailed review, research challenges and opportunities lying in the research area are thereafter concluded.

Chapter THREE defines the research scope, material consideration and specific mould types. Research framework and methodologies

with respect to the research points are then investigated. Also, the underlying relations within the research problem are revealed and finite element solutions are formulated in this chapter.

The experimental work is designed in Chapter FOUR. The effect of die geometry on resulting thermal stresses as well as the effect of welding on residual stresses is investigated for optimal design of specimens to simulate real dies and moulds. This Chapter also compares thermal fatigue testing methods for the testing method selection.

Chapter FIVE describes the details of thermal fatigue tests, both experimentally and numerically. The experimental work involves sample preparation, experimental procedures and experiment data treatment while numerical study utilises finite element method to simulate thermal fatigue cycling, thereby establishing fatigue propagation models for life evaluation.

The calculation of residual stresses after welding is investigated in Chapter SIX. This begins with the study of weld characteristics which are essential to the welding remanufacturing. The finite element solution to the specific welding facility is established by calibrating the heat source model.

Chapter SEVEN further describes the effect of welding residual stresses on thermal fatigue life of dies and moulds. Case studies of life assessment of thermal cracked dies and moulds after welding remanufacturing are then conducted. And the feasibility of the evaluation is validated with experimental results, accordingly.

The research work of this thesis is summarised in Chapter EIGHT, followed by the conclusions drawn from discussions in previous chapters. Also, future work regarding this topic is discussed as well.

Chapter 2

Literature review

2.1 Introduction

Dies and moulds, which are essential tools for manufacturing engineered products, usually fail or become obsolete after a certain period of use for a variety of reasons. Thus, they often need remanufacture. The objectives of this chapter are to review the current state of the art in remanufacture of dies and moulds and to investigate the potential benefits and opportunities associated with remanufacturing.

In this chapter, the unique characteristics of remanufacturing of dies and moulds, compared to those of other products, is firstly summarised, followed by the examination of industrial repair strategies of the main types of dies and moulds. Key technologies needed for remanufacture are then reviewed in detail including welding repair technologies, remaining useful life evaluation methods, and reliability analysis. Finally, challenges and opportunities facing the industry and academia are discussed in order to draw several key conclusions.

2.2 Characteristics of remanufacturing dies and moulds

Figure 2.1 illustrates a typical practice of mould repair in the dies and moulds industry. The worn and quite heavily eroded mould, as shown in Figure 2.1.a, would normally be disposed and replaced with a new one. However, through mould repair/remanufacture, its service life can be extended. Figure 2.1.b shows the mould milled back to reveal the under-surface in good condition. Figure 2.1.c depicts the mould after laser cladding process, while the finished product machined to its original shape is shown in Figure 2.1.d.

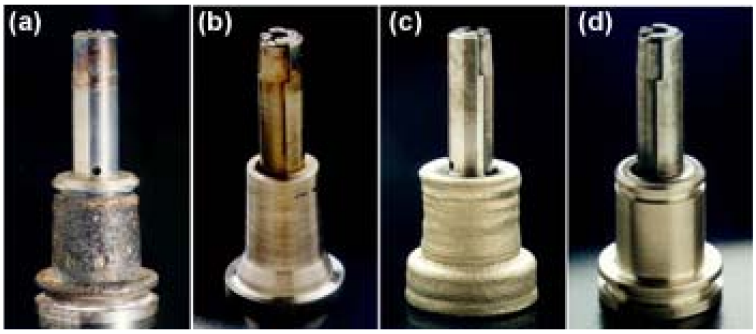

Figure. 2.1 Injection mould tooling for toothbrush holder. (a) Eroded, (b) Ground back, (c) Laser clad and (d) Milled to original tolerances. Photos courtesy of Fraunhofer ILT (Aachen, Germany).

Generally, as shown in Figure 2.2, the typical sequence of remanufacture is disassembly, cleaning, repairability analysis, refurbishment, replacement or repair, and reassembly of parts. The remanufacturing process enables the salvation of functionally failed but repairable products that are otherwise discarded in order to return them back to use, thus extending the useful life of moulds/dies.

Though remanufacturing activities of products have been widely conducted and contribute a large amount to economies in the U.S., Europe and China, not all products are suitable for remanufacture

and therefore a remanufacturability analysis is necessary prior to the actual remanufacture process. Based on 25 years of research into the remanufacturing industry, Hauser and Lund (2003) proposed a set of remanufacturability criteria required for a product to be successfully remanufactured, which are listed as follows:

- Technology exists to restore the products.
- The product is made up of standard interchangeable parts.
- Cost of core is low relative to savings in product cost achieved by core reuse.
- Product technology is stable over more than one life cycle.
- Market demand is sufficient to sustain enterprise.

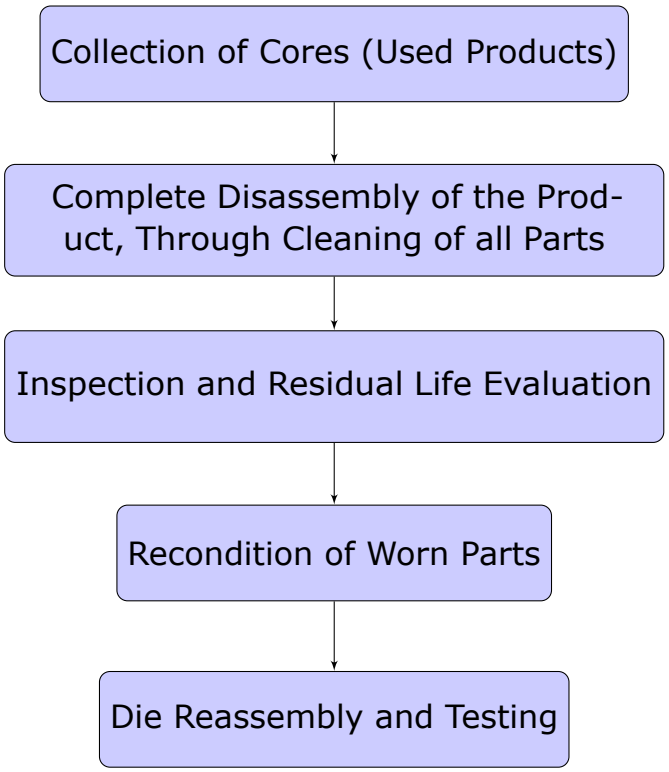

Figure. 2.2 Typical sequence for the remanufacturing of dies and moulds

Dies and moulds meet most of the proposed criteria as they are usually utilized for products of large volume and thus inherently retain a high value over common products and standardized components are increasingly adopted. Moulds remanufacture becomes feasible owing to recent scientific and engineering advances in repair technologies. Moreover, market scale of dies and moulds are booming steadily, which makes the collection of cores more accessible.

However, the remanufacture of dies and moulds is quite different from that of mass products:

(a) Quantity. Moulds/dies are dedicated and one-off, whilst other products e.g. automotive engines, are normally mass produced. This leads to a different remanufacturing strategy;

(b) Remanufacturing strategy. Generally, the remanufacture of mass produced products is the replacement of worn/failed parts with new ones, and the worn parts are recycled to recover materials because of their relatively low costs, whilst the remanufacture of dies and moulds is mainly focused on the repair of the failed dies and moulds using welding and machining technology instead;

(c) Enabling technologies for repair. Welding is the most popular enabling technology for the repair of injection moulds and die casting dies whilst machining of the worn surfaces to create the original geometry and surface roughness is often required for the repair of stamping forming moulds.

(d) Uncertainty. The unknown condition and unknown geometry of worn/ failed moulds/dies makes the remanufacturing process much more time-consuming and expensive. Currently, the

repair of moulds involves the assessment of mould conditions and the identification of the areas on the mould that need repair, including the manual or semi-automatic additive build-up of extra material, NC programming for rough and finish machining at separate work stations as well as several inspections to ensure quality control of the repair processes. All this causes long turnaround and processing times, resulting in high repair costs, long cycle times and lead times.

(e) Interference with production. Productions using dies/moulds are stopped when dies/moulds wear or fail since they are normally dedicated and one-off, therefore fast repair of moulds/dies is often urgently needed.

2.3 Failure modes of dies and moulds

Generally, dies and moulds are designed to have the capacity for mass production. With modern hard materials and proper mould design, an injection mould is capable of producing 100,000 parts or more. According to Klobcar and Tusek (2008) and Klobcar et al. (2008), the production capacity of a die casting die can reach up to 300,000 castings.

Though there are various types of moulding processes including injection moulding, die casting, forging, vacuum forming, etc., the major failure modes that lead to damage and failure can be generalized as below.

(a) Heat checking (also called thermal cracking). With dies or moulds constantly heated and cooled down during the operation cycle, large thermal gradients are created causing the die surface to be in compression during heating, and tension during

cooling of the die. Surface cracks are thus produced resulting in poor product surface finish and ultimately failures. Heat check is the main failure mode in hot working and specifically accounts for 70% of failures in die casting dies (Starling and Branco, 1997). Figure 2.3 illustrates the typical surface of a failed die with thermal cracks.

(b) Wear. During the moulding process, dies and moulds are cyclically exposed to different mechanical, thermal, tribological and chemical loads, thereby leading to the slow removal of die material and finally poor part tolerances. Mechanical and tribological loads usually account for the failure of cold working moulds while thermal and chemical loads for that of hot working moulds. Wear, as shown in Figure 2.4, decisively affects tool service life in approximately 70% of hot forging dies according to Turk et al. (2004) and Behrens and Schaefer (2005) and 85% of stamping dies (Abachi et al., 2010). Complicated geometrical features such as cores, pins, ribs and corners are especially inclined to wear. The wear causes the die to deviate from dimensional tolerances and often requires the repair of parts of the die after extensive damage.

(c) Plastic deformation. This failure mode is frequently encountered in both cold working and hot working moulds. When the contact pressure exceeds the compression yield stress of the tool material, the die suffers from plastic deformation which also leads to poor dimensional tolerances. For hot forging dies, plastic deformations influence tool endurance in nearly 1% of cases.

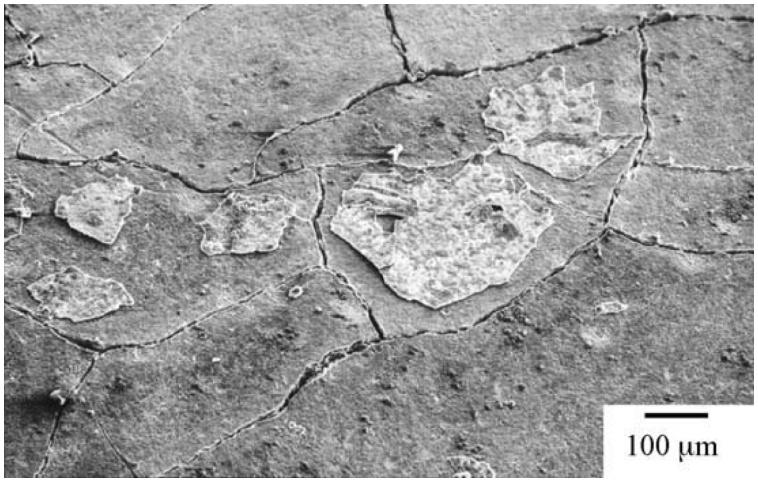

Figure. 2.3 Typical surface cracking in a failed die (SEM image, (Persson et al., 2005))

(d) Soldering and corrosion. This is a result of chemical interactions between the workpiece and the die material during the hot forming process. Thus, parts of the workpiece materials stick to the die surface (soldering) with defective products being produced, or part of the die surface becoming corroded. Figure 2.5. shows the appearance of pins after accelerated tests in aluminium die casting.

(e) Gross failures. Catastrophic failures due to thermal shocks and the heating of die material can lead to die malfunction and instability of mechanical properties.

2.4 Repair of dies and moulds

2.4.1 Repair strategies

Among the numerous types of dies and moulds, the predominant ones are stamping dies, hot forging dies, die casting dies and injection moulds and they play a key role in manufacturing industries. Therefore, it is of huge significance to study repair strategies for

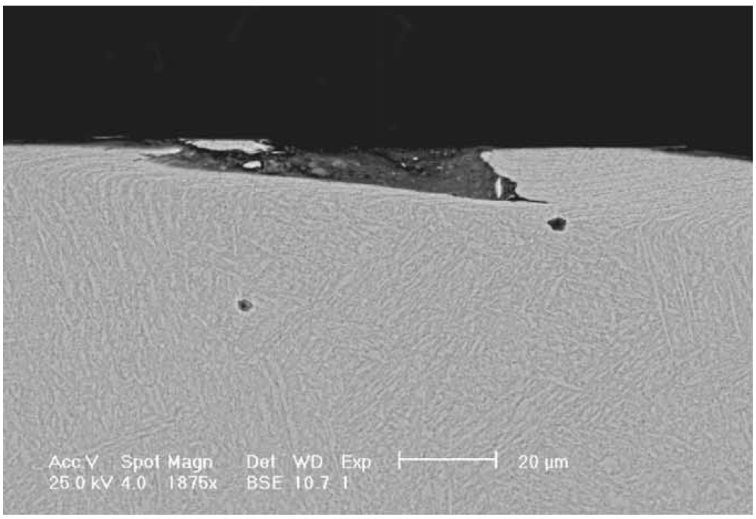

Figure. 2.4 Worn surface of a die pin(Barrau et al., 2003)

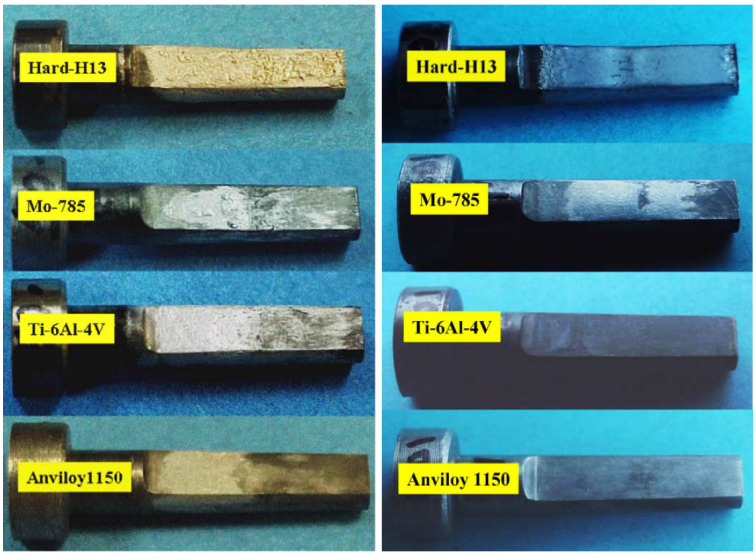

Figure. 2.5 Pins after 50 shots of accelerated tests with and without soldering(Zhu et al., 2004)

extending their service life and putting them back into operation. Table 2.1 depicts the main attributes of these main dies/moulds and their corresponding repair strategies.

All these moulds are designed for high volume production and have high values as well. In addition, the evolution rate is definitely dependent on the products for moulding, thus attention needs to be paid to establishing design methods for the remanufacture of dies and moulds at the design stage of products.

For repair strategies, as shown in Table 2.1, it is apparent that the major job for remanufacturing dies and moulds lies on repairing wear and thermal cracks in dies and moulds. Die casting dies and injection moulds have been popularly investigated in the literature while stamping dies and hot forging dies are generally industrially repaired. Welding is the most popular means for restoring damaged die casting dies and injection moulds. Industrial companies normally prefer to machine the damaged layer of stamping dies and hot forging dies to regain the dimensional tolerances of die cavities. However, the disadvantage of this machining method is that the mass and structure of dies are constantly reduced after every repair and its potential consequences are still unrevealed. Additive repair method like laser welding with equivalent quality and increasingly low costs is considered a better solution.

Table 2.1 Main attributes of types of dies and moulds and their repair strategies

Attribute	Stamping dies	Hot forging dies	Die casting dies	Injection moulds
Production Quantity	High Volume	High Volume	High Volume	High Volume
Value	High	High	High	High
Evolution Rate	Low	Low	Low	Medium
Mould Material	Cold work	Hot work	Hot work	Hot Work
Main Failure Modes	Wear(85%), Plastic De-formation	Wear(70%), Thermal Cracks, Plastic Deformation	Wear, Thermal Cracks(70%), Soldering	Wear, Thermal Cracks, Plastic De-formation
Repair Strategies	Machining	Machining	Tungsten Inert Gas (TIG) Welding, Laser Welding, Surface Engineering	TIG Welding, Surface Engineering

2.4.2 Repair enabling technologies

Dies and moulds fail in a variety of ways as mentioned above and measures must be taken to avoid or postpone the advent of these failures as much as possible. There are many alternative ways to extend the service life of dies with respect to the whole life cycle, including utilization of new wear resistant die materials, reduction of the intensity of wear by optimizing die geometries, reduction

of molten metal corrosion and erosion to the die by coatings and the improvement of the toughness of existing dies with better heat treatments, etc. While there are a variety of measures to prevent dies from failure, dies will finally reach the end-of-life phase. Welding is the most popular technology fit for repairing damaged dies and moulds so that they may be put into operation again (Tusek et al., 2007). Furthermore, the cost of repair accounts for only a small proportion, maximum of 30% of the cost of a new mould (Thompson, 1999). Among countless welding technologies, three of the most frequently used processes for the repair of dies and moulds are TIG Welding, Plasma arc welding (PAW) and laser-beam welding.

TIG welding (also called Gas Tungsten Arc Welding, GTAW) is a fairly mature technique and is widely applied in industry to obtain a better performance from repaired tools, dies and moulds. The process is often optimised in terms of welding procedure, material and filler wire, etc (Thompson, 1999).

Plasma arc welding advances the GTAW process, as the plasma is forced through a fine-bore copper nozzle at high velocities (nearly the speed of sound) and at a temperature of almost 20,000^{o}C. Compared to GTAW, Plasma Arc Welding has a stable arc that is more tolerant to arc length changes and penetrates weld materials more deeply and uniformly due to the constricted orifice. In addition, PAW needs a more simplified fixture and is more suitable for automation. With the exception of magnesium, PAW is suitable for welding most of the materials that can be welded by GTAW.

Laser welding is characterised by its concentrated density of energy and accuracy allowing narrow, high quality and deep weld beads. Due to its advantages over traditional welding techniques, laser repair technology has been widely adopted for the restoration

of moulds and dies as well as other components, such as steam generator, navy aluminium components, and turbine components.

Apart from these main stream welding techniques, other processes like the electro spark process and cold spray are adopted for the repair of dies and moulds.

The electro-spark process is an efficient technology used to restore damaged die-casting dies, and can also improve overall casting efficiency by applying a high performance coating in the critical areas of the dies. The electro-spark process may be used to extend the service life of die casting dies at both pre-damaged and damaged stages (Aoshima, 1999). The damage of erosion and abrasion in aluminium die casting dies can be reduced dramatically by applying tungsten and/or titanium carbide coating in problem prone areas, and worn dies can be repaired by applying an alloy overlay.

Cold-spray, as an emergent repair technique, has the advantage of minimum thermal stress over fusion welding techniques because it operates at room temperature and does not involve the melting of materials. The initial research work conducted by Lee et al. (2007) showed good quality of repaired parts and demonstrated the industry potential of the application of this method into wear repair.

Additionally, studies of laser glazing (Jiang and Molian, 2001), powder alloying and laser coating (Shah and Dahotre, 2002) also show great capability in extending die service life.

2.4.3 State-of-the-art mould repair

Despite the fact that devices for tool steels repair are available on the market, there is a lack of know-how related to the weldability and welding procedures of moulds. Thus, the influences of welding

parameters on the metallurgical behaviour of AISI P20 and H13 as well as welding procedures of TIG welding were analysed by Silva et al. (2008), and pre and post heat treatment advised in order to avoid risk of failure and to obtain uniform properties.

Regarding the repair methods, laser welding is the most popular repair technology among the three mainstream welding technologies (Grum and Slabe, 2004), and considerable effort has been devoted to implementing laser-based repair technologies so as to obtain the high restoration quality of worn parts. For instance, a laser-based free form fabrication process, named Direct Metal Deposition (DMD) (Mazumder et al., 1997), for applications specific to the repair of plastic injection moulds and die casting dies was successfully commercialized by the POM Company. The developed process, DMD, was then widely adopted for improving the service life of AISI H13 tool steel. Because AISI H13 tool steel, as the primary building material for die casting dies and injection moulds, is difficult for deposition due to residual stress accumulation from martensitic transformation. Parishram et al. (2006) and Parishram (2007) studied the effects of laser process parameters on the repaired AISI H13 tool steel. The observations are that the power levels have a significant correlation to the depth of the processed region and scan speeds affect the width and micro-hardness. Lee et al. (2009) used a 200W fibre laser to investigate the hardness of AISI H13 tool steel after laser hardening and laser melting respectively. It was found that the hardness after laser surface hardening is improved from HV240 to HV480-510 and after melting the melted zone near the base metal has a dense martensite microstructure which leads to higher hardness than that near the surface.

Much research has been devoted to the restoration of dies and moulds which have failed in one or more modes. As summarised in Table 2.1., thermal cracks are the principal failures faced by hot working tools which usually cause operation interruption and require the repair or replacement of dies and moulds. Sun et al. (2003, 2001) repaired the cracks of hot work tool steel using the laser melting process and found that the impact strength and fatigue strength of repaired specimens was remarkably low, but could be recovered after heat treatment. Laser repair was considered as a feasible means for the life extension of the damaged tool. The repair feasibility of using laser welding for the thermal cracks on aluminium die casting dies was investigated by Parishram et al. (2006) and Pleterski et al. (2008).

Compared to other welding technologies, laser repaired dies have some disadvantages, such as the fact that laser melting may generate hard structures resulting in a detrimental reduction in impact toughness (Sun et al., 2001). Weld defects due to overalloying of the weld metal have also been observed (Vedani et al., 2007). The solutions to these problems were suggested by using proper parameters of the laser pre-heating process (Vedani et al., 2007) and heat treatment at secondary hardening temperature (Sun et al., 2003).

2.5 Life evaluation technologies

Life evaluation technology plays a significant role in the component design, maintenance, and operation management. It is frequently used to predict the remaining useful life (RUL) of a component or system to investigate the length from the current time to the end of life. Recently, prediction of RUL has been widely conducted

in operational research, reliability and statistics with important applications in other fields such as material science, biostatistics and econometrics (Si et al., 2011). Accurate RUL prediction is the key to preventing unexpected failures and minimizing overall maintenance costs and losses due to interrupted production (Tian et al., 2010). Also, evaluation of RUL is an important step in the remanufacture for deciding whether or not to remanufacture the collected cores.

2.5.1 Remaining useful life prediction

Remaining useful life prediction is the main task in prognostics which estimates time to failure and risk for one or more existing and future failure modes (Sikorska et al., 2011). Therefore, the prognostic models for estimating the RUL of a component or system have been frequently studied. To evaluate whether a structure, system or component of interest can perform its function throughout its lifetime with reasonable assurance, a variety of approaches have been proposed. Although there is little consensus among reviewers in the prognostic field on the most appropriate classification for grouping remaining useful life prediction models, they can be broadly categorized into two: deterministic and probabilistic models (Li et al., 2009). Deterministic approaches attempt to incorporate physical models of the system into the estimation of the RUL while probabilistic methods utilize monitored operational data related to system health. Therefore, prognostic models may also be classified by a physics-based approach and data-driven approach, respectively (Zio and Di Maio, 2010).

Physics-based methods quantitatively feature the behaviour of failure mode using physical models of components and damaged

propagation models based on damage mechanics. This assumes that the system behaviour in response to working conditions is thoroughly understood and can be described accurately and analytically. The remaining useful life of a component/machine is estimated by solving a set of deterministic equations. The main advantage of this group of models is the ability to directly incorporate existing understanding of the physical mechanisms of failure. As physical understanding of the system improves, the accuracy of the RUL prediction can be improved simultaneously. Few data are required when applying physical models to estimate the RUL. Consequently, when available and sufficiently complete, physics-based models tend to significantly outperform other types of models (Luo et al., 2003). However, it may not always be realistically possible to perfectly understand the failure mechanisms under the range of relevant operating conditions and lifetimes are often modelled using only static probability distribution without taking into account any condition monitoring data, or by deterministic deterioration models even though the phenomena are stochastic by nature (Banjevic, 2009).

On the other hand, data-driven methods utilize collected condition monitoring data for RUL prediction without deep understanding of the physical principles. The data-driven methods are based on the understanding that condition monitoring data and the extracted features will change during the damage evolution process. Thus, the relationship between equipment age, condition monitoring data, equipment degradation and remaining useful life is modelled. The most frequently applied techniques for data-driven methods are statistical techniques (regression models, Autoregressive moving average (ARMA) models, etc.) and Artificial Intelligence (AI) models (neural networks, fuzzy systems, etc.). The obvious advantage is

that there is no need for a thorough understanding of physical laws. Moreover, this approach is especially effective for complex systems of which physical modelling is impossible to be sufficiently accurate. However, this technique needs a large amount of data to make the system as close to real applications as possible (Li et al., 2009).

For a detailed review of data-driven approaches, Sikorska et al. (2011) carried out a thorough review of prognostic modelling options for remaining useful life estimation implemented by industry. In this review paper, the exact demarcation between diagnostics and prognostics has been defined with little disagreement by those in the published literature, and the models for remaining life prediction have been classified into four main groups: Knowledge-based (expert and fuzzy), Life expectancy (stochastic and statistical), Artificial Neural Networks, and Physical models. The strengths and weaknesses of each of these four main prognostics model classes have been explored. They concluded that Artificial Neural Networks may be the best option for remaining life prediction since they require a minimal understanding of the processes governing failure. While a larger input of domain-specific expertise rules are necessary for expert and fuzzy systems, life expectancy models need a larger amount of statistical calculations and detailed data collection process. On the other hand, physical models require a comprehensive knowledge pertaining to all physical mechanisms and environmental factors that influence equipment failure for their successful applications. Another detailed review article for RUL prediction has been presented by Si et al. (2011). The collected data were divided into direct condition monitoring (CM) and indirect CM data. The reviewed models related to direct CM data were regressive ones, Wiener process, Gamma process and Markov based

models, while stochastic filtering-based models, covariate based hazard models, Hidden Markov models and Hidden semi-Markov models were delineated as indirect CM data models.

2.5.2 Die/mould damage modelling

To evaluate the remaining useful life of dies and moulds, physics-based models are mostly applied. The service life of dies and moulds is limited by several factors, which are the dimensional error caused by macro-wear, overstress caused by stress concentration and the fracture caused by fatigue (Kim and Choi, 2009). While industrial practices have attached great importance to die life, it has not been so in academia. As already discussed in the failure mode section, dies and moulds frequently suffer from heat checking, wear, plastic deformation and soldering, etc. Therefore, the essence of RUL estimation is to predict the damage evolution of die halves, predominantly the degree of wear and fatigue. In general, die failures caused by wear are important for warm and hot forging, while it is the sudden fracture or fatigue that affects the die service life in cold forging and die casting.

Wear modelling

Wear, the most predominant form of die failure, is the slow removal of die material resulting in poor part tolerances and poor die surface roughness. Unfortunately, it is the most difficult to mathematically model because of an abundant number of factors affecting wear. The three major forms of wear are abrasive wear, adhesive wear and plastic deformation. A number of different approaches have been proposed with aims to accurately predict the die wear volume.

Archard's wear model (Archard, 1953) is the earliest and most widely used one for the estimation of wear quantity. The amounts of wear, for adhesive and abrasive mechanisms, are proportional to the wear coefficient between the die and the workpiece, the surface pressure of the die, the relative distance between the die and the workpiece and an inversion to the hardness of the die. Recently, based on Archard's wear model, new models have been studied to take more factors into consideration. Kang et al. (1999a,b) studied the effects of thermal softening on die wear, which was then embodied by a new model used for the calculation of wear profile. Lee and Jou (2003) proposed a new wear model considering the wear coefficient and the hardness of tool steel as functions of temperature. Kim and Choi (2009) also applied a similar wear model to investigate the wear quantity of forging dies.

Another approach is an energy balance approach to wear modelling. This model accounts for the energy supplied by the machine, using the first law of thermodynamics. This assumes that the amount of material removed is proportional to the energy dissipated on the tool/workpiece contact interface. Stahlberg and Hallstrom (1999) did a comparison between these two wear models and found that both models showed satisfactory agreement with the experimental results, but the energy method had better capacity of indicating the location of wear-sensitive parts.

Fatigue modelling

Fatigue is a process that causes the premature failure or damage of a component subjected to repeated loadings far below the static yield strength of the material. Traditionally, RUL prediction of fatigue behaviours has been of particular interest. The fatigue process can

be broken down into three major phases – initiation life, propagation life and catastrophic failure. Due to the extreme complexity of this process, it is difficult to accurately describe and model fatigue at a microscopic level. However, the necessity of fatigue life prediction has led to three different approaches: stress life approach, strain life approach and Linear Elastic Fracture Mechanics (LEFM) approach.

The stress life approach (or Wohler approach) uses a log-log stress versus cycles till failure diagram to display fatigue property data (Bannantine et al., 1990). It treats all strains as elastic and thus is mostly used for high cycle fatigue failure. Also, it does not distinguish between crack initiation and propagation (Farahmand et al., 1997). The strain life approach is based on plastic strain which leads to crack initiation and thus is more suitable for high strain/low cycle situations. Nevertheless, it only accounts for initiation life and cannot be used to predict propagation life (Bannantine et al., 1990). The LEFM approach offers better insights into the actual mechanisms of fatigue that are significant in research. It directly deals with the propagation phase of fatigue cracks with an initial crack size being known or assumed. However, it has problems dealing with crack initiation. The general comparison of these fatigue life approaches in nature is shown in Table 2.2.

When stresses in a die are generally in the elastic region, the stress-life method is very suitable for fatigue life prediction. For instance, Kim and Choi (2009) applied Goodman's and Gerber's equations, and used the stress-life method to estimate the fatigue life of hot forging dies. However, due to the heavy loadings applied to the dies and moulds, plastic deformation may occur at stress concentration positions. This may lead to a dramatic drop in die fatigue life and consequently, the fatigue model often requires

the considerations of low-cycle fatigue failure. Therefore, strain-life fatigue approaches are more frequently adopted for die life prediction. Rosbrook (1992) applied the finite element method to model the thermal fatigue of Wallace test samples using the Universal Slopes method (strain-life). This has the advantage of using material-independent exponents to understand the fatigue behaviours of die-casting dies. Sakhuja and Brevick (2004) also employed the method of Universal Slopes for thermal fatigue life predictions of copper rotor die casting dies. Lee and Chen (2001) proposed a simple strain-life model using the die hardness and fatigue total strain as parameters to predict the fatigue life of cold-forging dies. Since the die hardness is easily measurable, the advantage of such a simplified model is that it conveniently indicates the estimation of the die quality.

Table 2.2 Comparison between different fatigue analysis methods

Approaches	Strengths	Weaknesses
Stress life ($S-N$) approach	Simple to estimate material constants; Fit for designs involving long life; Constant amplitude histories; Available data for correction.	Completely empirical and lack of physical insights into fatigue mechanism; Ignores the true stress-strain response; No distinction between initiation and propagation.
Strain life ($\varepsilon-N$) approach	Accurately models plastic strain; Able to model the residual mean stressed from the sequence effect in load histories; Easily extrapolated to situations involving completed geometries; Useful for high temperature applications; Able to incorporate transient material behaviour.	More complicated than $S-N$ method; Only accounts for initiation life; Still empirical in several aspects; Need for additional testing for corrections.
LEFM approach	Directly deals with crack propagation; Able to be incorporated with non-destructive inspection techniques; Offers better insights into fatigue mechanism.	Difficult to deal with crack initiation; Difficult for situations where the assumptions of LEFM are not valid; Difficult to determine the stress intensity factors for complicated geometries.

In order to take more stages of fatigue into account so that a better accuracy is possibly obtained, much research has focused on modelling the crack propagation life via LEFM. Qamar et al. (2008) studied the crack propagation life of an extrusion die by using the Paris law with initial cracks in the range of 0.05 to 0.10 mm. Skov-Hansen et al. (1999) defined the life of cold-forging dies as the number of cycles needed to crack initiation and the number of cycles to crack propagation to the critical length. The life was assessed by combining the strain-life approach and dynamic fracture mechanics to calculate these two parts of life, respectively. Persson (2004) modelled the thermal fatigue life of hot work tool steels by representing the thermal crack initiation and propagation using strain-based models. This model is capable of predicting the

tendencies in the lifetime of the tool steels but further improvement is needed for actual thermal fatigue life prediction.

Die life prediction

With the wear and fatigue appropriately modelled, it is possible to evaluate the remaining useful life of dies and moulds. Recently, numerical simulation technologies have been widely applied to many metal forming applications to estimate tool life. A typical architecture of RUL evaluation using fatigue life approaches mentioned above is shown in Figure 2.6.

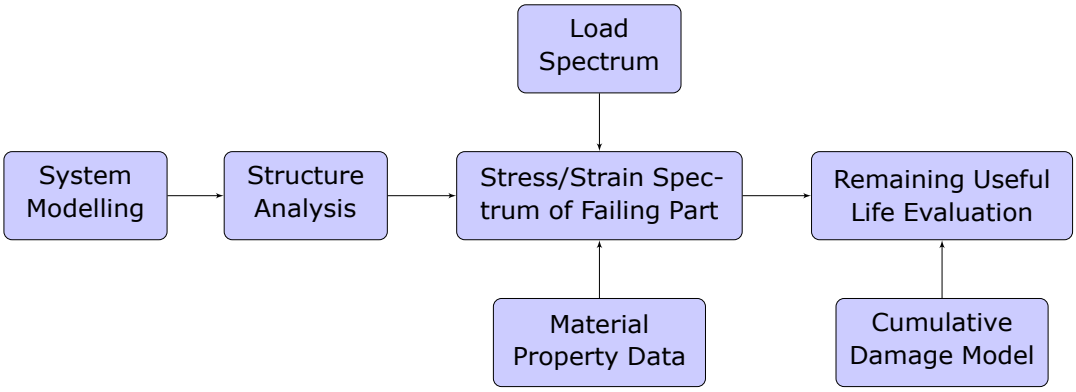

Figure. 2.6 A typical architecture of RUL evaluation using fatigue life approaches.

Finite Element Method, as a dominant numerical simulation technique, plays a leading role in estimating the residual life of dies and moulds. Behrens (2008) and Behrens and Schaefer (2005) used finite element analysis (FEA) to calculate tool wear taking into account hardness changes. Kim et al. (2005) and Kim and Choi (2009) presented two methods for estimating die service life against plastic deformation and wear. Other methods were occasionally selected as simulation tools for die life prediction. For example, Behrens (2008) and Abachi et al. (2010) recently carried out the simulation of forging process based on Finite Volume Method (FVM) to evaluate the wear of die halves and Watson et al. (2005) built

the physical model of a high power clutch system using the MATLAB Simulink modelling environment for wear prediction.

In order to reduce the maintaining cost and improve the life-cycle value of components, it is necessary to rapidly estimate the residual life of used parts so that the operation process can be conducted continuously. Thus, advanced inspection technique based methods are becoming preferable. The non-destructive evaluation (NDE) has the advantage of no removal of studied components for condition data acquiring over traditional sectioning and metallurgical examination (Shannon et al., 2010). One newly developed method to evaluate the residual life of used components is based on such non-destructive testing techniques. For this method, researchers tend to use continuum damage theory to study the damage evolution in metals and predict their lifetime. The measuring parameters are firstly determined in the testing apparatus with respect to the entire damage evolution and then are implemented for lifetime prediction. Parameters that are more correlated to damage and more easily tested usually become successful measurement inputs for NDE, for instance, modulus degradation, micro-hardness, electrical resistance, ultrasonic signal, and lock-in thermography, etc. Sun and Guo (2004) presented a method to obtain the damage information in metallic materials by means of capturing electrical resistance change under the hypothesis that the current-conducting cross-sectional area is equivalent to that of load-bearing.

Simulation based approaches and inspection based methods both have their own strengths. Simulation based approaches are able to take more variables into account and provide manufacturers with a panoramic view of components or systems being investigated. However, this is usually based on some simplifications. On the

other hand, inspection based methods have the advantage of rapid checking after the damage evolution is established. Nevertheless, because of the variety of damage mechanisms that are present in a structure or component, and the limitations of any NDE method, no single technique is capable of providing sufficient information to enable accurate assessment of the RUL (Shannon et al., 2010).

While remaining useful life has been widely evaluated in the maintenance of critical components or systems, less attention has been paid to the prediction of RUL for remanufacturing purposes until the recent growth of the remanufacture industry. Mazhar et al. (2007) proposed a two-step approach to assessing the remaining useful life of used components of washing machines. First, the mean life of components was assessed statistically; then, the actual (used) life was determined by analysing the degradation and condition monitoring data through an Artificial Neural Network model.

2.5.3 Reliability analysis

Wear and fatigue based models for life predictions are generally deterministic in nature. However, a variety of random variables such as geometric parameters and material properties result in the life prediction of components largely probabilistic in character (Qamar et al., 2008).

Deterministic life evaluation technologies normally investigate the service life of components under the assumption of certainties. On the other hand, reliability performance studies the underlying uncertainties. It plays a more important role in remanufacture as it is only the equivalent quality that can assure customers' confidence over remanufactured products. As with manufacturing, reliability control is also required through the entire remanufacture process.

Reliability performance prediction is a common problem faced by all product developers. However, differences in collected cores, required processes, and machining methods between manufacture and remanufacture, make it an even more difficult task for a remanufactured product because remanufacturers typically have much less information available to them. Similar to remaining useful life evaluation, reliability performance prediction of remanufactured products is still a "niche" part of remanufacture as well. However, such importance has already drawn considerable attention and some work has been published in the literature. Esterman et al. (2006) combined Failure Modes and Effects Analysis (FMEA), Experimental Model Building, Monte Carlo Simulation and LEFM to generate a reliability estimation of a remanufactured engine cylinder head with a fatigue crack repaired by the welding process. The effect of the laser melting process on hot work tool steel (SKD6) was evaluated by a rotating bending fatigue test by Song et al. (2008) and it is reported that the fatigue strength of the laser processed specimen decreases remarkably in comparison with that of base metal but can be recovered by heat treatment at 773 K.

There are a number of reasons as to why reliability analyses of remanufactured products are rarely carried out. The first reason is that remanufacture activities not being widely implemented yet. Secondly, the reliability performance of remanufactured products and remaining useful life evaluation of parts to be remanufactured retain a close relationship, i.e. the development of the latter technology can directly facilitate the former one; and since remaining life evaluation is not yet fully established, more research is needed. And lastly, more variables are encountered in remanufacture which

makes the reliable prediction of remanufactured products more complicated.

2.6 Challenges and opportunities

In regards to the remanufacture of dies and moulds, it can be concluded that the majority of research has focused on repair technology, especially, welding technology. Whilst welding technology is relatively mature, the industry of the remanufacture of dies and moulds is still in its infancy. With the demand for sustainable manufacturing across the world, it is expected that the industry of mould remanufacture will play an increasingly important role in the near future. However, the industry of remanufacture of moulds and dies can only be financially viable if it can be conducted in centralised factories to achieve mass production with high efficiency, reduced cost and low lead time. To this end, the challenges and research opportunities lie in:

i Reverse logistics and business model: Obtaining sufficient cores (worn /failed moulds/dies) from different factories at different locations to achieve the scale for mass production is essentially the first step for the industry to achieve its full potential. Also, cores acquired by a remanufacturer highly fluctuate in quality, even if the expected fractions of the various quality levels are known (Teunter and Flapper, 2011). Research should be focused on building a reverse logistic network for sufficient cores while addressing the increasing difficulties of forecasting quality levels of collected products;

ii Need for automation: Although remanufacturing inherently entails the customisation of products, with the purpose of

maximum benefits, it is also necessary for remanufacturers to achieve automation for mass customisation. However, the large degree of customisation of remanufacture requires much more flexible remanufacture equipment than normal manufacture processes. Unfortunately, no or little work has been done in this field;

iii Remaining useful life evaluation involves two aspects: the residual life evaluation of core and service life estimation of dies and moulds after remanufacture. It is not only a significant measure for a remanufacturer to make a decision on whether the core is worth repairing or not, but also one important feature that makes remanufacture different from other close loop strategies, e.g. recycling. Although RUL of common products has been studied, differences in the initial conditions between used products and new products are huge, which makes it difficult to assess their residual life. Additionally, dies and moulds are manufacturing tools by nature and require more accurate evaluation techniques. Little research has been conducted on the RUL of failed dies and moulds;

iv Design for remanufacture: To successfully apply remanufacturing to a product, it needs to be designed for this purpose at conceptual stage with some characteristics such as ease of disassembly, ease of replacement, and ease of reassembly, etc. included (Pigosso et al., 2010). The literature review conducted by Hatcher et al. (2011) has indicated that life cycle thinking is one significant potential path for further research on design for remanufacture. Remanufacture of used components cannot be realised without the whole life cycle thinking of products because the remanufacture process is composed of a set of

reverse operations. Traditional perspectives on product design and application have to be updated with considerations about the remanufacture of dies and other tools: the pre-failure stage to reduce the need to repair and the post failure stage to make remanufacture easier. Standardisation and module design can greatly improve the reusability of die components as well. Another aspect for consideration is design for no or acceptable failures because components failing in one or more modes, e.g. wear, contributes a huge fraction to the waste stream (Sherwood et al., 2000). Excellent design would prevent failures, leading to the reuse of parts without repair, or afford economic repair of failed parts;

v Life oriented repair technologies: After remanufacturing, failed products are expected to serve another predetermined life cycle. Unfortunately, the relationship between repair process parameters and the service life of repaired components has not been well established by recent studies on repair technologies, such as welding. Life models are necessarily investigated for different failure modes encountered by dies and moulds so that more efficient remanufacture processes may be applied in response to specific failure mode;

vi Cost model: Usually, dies and moulds are urgently repaired without consideration of repair costs due to their tooling roles in manufacturing. When used dies or failed moulds are collected for remanufacture, the changed situation makes it necessary to analyse the cost needed in order for remanufacturers to pursue maximum benefit. Practical cost models related to the remanufacture of dies and moulds should become another research focus;

vii Life cycle assessment (LCA): Although it is generally acknowledged that remanufacture improves environmental and economic performances, not many studies have been conducted to quantify the full benefits of remanufactured products. Smith and Keoleian (2004) performed an LCA to investigate the energy savings and pollution prevention achieved through remanufacturing a midsized automotive gasoline engine as compared to a new one. Biswas and Rosano (2011) carried out a similar LCA to evaluate the greenhouse gas emissions from the production of a remanufactured compressor versus a new compressor. These utilised methods usually considered only one life cycle, i.e. cradle-to-grave. However, various End-of-Life (EOL) options, such as reuse, remanufacturing, recycling and landfill, have led to a closed-loop system. Therefore, linear classical models should be improved to allow the consideration of this complexity. Goldey et al. (2010) analysed the environmental benefits associated with remanufacturing network telecommunications equipment by employing a LCA model of two successive life cycles. Amaya et al. (2010) proposed life cycle bricks and parameters in the LCA model to quantify the environmental benefits related to closed-loop strategies of multiple life cycles. The benefits of this method include better relevance to real practice, and more reliable data in evaluation. For dies and moulds, the number of life cycles is specifically dependent on the degree of damage they suffer. Therefore, specific number of life cycles should be an important consideration factor in developing new methodologies in LCA.

2.7 Summary

Dies and moulds play a significant role in mass production. Failure leads to a reduced service life. Not only can the remanufacture of dies and moulds put failed dies back into application but also releases the pressure on landfill and hence reduces the environmental impact.

With the purposes stated, tremendous contributions relating to the remanufacture of dies and moulds have been made in terms of the involved process. Characteristics of the remanufacturing of dies and moulds have been discussed in detail and showed how they differ from the remanufacture of common products. Failure modes of dies and moulds have been reviewed and their corresponding repair technologies summarised, among which welding dominates and is readily used for the remanufacturing of dies and moulds. Residual life evaluation and reliability analysis, though well researched in other fields, are still immature within the remanufacture of dies and moulds.

The remanufacture of dies and moulds has already shown great potential for the near future. However, to successfully carry out the remanufacture of dies and moulds, both industry and academia are facing many challenges. Such challenges mainly lie in reverse logistics, automation, residual life evaluation, design for remanufacture, and cost control.

Chapter 3

Research methodologies

3.1 Introduction

As concluded in the literature review, remanufacture has not been carried out in the die and mould industry. Research interests within remanufacturing activities are evidently also research gaps for the remanufacture of dies and moulds. Research gaps for remanufacture of dies and moulds are thus both extensive and intensive. Therefore, this chapter focuses on the definition of research methodologies to be applied.

The chapter firstly narrows down the huge research gap within the remanufacture of dies and moulds to the crucial scope - remaining useful life assessment of remanufactured dies and moulds. The aspects to be concerned within the scope are then identified and methodologies for them are proposed correspondingly. Last but not least, common problems encountered by these aspects are investigated with theoretical solutions.

3.2 Research scopes

Remanufacture of dies and moulds is still in its infancy. All aspects related to remanufacturing activities are research gaps for the remanufacture of dies and moulds, as concluded in the previous chapter. Remaining useful life evaluation is a key technology to ensure the reliability of remanufactured products. It plays an even more important role in remanufacturing failed dies and moulds because they are generally product specific and one-off design. Although recently repair of damaged dies and moulds has been regularly performed in the industry, remaining useful life prediction is scarcely conducted after that, which renders manufacturers unsure warranties. For more accurate prediction and better warranties, remaining useful life evaluation technology needs to be well developed for remanufacturing dies and moulds. Thus, this research is mainly narrowed down to the fatigue life assessment of thermal cracked hot work dies and moulds for remanufacturing.

3.2.1 Target moulds

Dies and moulds differ from each other from their types, through the products they produce, to tool materials and their failure modes. This research targets specifically at failed hot working dies and moulds with thermal cracks. One reason is that heat checking is the main one in hot working processes and is responsible for 70% failure cases in die casting (Starling and Branco, 1997). Additionally, hot working processes allow materials to recrystallize to keep the materials from strain hardening. Generally, hot working dies and moulds are usually designed for complex products and for high volume production. Consequently high values are built in these

types of dies and moulds. The potential demand for remanufacturing is huge.

Therefore, this study focuses on thermal cracked dies and moulds from hot working processes, especially die casting dies.

3.2.2 Material considerations

AISI H13 is a hot working tool steel with 5% Cr and a higher content of vanadium than other steels in its class. Therefore it combines good toughness, resistance to abrasion and high red hardness with the ability to resist heat checking. It also has high tensile and impact strength. These properties make H13 the material of choice for aluminium and magnesium die casting in addition to other hot working applications such as forging, extrusion and swaging. However, H13 has low fracture toughness and is susceptible to hydrogen embrittlement.

8407 Supreme is a premium high quality H13 die steel. It has significant improvements in isotropic properties compared to conventionally produced AISI H13 grades. These improved isotropic properties are particularly valuable for tooling subjected to high mechanical and thermal fatigue stresses, e.g. die casting dies, forging tools and extrusion tooling.

Therefore, 8407 Supreme is chosen as the material choice for sample specimens in this research. The chemical composition and mechanical properties of the tool steel are depicted in Table 3.1 and Table 3.2, respectively.

Table 3.1 Chemical composition of the mould steel (wt%)

	C	Si	Mn	Cr	Mo	V
8407 Supreme	0.39	1	0.4	5.2	1.4	0.9

Table 3.2 Typical mechanical properties of the mould steel (Room temperature)

Hardness(HRC)	Tensile Strength, R_m (MPa)	Yield Strength, R_p (MPa)
52	1820	1520
45	1420	1280

3.3 Research framework

To accurately predict the remaining useful life of structures, it is necessary to consider as many as possible aspects that affect the structure. Generally, three aspects need be considered when conducting remaining useful life evaluation. The first significant factor is their changed initial status due to remanufacturing. Remanufactured dies and moulds are not the same as they are in their first service life cycle. The damage process starts from a different state. Also, there has been some variance in the damaged area introduced by remanufacturing processes as well. Another factor that determines the post-remanufacture service life is the working condition they are being operated. The more severe the conditions they experience, the shorter their service life. Last but not least, the damage evolution process of the material is also an important part for the service life evaluation. Different materials and their applications require different life evaluation models.

Figure 3.1 depicts major parts involved in the remaining useful life assessment of remanufactured dies and moulds. The process begins with initial status modelling of die halves introduced by remanufacturing processes. For welding processes, residual stresses would be the dominant factor influencing the fatigue strength of welded area if the weld profile is optimized. Therefore, the main job of initial status modelling is to calculate residual stresses due

to remanufacturing process. Loadings and boundary conditions are extracted and simplified from their industrial working environment. Hitherto, cyclic loading profiles of die halves can then be computed via finite element analysis (FEA). With damage evolution model obtained from simulative damage tests, remaining useful life of remanufactured die halves can be assessed either by a separate evaluating process or by integration of the damage model into the previous step.

Therefore, this research mainly includes three parts, finite element modelling (FEM) of residual stresses due to laser welding repair, work loading calculation of die halves under moulding operations and fatigue life modelling of the die material taking into account the resultant impacts of working load for next service life and the residual stress from remanufacturing. The detail of each aspect is discussed in the following parts.

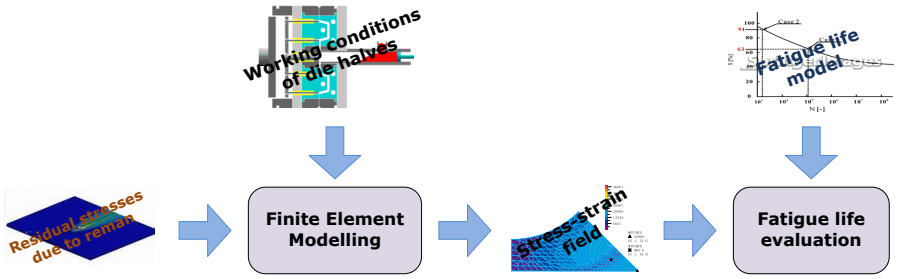

Figure. 3.1 A schematic diagram of proposed research framework

3.3.1 Die casting process

To evaluate the remaining useful life of remanufactured dies and moulds, it is certainly necessary to take into consideration working conditions because they directly affect the loads dies and moulds suffer and thus decide their service life.

There are two basic types of die casting machines, namely hot-chamber machines and cold-chamber machines. Both die casting machines follow a similar operation cycle. Typically, a die casting process consists of the following four steps. (a) Die closing: the cleaned and lubricated two halves of the die are closed and clamped together inside the die casting machine. (b) Injection and solidification: the molten metal is forced into the die at high pressures and velocities for low cycle times. The casting metal then rapidly solidifies in the die cavity. (c) Part ejection: after solidification, the casting is removed from the die halves. (d) Clean and lubrication: the open die halves are sprayed with releasing agent and water based lubricants. Figure 3.2 depicts the most common stages during a cold-chamber manufacturing cycle.

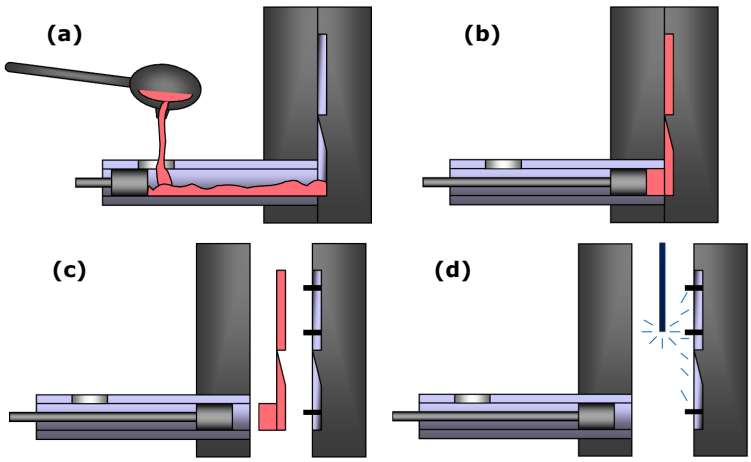

Figure. 3.2 Operation stages in a typical cold chamber die casting cycle(Vinarcik, 2003).

Die casting dies are subjected to cyclic mechanical loads of machine clamping force and the cavity pressure, as well as thermal loads due to cooling and solidification of the casting alloy, and to the cooling of the lubricant. It is the repeated, rapid, non-uniform heating and cooling that results in thermal-mechanical loadings and finally leads to thermal cracking of die surfaces. The cyclic profiles

of damage field within the die are influenced by all these factors. The extent to which these loads affect the damage behaviour and cyclic life of the die is largely determined by their magnitudes and exerting locations(Rosbrook, 1992).

On a properly adjusted machine, the clamping force is supported evenly by the contact area of die surfaces and thus the force per unit area on the die is relatively small, even though the locking force on a large machine may be as large as several thousand tonsGarza-Delgado (2007); Rosbrook (1992). Cavity pressures are more significant to the problem of heat checking than the pressures due to the locking forces are because of their greater magnitudes and acting areas where maximum thermal loading is observed. The largest thermal loads experienced by the die occur during cooling and solidification of the casting alloy, and during spray cooling of the die. During injection, compressive stresses are induced near the die surface as the expansion of the surface elements is constrained by cooler neighbouring elements while during spray cooling, tensile stresses are created near the die surface as the contraction of surface elements is restricted by warmer neighbouring elements.

Therefore, the task of moulding process modelling is to reveal the contributions of cavity pressures and thermal loads to work loadings of die casting dies. Figure 3.3 presents the approach to modelling the stress and strain profiles of die casting dies under cyclic operations using finite element method. Specifically, the die operation cycle is firstly summarized as several stages so that loads and boundary conditions can be conveniently identified for each stage. Simplifications may be made for insignificant stages. Then, for each stage, mechanical loads, thermal loads as well as boundary conditions are specified and attained accordingly. With material

properties, finite element models are solved for the working profiles die casting dies experience.

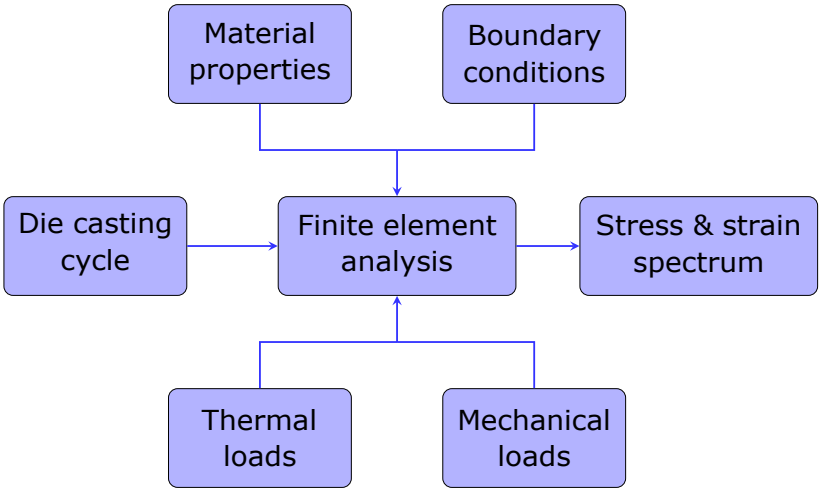

Figure. 3.3 Finite element modelling die casting process

3.3.2 Thermal fatigue life assessment

Not only are the service lives of die halves affected by the time-varying stress-strain behaviour during the production cycle, they are also significantly dependent on the thermal fatigue evolution behaviour of the tool material. With die halves constantly heated and cooled during the operation cycle, large thermal gradients are created causing the die surface to be in compression during heating, and tension during cooling of the die. The stresses due to the cyclic thermal loads may be high enough to impose plastic deformation on the die surface, and eventually cause thermal cracking (Velay et al., 2002). Failure of die halves causes a significant loss for the die casting industry because of the high cost of dies and the production suspension due to die downtime. Therefore, a great deal of effort has been paid to understanding the fundamental of thermal fatigue evolution.

Traditionally, the Strain life ($\varepsilon - N$) approach is utilized to predict the fatigue life based on the strain damage evolution laws when the

structure's response is stabilized after many cycles. The popular equation relating the total strain $\Delta\varepsilon$ and number of reversals to failure $2N_f$ is the Coffin-Manson relationship (Coffin, 1954; Manson, 1953):

$$\frac{\Delta\varepsilon}{2} = \frac{\sigma'_f}{E}(2N_f)^b + \varepsilon'_f(2N_f)^c \tag{3.1}$$

where σ'_f and ε'_f are the fatigue strength coefficient and ductility coefficient, E is the modulus of elasticity, b and c are the fatigue strength exponent and the fatigue ductility exponent, respectively.

However, this approach usually models the response of the structure subjected to a small fraction of the actual loading history and then extrapolates it over many load cycles using empirical formulas to predict the likelihood of crack initiation and propagation. The assumption of a constant crack/damage growth rate may not be the realistic situation.

Continuum damage mechanics (CDM) is a relatively new development in solid mechanics. It defines a damage variable to reflect the current physical state of the studied system(Lemaitre, 1992). The state variable ranges from 0 (no damage at the material point) to 1 (the material point completely loses the stiffness). If the damage is considered isotropic and homogeneous, a scalar quantity can represent the damage in the material(SIMULIA, 2012). The damage variable can then be defined as:

$$D = \frac{A}{A_0} \tag{3.2}$$

Here, D is a positive, monotonically increasing function. A is the lost area due to damage and A_0 is the original area. After definitions of constitutive equation of the material and the damage evolution law,

the number of cycles to failure (when D reaches to D_c, the critical damage) can be computed.

This method is capable of locating initial crack formation and calculation of crack growth path. It offers a full field damage investigation and can apply to complex structures. However, the technique integrates damage evolution models with the constitutive equations, which requires extensive computational expense and complicated implementation. In addition, the approach needs more experiments to determine the material constants.

A computationally effective modelling technique is to perform low-cycle fatigue calculations under direct cyclic analysis environment in ABAQUS(SIMULIA, 2012). The direct cyclic low-cycle fatigue procedure also uses the CDM approach to model the progressive damage and failure in bulk materials. Instead of updating damage variables every cycle, the technique in ABAQUS evaluates the behaviour of the structure at discrete points along the loading history, as shown in Figure 3.4. The degradation and evolution of material properties for next increment is predicted via the solution at each of these points. The damage growth rate is updated accordingly throughout the analysis.

In a low-cycle fatigue analysis, the damage initiates when the accumulated inelastic hysteresis energy per cycle fulfils the initiation criterion, as formulated as follows:

$$N_0 = c_1 \Delta w^{c_2} \tag{3.3}$$

where N_0 is the number of cycles to damage initiation, Δw is the accumulated inelastic hysteresis energy per cycle, and c_1 and c_2 are material constants.

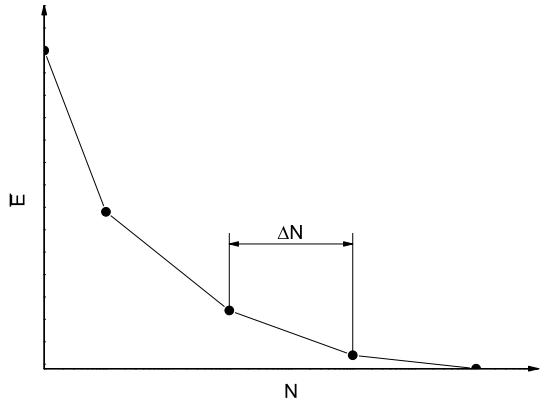

Figure. 3.4 Elastic stiffness degrades as a function of the cycle number

Once the damage initiation criterion is satisfied at a material point, material stiffness at this point is degraded. The damage state is then calculated and updated based on the inelastic hysteresis energy for the stabilised cycle.

The rate of the damage per cycle is given by

$$\frac{dD}{dN} = \frac{c_3 \Delta w^{c_4}}{L} \tag{3.4}$$

where c_3 and c_4 are material constants, L is the characteristic length associated with the material point.

Therefore, the damage variable D_N is updated from the current cycle forward to the next increment over a number of cycles, ΔN, by

$$D_{(N+\Delta N)} = D_N + \frac{\Delta N c_3 \Delta w^{c_4}}{L} \tag{3.5}$$

The procedure of thermal fatigue modelling is illustrated in Figure 3.5. Due to the one-off characteristic of die casting dies, it is necessary to propose samples for thermal fatigue tests. Also, experimental arrangements for fatigue testing need be designed to result in a panoramic view. Crack length v.s. number of cycles to

fatigue data, $N_f - a$, are observed during thermal fatigue testing. The data are then analysed to establish thermal fatigue life model.

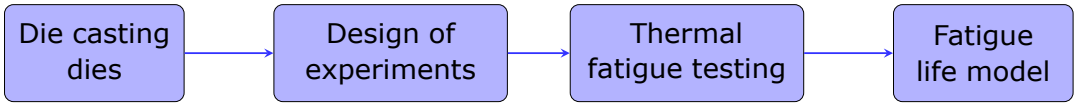

Figure. 3.5 Thermal fatigue life modelling process

3.3.3 Residual stress modelling

Selection of welding

With repair alternatives reviewed in Chapter TWO, it is necessary to make a selection of a proper welding process for remanufacture of dies and moulds. To contribute to the knowledge about the mould repair by welding, Pecas et al. (2006) compared three main processes by classifying their performance for several repair factors. The comparison was based on 10 criteria which were viewed as the most important in terms of welding process, operation characteristics and effect on the mould, as shown in Table 3.3.

Table 3.3 Welding processes classification in each criterion in injection mould repair (Pecas et al., 2006)

No.	Criteria	TIG	Plasma	Laser
I	Deposition Rate	★★★★★	★★★★☆	★★☆☆☆
II	Equipment Portability	★★★★★	★★★★☆	★☆☆☆☆
III	Accessible Geometries	★★★★☆	★★★★☆	★★★☆☆
IV	Weld Bead Complexity	★★★★☆	★★☆☆☆	★★★☆☆
V	Cost per hour	★★★★★	★★☆☆☆	★★☆☆☆
VI	Weld Bead Appearance	★★☆☆☆	★★★★☆	★★★★★
VII	Metallurgical Quality	★★☆☆☆	★★☆☆☆	★★★★★
VIII	Operator Dependence	★★☆☆☆	★★☆☆☆	★★★★★
IX	Equipment Set-up Time	★★★★★	★★★★★	★★☆☆☆
X	Need of Heat Treatment	★☆☆☆☆	★★☆☆☆	★★★★☆

★★★★★ Excellent; ★★★★☆ Good; ★★★☆☆ Average; ★★☆☆☆ Bad; ★☆☆☆☆ Very Bad; ☆☆☆☆☆ Mediocre.

From Table 3.3, it is apparent that laser beam welding process is the best choice for repairing failed dies and moulds in terms of metallurgical quality, weld bead appearance and operator dependence. Additionally, with recent scientific and engineering advances, laser based welding technology make tool remanufacturing technologically accessible and feasible. Although the relative capital cost of a laser facility is definitely higher than other common repair technologies, it is possible to minimise the operating cost by keeping the laser working. Therefore, laser based fabrication technologies are the preferred choice for remanufacturing failed dies and moulds.

Simulation

The overall aim of simulating welding, as far as remanufacture of dies and moulds is concerned, is to disclose the effects of welding process parameters on the performance such as hardness, impact strength, fatigue resistance and repair cost, et al. The scope of computational welding mechanics (CWM) and pertaining accuracy levels are of great importance and must be determined before simulation.

Lindgren divided the simulations into different scope and accuracy categories, from which one can have a clear determination of what kind of simplifications that can be done when modelling the welding process (Lindgren, 2006). Possible questions ordered by increasing complexity are tabulated in Table 3.4 while accuracy levels required from a welding modelling are shown in Table 3.5.

The welding simulations in this research are used for correlating welding process parameters with fatigue life. Therefore, models with basic or standard accuracy are adequate for obtaining residual state of welded dies/moulds, i.e. the high temperature behaviour could be considerably simplified and models of microstructure and/or criteria for fracture may not be needed as well. In addition, 3D geometric models can be applicable with acceptable accuracy performed.

A schematic diagram is then presented in Figure 3.6 to describe the calculation process. Firstly, the weld profiles are characterised and optimized to obtain the welding process parameters. Heat source models are then calibrated and, together with material properties, are used in the finite element modelling to obtain residual stresses.

Table 3.4 Questions that may be the scope of a welding simulation (Lindgren, 2006)

No.	Questions
1	What are the residual stresses? These will be used for determination of risk for buckling, fatigue, cold cracking or stress corrosion cracking etc.
2	What are the final deformations? These are wanted in order to check if the tolerance requirements on component are fulfilled after the welding procedure.
3	What are the transient stresses and deformations? These may be wanted in order to find procedures that maintain the gap required for a successful weld.
4	What is the microstructure of the weld and the heat affected zone (HAZ)? This kind of analysis also requires a microstructure model.
5	What causes hot cracking? Note that hot cracking phenomena are on the limit of continuum mechanics as it may be caused by liquid material along grain boundaries exposed to tensile strains. The parameters obtained from simulations must be evaluated with care in order to ascertain if the model can be used to study how the welding process can be changed to reduce hot cracking.

Table 3.5 Accuracy levels wanted in a welding simulation (Lindgren, 2006)

Level	Accuracy
1	Reduced accuracy levels. Use of simple and fast models for evaluations at preliminary design stages.
2	Basic simulation where only the overall residual state is of interest, questions 1 and 2. A standard simulation (next level of accuracy) is required if the structure is more flexible.
3	Standard simulation where only the residual state is of interest. It is used when questions No. 1–3 are to be answered.
4	Accurate simulation where the transient strains and stresses are wanted. This accuracy level is needed when questions No. 3–4 in Table 3.4 should be answered.
5	Very accurate simulation where the high temperature behaviour and the zone near the weld is important. This is necessary in order to answer questions No. 4–5.

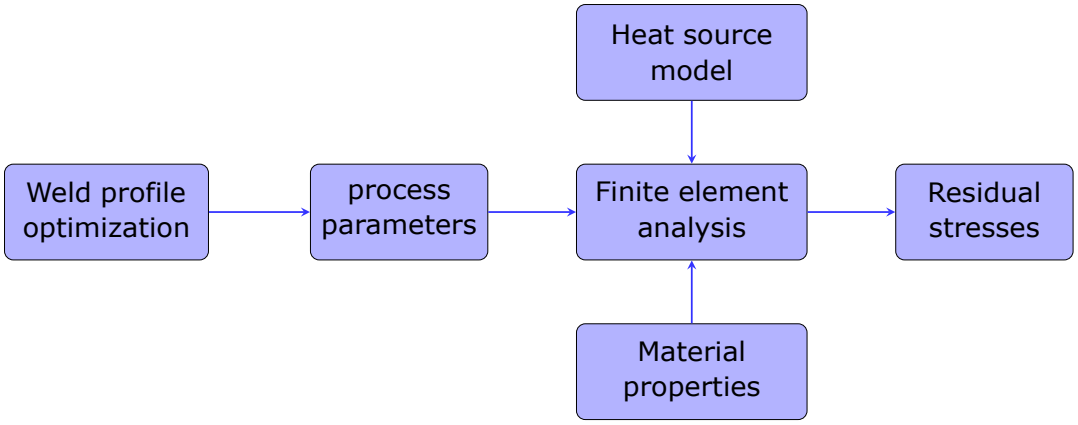

Figure. 3.6 Calculation of laser welding residual stresses

3.3.4 Underlying relations

Three aspects of the research problem have been defined in the previous three sections, respectively. Not only do they comprise the

research topic, these three aspects are closely related to each other. The relations among them are discussed in detail in the following, as illustrated in Figure 3.7.

The research problem comes from the die and mould industry which utilises numerous moulding processes for part production. Working conditions of dies and moulds are one crucial part in life assessment of dies and moulds after remanufacturing. Thermal fatigue tests are necessary to cover all the working conditions thereby obtaining a damage evolution model capable of predicting those states. Inversely, the resulting life model offers moulding processes a criterion for process optimisation.

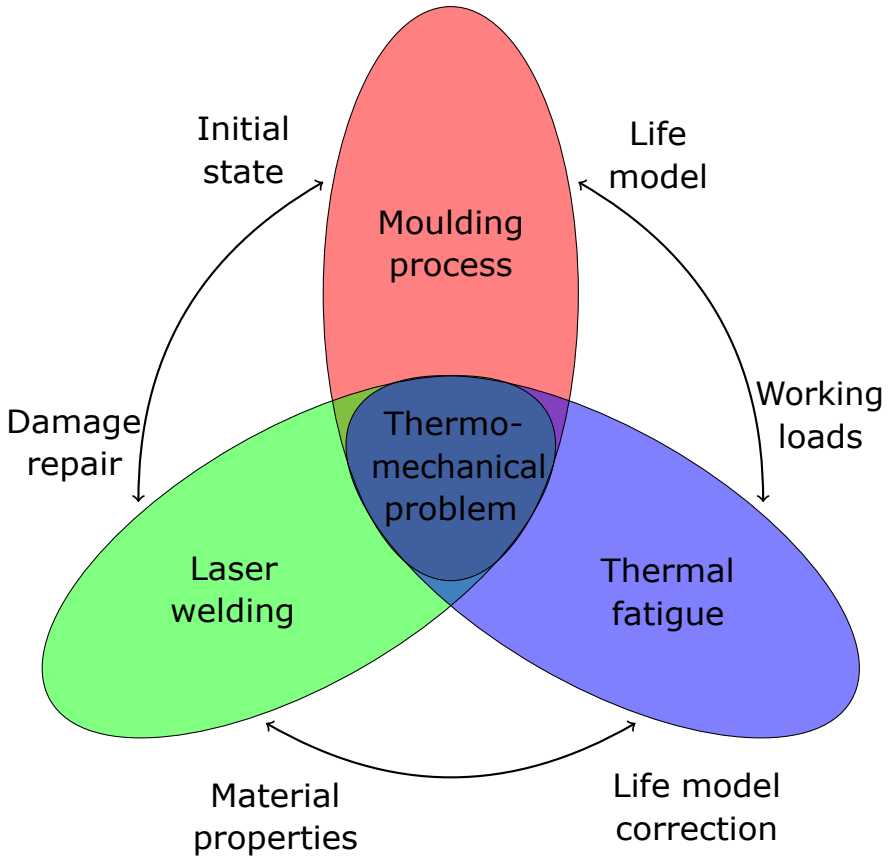

Figure. 3.7 Underlying relations among three aspects of the research problem

When failed, damaged dies and moulds are to be remanufactured using repair enabling technologies such as laser welding. Remanu-

facturing process modifies the damaged area of dies and moulds, which results in new initial states that should be considered in the life evaluation process as well.

Variation in remanufactured dies and moulds due to laser welding should be studied in thermal fatigue tests to correct obtained fatigue model from virgin mould materials. Conversely, material properties gained from thermal fatigue tests can be implemented into the simulation of laser welding.

One thing that these three aspects share in common is that they are all related to thermo-mechanical problems. Furthermore, these problems also share the same coupling manner. Specifically, the thermo-mechanical problems can be investigated using an uncoupled solution, i.e. the effect of mechanical problem on the thermal part can be neglected. This characteristic will facilitate numerical simulations of these three aspects of the research problem.

3.4 Thermo-mechanical solutions

Thermal cracking related moulding process, thermal fatigue and laser welding are in essence thermo-mechanical problems. This section states the principles within thermo-mechanical problems in terms of thermal and mechanical aspects, respectively. Solutions to thermo-mechanical coupling problems are then discussed as well.

3.4.1 Thermal problem

The equation governing heat transfer in a continuous medium can be derived by imposing the principle of conservation of heat energy over an arbitrary fixed volume, V, of the medium which is bounded by a closed surface, S, as shown in Figure 3.8.

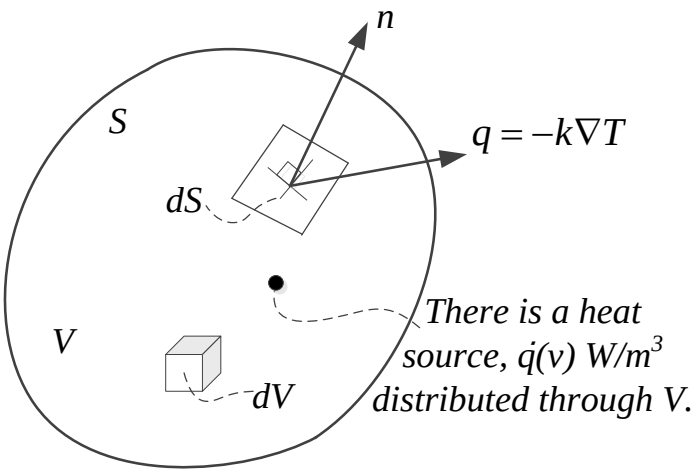

Figure. 3.8 Control volume in a heat flow field

The governing equation can be written as:

$$\int_V \left((\nabla \cdot \mathbf{k} \nabla T) + \dot{q} - \rho c \frac{\partial T}{\partial t} \right) \mathrm{d}V = 0 \tag{3.6}$$

where

$$\mathbf{k} = \begin{bmatrix} k_{xx} & k_{xy} & k_{xz} \\ k_{yx} & k_{yy} & k_{yz} \\ k_{zx} & k_{zy} & k_{zz} \end{bmatrix} \tag{3.7}$$

is the conductivity tensor, ∇ Laplace operator, T the temperature, $\dot{q}$ the rate of heat distributed in the volume V, ρ the density of the medium and c the specific heat.

Since the volume, V, is arbitrary, the integrand must vanish identically, therefore

$$\nabla \cdot k \nabla T + \dot{q} = \rho c \frac{\partial T}{\partial t} \tag{3.8}$$

Boundary conditions frequently encountered can be of the following types:

(a) Specified temperature $T_s = T_1(x, y, z, t)$ on S_1,

(b) Specified heat flux $q \cdot \mathbf{n} = -q_s$ on S_2,

(c) Convection boundary condition $q \cdot \mathbf{n} = h(T_s - T_e)$ on S_3,

(d) Radiation boundary condition $q \cdot \mathbf{n} = \sigma_{sb}\varepsilon_{sec}(T_s^4 - T_0^4)$ on S_4,

where h is the convection coefficient; T_s is an unknown surface temperature; T_e is a convective exchange temperature; σ_{sb} is the Stefan–Boltzmann constant; ε_{sec} is the surface emission coefficient and T_0 is a radiative exchange temperature. For a transient analysis it is necessary to specify the temperature initial conditions for a body at the time $t = 0$:

$$T(x, y, z, 0) = T_0(x, y, z) \tag{3.9}$$

3.4.2 Mechanical problem

For the mechanical field, the law of balance of energy rate also applies: the rate of change of total energy in a medium equals to the corresponding rate of work done by external forces on the medium together with the rate of heat added to the medium. Consider the same fixed volume, V, the balance of energy principle can be stated as follows:

$$\dot{U}_V = \dot{W} + \dot{Q}_H \tag{3.10}$$

where $\dot{U}_V$ is the rate of increase of energy in V, $\dot{W}$ the rate of work done by external forces across S and $\dot{Q}_H$ the rate of heat generation within V.

Since the total energy in the medium includes internal energy and kinetic energy, as formulated as:

$$\dot{U}_V = \dot{U}_I + \dot{U}_K \tag{3.11}$$

where,

$$\begin{cases} \dot{U}_I = \int \rho\dot{\epsilon}\,\mathrm{d}V \\ \dot{U}_K = \int \rho\dot{\mathbf{u}}^T\frac{\mathrm{d}\mathbf{u}}{\mathrm{d}t}\,\mathrm{d}V \end{cases} \tag{3.12}$$

$\dot{U}_I$ and $\dot{U}_K$ are the internal energy rate with density ϵ and the kinetic energy rate, respectively.

$$\dot{W} = \sum_i \dot{\mathbf{u}}^T\mathbf{F}^{(i)} \tag{3.13}$$

Therefore, the mechanical problem can be described as:

$$\int \rho\dot{\epsilon}\,\mathrm{d}V + \int \rho\dot{\mathbf{u}}^T\frac{\mathrm{d}\mathbf{u}}{\mathrm{d}t}\,\mathrm{d}V = \sum_i \dot{\mathbf{u}}^T\mathbf{F}^{(i)} + \dot{Q}_H \tag{3.14}$$

Assuming isothermal and adiabatic conditions, the problem is then simplified as:

$$\int \mathbf{E}^T\cdot K\cdot\mathbf{E}\,\mathrm{d}V = \sum_i \dot{\mathbf{u}}^T\mathbf{F}^{(i)} \tag{3.15}$$

3.4.3 Thermal mechanical coupling

The thermal to mechanical coupling effects include:

- Thermal expansion, which creates thermal strain ε_{th} within the medium as:

  $$\varepsilon_{th} = \alpha(T - T_0) \tag{3.16}$$

  where α is the coefficient of thermal expansion. And the total strain becomes the sum of mechanical strain and the thermal counterpart:

  $$\varepsilon_{tot} = \varepsilon_{th} + \varepsilon_{mech} \tag{3.17}$$

  Here, ε_{tot} and ε_{mech} are the total strain and mechanical strain, respectively.

- Temperature-dependent mechanical properties, including Young's Modulus, yield stress, Poisson's ratio and so forth.

While mechanical effects on thermal part usually contain the following points:

- Internal heat generation due to plastic deformations or viscous effects.

$$\dot{Q}_H = \int \sigma \dot{\varepsilon} \, \mathrm{d}V \tag{3.18}$$

- Heat transfer between contacting bodies.

- Heat generation due to friction. When an object is pushed along a surface along a path C, the energy converted to heat is given by the integral as bellow:

$$E_{th} = \int_C \mathbf{F}_f(\mathbf{x}) \, \mathrm{d}\mathbf{x} = \int_C \mu_k \cdot \mathbf{n} \cdot \mathbf{F}_f(\mathbf{x}) \, \mathrm{d}\mathbf{x} \tag{3.19}$$

where $\mathbf{F}_f(\mathbf{x})$ is the friction force, μ_k is the coefficient of kinetic friction, $\mathbf{n}$ is the unit normal vector of the surface, and $\mathbf{x}$ is the position of the object.

Generally, there are three ways of coupling: uncoupled, sequentially coupled and fully coupled, as shown in Figure 3.9. Uncoupled thermo-mechanical problem is that two types of problems are not affected by each other. Therefore, it is simple to get two problems solved separately. sequentially coupled refers to that thermo-mechanical problems are coupled in one direction. The solution to that is to run analyses sequentially. The result of previous analysis is input into the next for analysis. The fully coupled problem must solve both the problems at the same time since they are affected by each other.

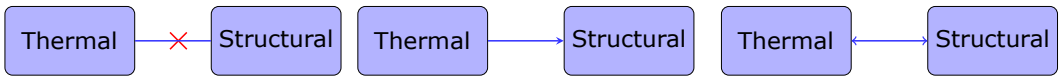

(a) Uncoupled (b) Sequentially coupled (c) Fully coupled

Figure. 3.9 Common ways of thermo-mechanical coupling

In cases such as laser welding, die casting and its corresponding thermal fatigue testing, large spatial temperature gradients exist in the body, and the plastic strain rate with the body is small. Heat generation due to irreversible deformation can therefore be neglected (Alblas, 1969; Rosbrook, 1992). This allows the coupled thermo-mechanical problem to be decoupled into two separate problems: one thermal and one mechanical. With this assumption, such thermo-mechanical problems can be addressed by conducting sequentially coupled thermo-mechanical analyses.

To demonstrate the aforementioned conclusion, a benchmark case study was conducted. The scenario is the same as in the literature (Klobcar et al., 2008). A comparison of temperature and stress results computed from two methods, i.e. fully coupled and sequentially coupled, is illustrated in Figure 3.10. From the figure, we can tell that the divergence due to different methods applied is extremely tiny and therefore it indicates that the accuracy of sequentially coupled method is satisfactory for the problems like die casting.

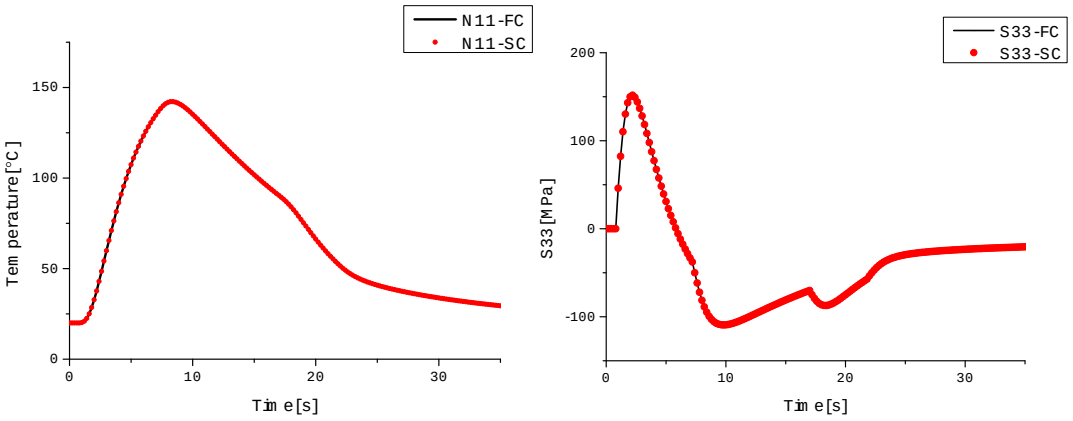

(a) Fully coupled (b) Sequentially coupled

Figure. 3.10 Comparison of results calculated from fully coupled method and sequentially coupled method

3.5 Summary

The research scope is restricted to fatigue life assessment of thermal cracked dies and moulds for remanufacturing. Within the scope, three main problem were identified and corresponding frameworks were proposed. The underlying relations among these problems were investigated and a common solution was concluded.

Chapter 4

Design of experiments

4.1 Introduction

This chapter describes the design of specimens used in the rest of chapters for experimental verifications. Because realistic die halves are product specific and one-off, it is impossible and unnecessary to consider a real set of dies for research purpose. Therefore, the varieties of die geometry need be simplified by representative specimen geometry.

In this chapter, a series of preliminary studies using finite element modelling were conducted to obtain a guideline for the specimen design. Firstly, realistic die geometries were scaled down by the effect of die geometry on the thermal behaviour of dies and moulds. The effect of thickness on maximum principal stress of laser welded sample was also investigated by simulations of laser welding process. These thereby lead to the design of specimens for study accordingly. Then, the difference among three thermal fatigue test methods which are commonly used in the die and mould industry was disclosed by investigating thermal profiles of specimens. Lastly,

an optimal specimen for experimental purpose is concluded and thermal fatigue test method is selected.

4.2 Representative die geometries

Die casting dies in real applications are usually of huge size. Furthermore, dies and moulds are commonly product specific. It is necessary to design die geometries capable of representing real ones for research purpose. This section first defines the die geometries to represent real die casting dies, followed by the investigation of their effects on thermal loadings resulting in dies. Optimal representative die geometries are concluded at last.

4.2.1 Thermal representations

Typically, a die casting process consists of the following four steps. (a) Die closing: the cleaned and lubricated two halves of the die are closed and clamped together inside the die casting machine. (b) Injection and solidification: the molten metal is forced into the die at high pressures and velocities for low cycle times. The casting metal then rapidly solidifies in the die cavity. (c) Part ejection: after solidification, the casting is removed from the die halves. (d) Clean and lubrication: the open die halves are sprayed with releasing agent and water based lubricants.

Die casting dies are subject to cyclic mechanical and thermal loading which are closely related to the production conditions imposed. Table 4.1 summarises the boundary conditions of die casting dies over a whole production cycle (Garza-Delgado, 2007). At each production cycle, the die halves are exposed to the mechanical loads of clamping force and cavity pressure, as well as the uneven thermal

profile of the die resulted from the cooling and solidification of the casting alloy and the cooling by lubricant spray. Each of these forces affects the time-varying stress-strain field within the die. The extent to which the forces affect the stress-strain behaviour and cyclic life of the die is largely determined by their magnitude and the area upon which they act.

Table 4.1 Boundary conditions for the die casting operation cycle

Stage	Boundary conditions
Die closing	•Contact between the casting/die is disabled
	•Contact between the die halves is enabled
	•Free convection on exposed surfaces of die
	•Free convection on the die cavity surface
	•Free convection on exposed surface of cover platen
Injection and	•Contact between casting/die is enabled
solidification	•Free convection on die cavity surface is disabled
Part ejection	•Contact between casting/die is disabled
	•Contact between the die halves is disabled
	•Free convection on exposed surfaces on the die
Spray	•Forced convection on the die cavity
	•Free convection on remaining surfaces of the die

4.2.2 Die geometry definition

Industrial die casting dies are frequently designed for products of complex geometry. The feature of specific product targeting also makes die casting dies of multiple varieties. Therefore, it is impossible to study every die casting die in reality. Instead, geometry capable of representing major features that die casting dies contain is necessarily designed. For simplicity, the die is assumed to

be axisymmetric with a cavity represented by a cone shape at its centre. Figure 4.1 illustrates the cross section of representative die geometry proposed. Die cavity is symbolised by a notch as shown in Figure 4.1. Dimensions defining the geometry include the diameter and height of the die, and the width, angle and radius of the notch.

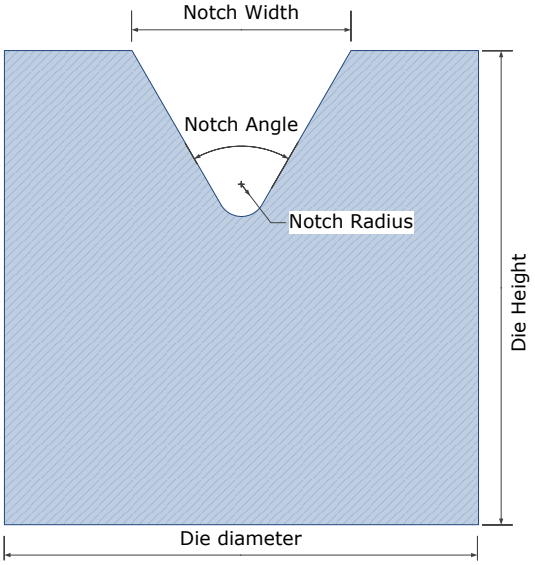

Figure. 4.1 Cross-section of axisymmetric geometry of die casting die representation

4.2.3 Effects of die geometry on thermal equilibrium

The effect of die geometry defined in the previous section on thermal equilibrium of the die is investigated by conducting thermal analyses of the representative die under immersion tests. Test specimens are cyclically heated by their immersion in the bath of molten casting metal, followed by the cooling in the bath of lubricant. And in this study, the immersion tests are assumed to be performed at the represented die cavity.

The simulations of immersion tests of the proposed representative die are conducted by ABAQUS® FE package. The test cycle is divided into four steps: (1) heating for 6.4s; (2) air cooling for 10s; (3)

lubricant cooling for 3s; and (4) air cooling for 10s in accordance with the die casting process. For each analysis, ten thermal cycles are performed to assume a thermal equilibrium state achieved within the test sample. The thermal behaviour of the point at the bottom of the cone is then extracted for comparison investigation. Material properties of H13 hot-work tool steel used in the literature (Klobcar et al., 2008) are considered in the FE model. Boundary conditions concerned are depicted in Figure 4.2. The analyses are conducted utilising one-factor-at-a-time (OFAT) method. And the set of parameters used as a reference are: 20 mm of both the die diameter and height, 60 degrees of the notch angle, a notch width with 2.0 mm and a radius of 0.2 mm at the tip.

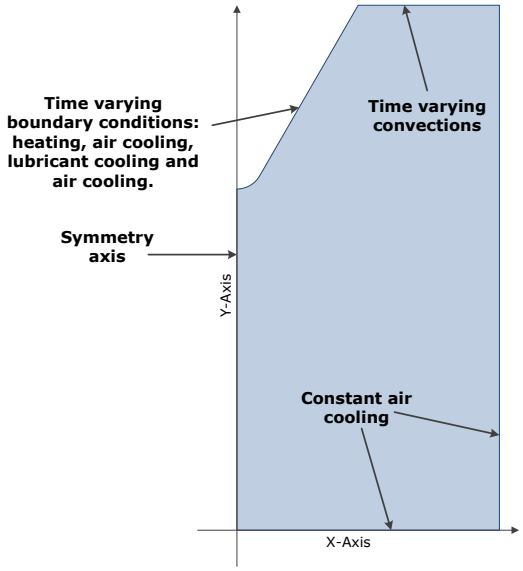

Figure. 4.2 Boundary conditions defined in the FE model

4.2.4 Results and discussion

Figure 4.3 - 4.7 show the result of thermal profiles of the cone tip in terms of variations in the designed geometry, i.e. die diameter, die height, notch width, notch angle and notch radius. The legends in these figures are denoted by the combination of the dimensions

used in thermal analysis in the order of die diameter, die height, notch angle, notch width and notch radius.

From Figure 4.3, we can observe that an increase in die diameter leads to a decrease in the temperature profile of the cone tip. Figure 4.4 shows a similar effect of die height on the temperature history of the notch tip. This is because the thermal capacity of the die increases with the die volume, thereby leading to a decrease in temperature field.

For the influences of the notch geometry on thermal profiles of its tip, different observations are made. The historical data in temperature field increase as the width or radius of the notch increase, and are in decrease with an increase in the notch angle. The reason is that more heat is input at the tip and less thermal capacity of the die is assumed when an increase in the notch width or radius, or a decrease in the notch angle is applied.

Further analyses are conducted to reveal the effect of the ratio of die diameter over the notch width assuming that die height equals die diameter. Figure 4.8 shows the result of maximum temperature over the thermal profile of the cone tip in terms of different die diameter and notch width ratios. Differences between lines are indicated by the notch width used in analysis as legend.

From the result, it is obvious that the maximum temperature declines as the ratio of die diameter over notch width increases. Also, declinations are dramatic at lower ratios while the maximum temperature is becoming constant as the ratio reaches to a certain value. This provides a reference for design of experimental specimens. For instance, a notch of 10 mm in the width should lead to a diameter of 60-80 mm in the die as influence due to increased ratio can be neglected.

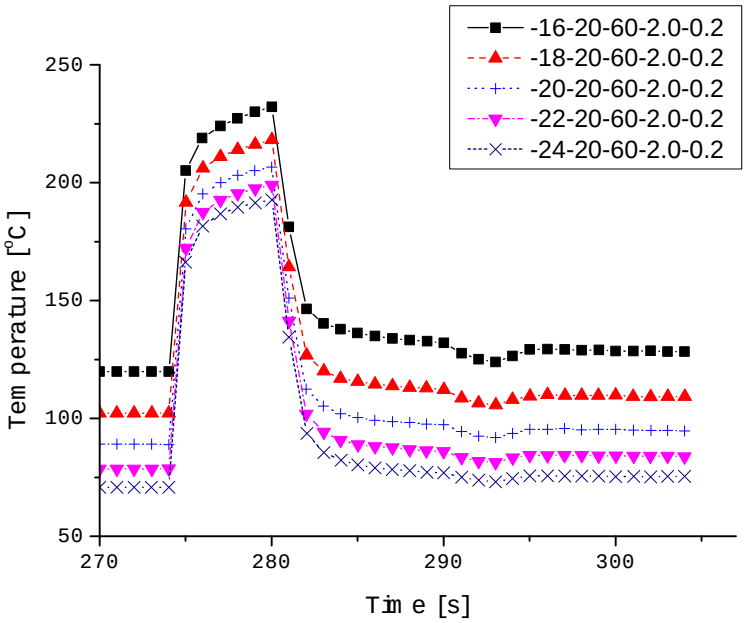

Figure. 4.3 Temperature profile with respect to die diameters

Legends for the data are indicating variables in the order of die diameter, die height, notch angle, notch width and notch radius. For instance, the legend -16-20-60-2.0-0.2 means that die diameter=16 mm, die height=20 mm, notch angle=60°, notch width=2.0 mm and notch radius=0.2 mm.

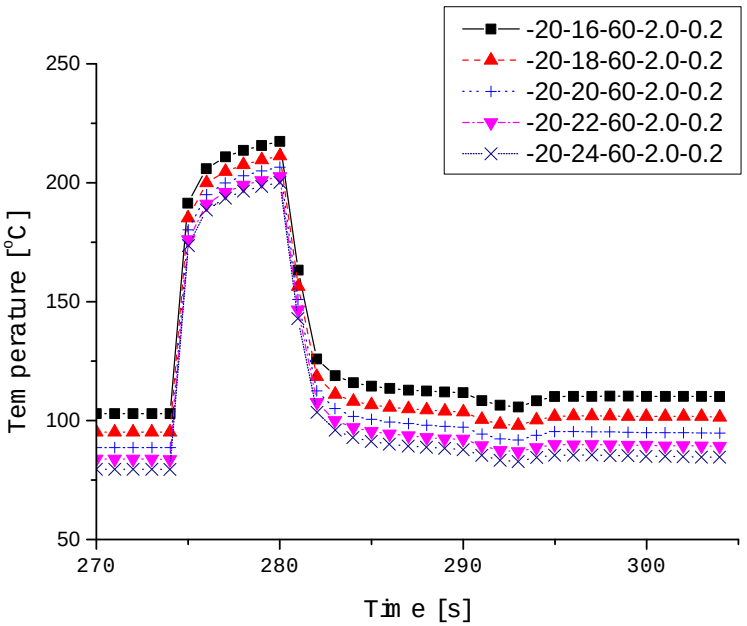

Figure. 4.4 Temperature profile with respect to die heights

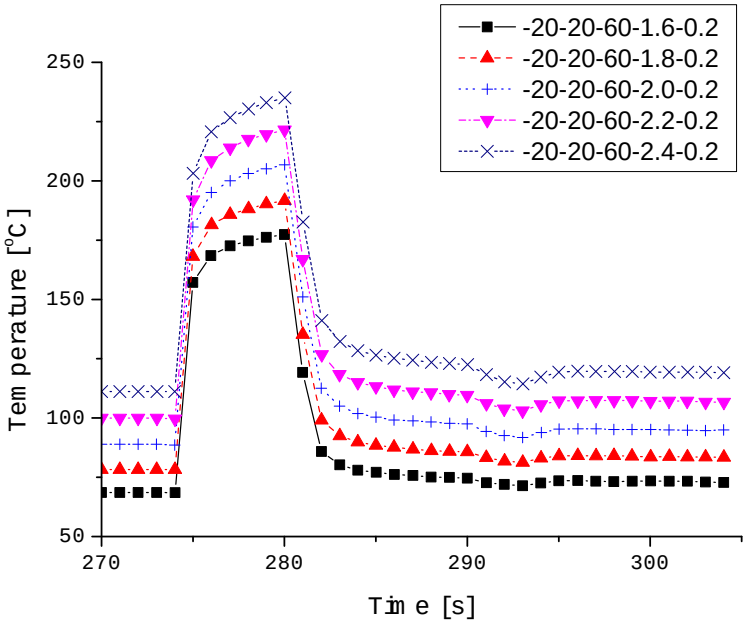

Figure. 4.5 Temperature profile with respect to notch widths

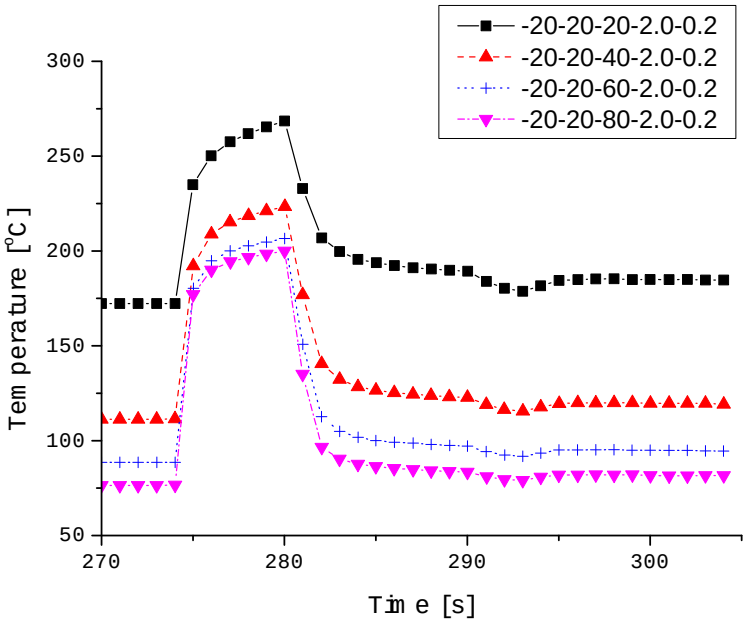

Figure. 4.6 Temperature profile with respect to notch angles

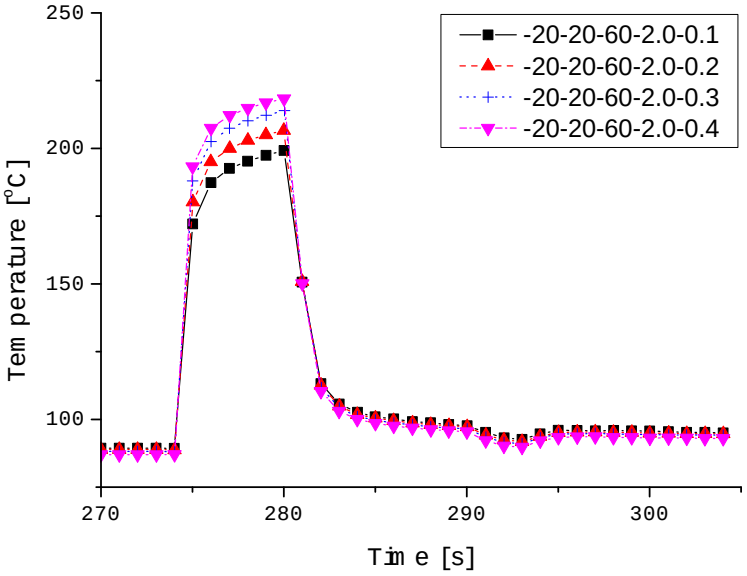

Figure. 4.7 Temperature profile with respect to notch radii

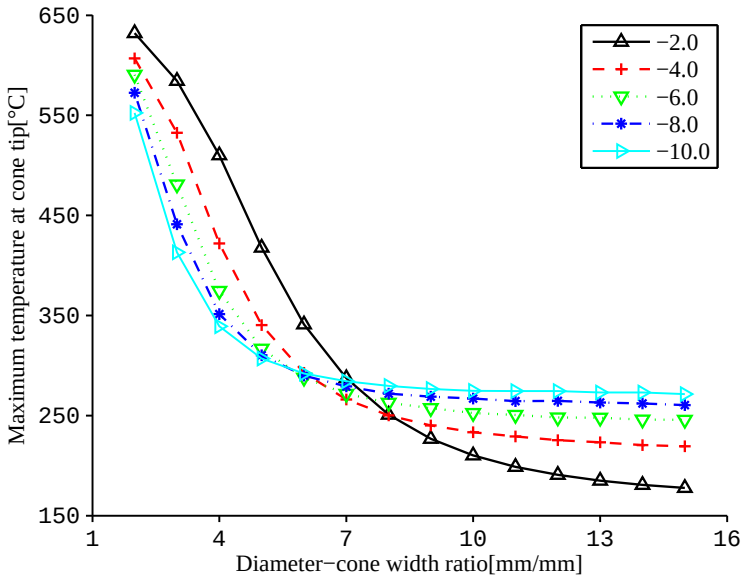

Figure. 4.8 Maximum temperature at cone tip with respect to diameter-cone width ratios

4.3 Geometry effect on welding residual stresses

The previous section studies the effect of die geometry on the thermal equilibrium using an axisymmetric model. However, it is difficult to achieve thermal shocks in test specimens under thermal

fatigue using an axisymmetric model when coolant spraying is used. Thereby, this section is concentrated on studying the thickness of test samples. It is accomplished by revealing the influence of sample thickness on residual stresses of test samples after laser welding.

The effect is uncovered by conducting a series of fully coupled thermo-mechanical finite element analyses of laser welding along the central part of a designed specimen. The specimen is designed according to ASTM E606–04e1, a standard practice for strain-controlled fatigue testing, with variation in its thickness. Since additional machining process is usually required to remove the extra material of welding repaired parts, the simulations of laser welding are therefore simplified as laser surfacing in this preliminary study. Finite element analyses were run by a commercial FE package ABAQUS®.

Figure 4.9 shows the geometry of laser surfacing specimen taken for finite element analysis, $132 \times 20 \times 5$mm. The material used for this purpose is AISI H13. Thermo-physical properties (temperature dependent) of the material are assumed to be isotropic and homogeneous. The material density and the Poisson's ratio were assumed to be independent on temperature. Specifically, density was taken to be 7820 kg/m^3 and Poisson's ratio 0.3. The latent heat of fusion is not taken into account in the FE model.

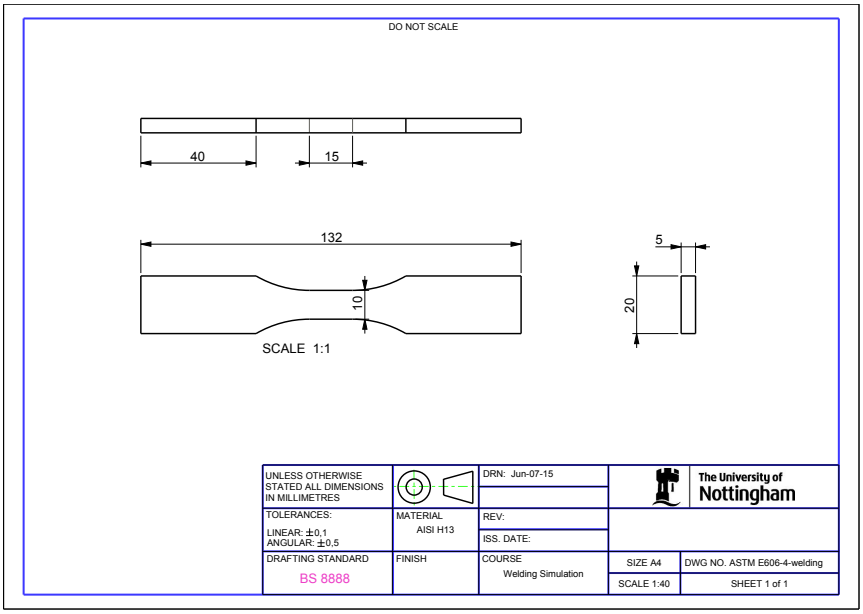

Figure. 4.9 Schematic diagram of specimen for preliminary welding simulation

Figure 4.10 and Figure 4.11 show the meshing detail and boundary conditions of this study. Due to the symmetry, only half of the specimen was modelled. The model contains 25600 eight-node linear brick elements with features of temperature-displacement fully coupled. Boundary conditions were applied to the model by specifying the value of heat transfer coefficient and the surrounding temperatures for the elements and at the nodes, respectively. The initial temperature of the specimen is assumed to be 20°C and the convective heat transfer is considered at all surfaces exposing to ambient environment. Constant coefficient of heat transfer and environmental temperature are considered during analysis as well, i.e. 80W/m^2°C and 20°C, respectively.

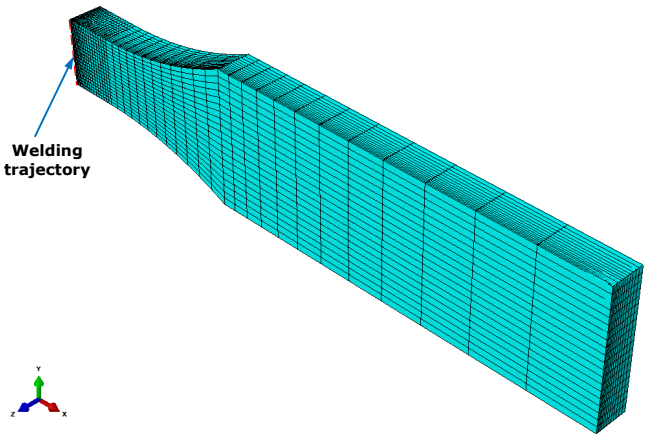

Figure. 4.10 Meshing of laser surfaced specimen for preliminary study

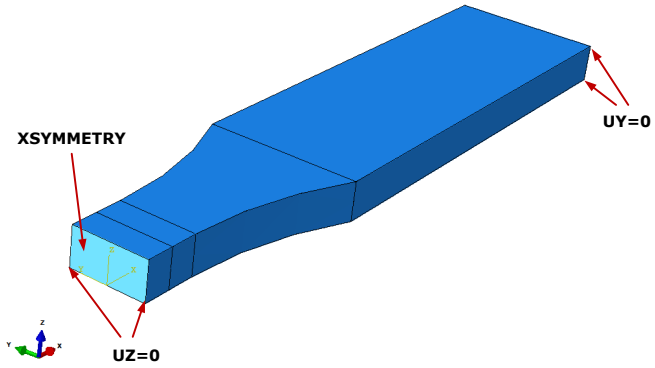

Figure. 4.11 Boundary conditions applied in laser surfaced specimen for preliminary study

In the analyses, a three-dimensional conical Gaussian heat source is used as a laser source applied to specific elements in finite element model. The heat source parameters from Table 4.2 were used to model the distributed heat flux. The heat was focused along the welding trajectory and then transferred throughout the rest of the specimen by conduction.

Table 4.2 Values of the heat-source coefficients used in FEM

Parameter	Symbol	Value	Unit
Width	a	0.3	mm
Length	c	0.3	mm
Depth	b	1	mm
Speed	*v*	2.5	mm/s
Power	p	125	W
Efficiency	η	0.7	-

The results of maximum principle stress of laser surfaced specimens due to the change of specimen thickness is plotted in Figure 4.12. From the figure, it is clear that the maximum principle stress of specimens increase with an increase in the thickness. And furthermore, as the thickness increase, the maximum principle stress infinitely tends to a constant. The difference of maximum principle stresses between thickness of 5mm and 8mm is approximately 3%.

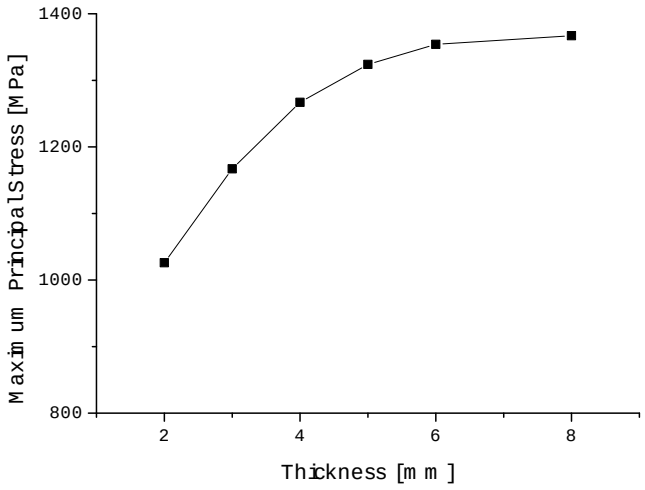

Figure. 4.12 Maximum principle stress of laser welded specimen in terms of thickness

4.4 Comparison of thermal fatigue test method

Fatigue tests are frequently carried out by alternating three parameters, i.e. stress, strain and temperature in a test sample until failure occurs. In thermal fatigue experiments, temperature is programmed to vary with time to produce the appropriate stress-temperature cycle (Carden, 1963).

4.4.1 Thermal fatigue tests

An extensive effort has been paid to establishing thermal fatigue test facilities capable of getting insight into the nature of the thermal fatigue process. In this study, generally, they are categorised into two families: conventional and mould-specific ones.

Conventional thermal fatigue tests, usually termed as isothermal strain fatigue tests, are conducted by varying the mechanical strain while keeping the temperature constant. In the case of isothermal conditions, temperature can be assumed uniformly distributed in the test coupon. Therefore, the test is free from difficulties in approximating temperature distribution among the test specimen. In essence, conventional thermal fatigue tests are mechanical fatigue tests under a series of temperature conditions. However, for applications like die casting, structures fail mainly due to thermal gradients existed rather than mechanical loadings. It is necessary to study the effect of thermal gradients on the fatigue behaviour. And therefore conventional thermal fatigue tests are not suitable for these applications.

Many other test facilities have also been developed to capture the thermal shocking behaviour of die materials as real die casting dies

experience. The difference among them mainly lies in the heating methods adopted while water or water-based lubricant cooling are commonly utilised in the tests. According to the heating system, the most frequently encountered thermal fatigue test methods for die casting dies can be categorized as immersion test, furnace heating based test and induction heating based test.

4.4.2 Mould-specific test methods

The apparatus for immersion tests contains a heating station with molten casting alloy and a cooling station with water at room temperature (Klobcar and Tusek, 2008; Klobcar et al., 2008). Test specimens are cyclically heated by their immersion in the liquid metal, followed by the cooling in the lubricant water. The cycle period can be controlled by setting up different immersion intervals. The heat transfer principles dominating in this method are quite identical to those in real die casting processes. And the test system could be quickly established as well. However, the heat capacity of specimens is much lower than die casting dies and therefore different thermal equilibriums are built in the test specimen and die casting dies.

Another test technique usually heats samples with a high temperature electric resistance furnace and cools them with running water as well (Tong et al., 2011). The samples are also free from any external load. Thermocouples are attached to the sample for temperature monitoring. It is not difficult to build a set-up of this method, neither. However, test coupons are heated through convection of heated gas around them, which is different from the die casting process. Another disadvantage is that this method usually takes a long period to heat test samples up to a high temperature.

The third type of test equipment uses an induction unit for the heating purpose and also cools specimens by water (Persson, 2004; Persson et al., 2005; Velay et al., 2002). In some case, surface strain measurements are also accompanied, which makes it possible to calculate the strains induced in the specimen surface during thermal cycling. With induction coils of high frequency and power, the test machine is capable of introducing thermal shocks to specimens. The problem is that thermal loadings created are also different from the die casting process. Also, induction heating creates a layer of oxidization on the specimen surface.

4.4.3 Comparison of thermal fatigue tests

Preliminary analyses were also conducted to understand the difference among three thermal fatigue test methods. The thermal cycles of all three tests were assumed to be the same as the previous section, i.e. (1) heating for 6.4s; (2) air cooling for 10s; (3) rapid cooling for 3s; and (4) air cooling for 10s. Only the first stage is differently modelled for three methods. A series of 10 cycles is considered to accomplish a thermal equilibrium in test samples.

Finite element modelling of immersion tested samples is the same as the previous section and is used as a reference for comparison study. The other two methods are adjusted to obtain temperature profiles of the cone tip as close as possible according to their capacities.

Specifically, for furnace heating based method, the temperature of air in furnace is assumed to be 1500 ^{o}C. And the heat transfer coefficient between the air and tool sample is calibrated as an average of 0.000068 W/mm^{2}K according to the experimental procedure described in (Tong et al., 2011). The modelling of induction heating

is achieved by directly imposing heat flux on the heating area. A uniformly distributed heat flux of 4.15 MW/m^2 was designed by minimizing the divergence of maximum temperatures from immersion test and induction heating test at the 10th thermal cycle.

Temperature profiles of the 10th cycle of thermal fatigue test using three different methods are illustrated in Figure 4.13. From the chart we can see that there is little difference between immersion test and induction heating based method at the 10th cycle. This is probably related to the modelling method adopted. Surface heat flux application has basically the same influence of heat convection, see $q_s = h_s(T - T_s)$ where h_s is the heat transfer coefficient between two media, T and T_s are the temperatures of two media, and q_s is the resulting surface heat flux. Therefore, if fully calibrated as in this study, induction heating based test method can provide the same test capacity as immersion test has.

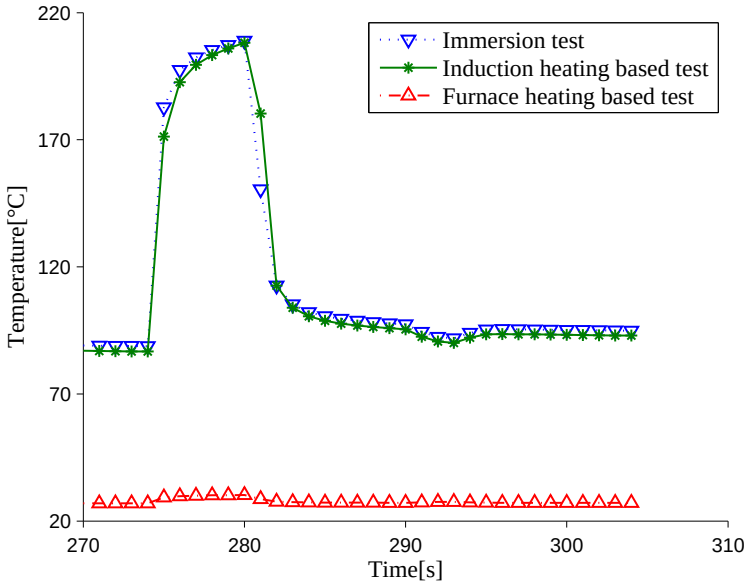

Figure. 4.13 Temperature profiles by different test methods

On the other hand, the thermal behaviour of test specimens under furnace heating based tests is drastically divergent from the others. The temperature arises only slightly and remains in a relatively low

range. It is caused by the low heat transfer coefficient between die material and air. That is the reason that such method takes long time to heat specimens up to a high temperature. Consequently, few thermal gradients exist in the die during heating period.

4.5 Summary

Due to the complex geometry and large varieties of industrial dies and moulds, in this chapter, a series of preliminary finite element simulations were carried out to support the design of test specimens. Also investigated is the capacities of three different thermal fatigue test methods commonly adopted in the die and mould industry. According to the analysis results, the following guidelines can be drawn for the design of experiments:

- The ratio of specimen width to notch width should be at around 10 in order to achieve a thermal equilibrium process similar to real dies and moulds.
- The maximum principal stress of laser welded specimens increases with the thickness but stabilises when the thickness is bigger than 5mm.
- Induction based thermal fatigue test method is capable of producing equal thermal loading on test specimens as immersion tests do. But low thermal gradients would be resulted by using furnace heating based test method.

Chapter 5

Thermal fatigue assessment

5.1 Introduction

This chapter establishes the damage evolution model of the die material of interest. Damage evolution model plays an important role in predicting the thermal cracking behaviour of the die material. Numerous models have been proposed to capture the material behaviour. Therefore, an appropriate model need be selected and established for the remaining useful life evaluation of remanufactured dies and moulds specifically.

The chapter is divided into three main parts. Firstly, a purpose designed thermal fatigue testing machine was used to experimentally investigate the crack growth process of test samples under uniformly designed runs. Then, in numerical terms, finite element modelling of thermal fatigue tested samples was conducted to study the thermal loadings they experience. By briefly reviewing damage criteria utilised in the die and mould industry, an energy based model taking into account the test period was selected and fitted for evaluating thermal fatigue life.

5.2 Experimental detail

According to the results of preliminary studies, induction heating based thermal fatigue test method has the flexibility of producing thermal shocks on test samples as immersion tests. Therefore, experimental work was carried out using an induction heating based thermal fatigue testing machine. It is specifically designed for testing thermal fatigue resistance of die steel materials. Test specimens are also designed to achieve severe thermal stress at the position of interest. The temperature profiles of the outer surface of test samples are measured using a thermal infrared imaging camera.

5.2.1 Sample preparation

With heat treatment to be harder than 54HRC as die casting dies, the test materials were machined into specimens with the dimensions of $20\times20\times5$mm, as shown in Figure 5.1, where a notch of 0.1mm in radius was wire Electrical Discharge Machining (EDM) cut. The geometry of the specimen is defined to (i) obtain an effective thermal gradient in the cross section of the specimen, (ii) guarantee efficient cooling in the central part of the specimen, (iii) generate a state of stress concentration, (iv) limit the manufacturing costs of the specimen, and (v) consider the die geometry effects on thermal cycling and welding residual stresses. Surface roughness of surfaces under major thermal loads was also designated to eliminate the effect of machining on thermal fatigue resistance.

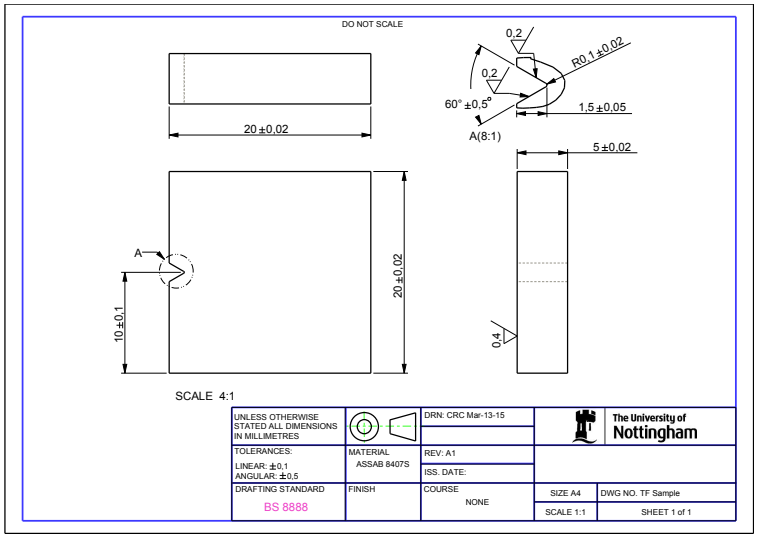

Figure. 5.1 Schematic diagram of thermal fatigue testing sample

5.2.2 Thermal fatigue test

Schematic representation of thermal fatigue test apparatus is depicted in Figure 5.2. Each specimen was heated by a high frequency induction coil, followed by immediate cooling by rushing water to achieve thermal shock effects as die casting dies experience. The controllable parameters include frequency applied for heating, holding time at the peak, and cooling time. Temperature profiles up to 50 cycles of the specimen surface were measured by a FLIR® T640 thermal imaging camera to record the thermal cyclic loadings that exist in test specimens. The data will then be applied in calibration of finite element modelling of thermal fatigue test as well.

During thermal fatigue testing, the samples were restrained at both top and bottom surfaces to avoid free movement. The samples were taken out to observe cracks firstly at 800 cycles and then every 400 cycles to 2400 cycles. Measurement of thermal cracks were conducted utilising an optical microscope(Axio Imager 2, Carl Zeiss®) after elimination of the oxide layer. The oxidized layer was firstly ultrasonic cleaned in dilute hydrochloric acid solution (10%)

for 10 to 15 minutes and then polished using Bruker automatic polishing machine.

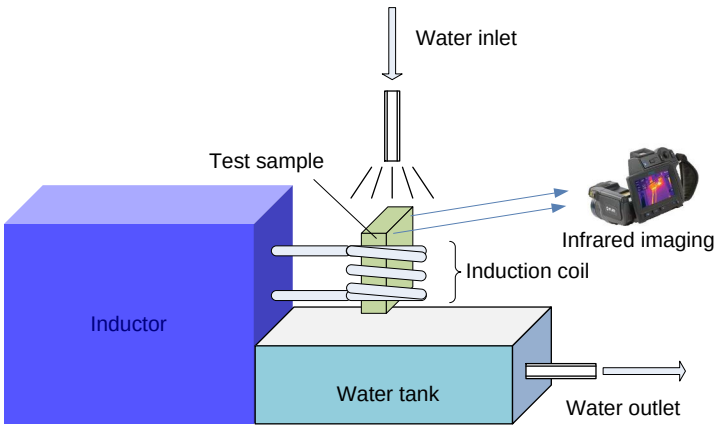

Figure. 5.2 A schematic representation of the thermal fatigue test equipment

5.2.3 Calibration of emissivity of test samples

An infrared camera measures and images the emitted radiation from an object. Since radiation is a function of object surface temperature, the temperature can therefore be calculated and displayed. However, the radiation measured does not only depend on the temperature of the object but is also influenced by other factors including the emissivity of the object, the reflected apparent temperature, the distance between the camera and the object, and the relative humidity and temperature of the atmosphere (FLIR, 2012).

To measure temperature accurately, it is therefore necessary to consider all these factors. And the most important is to set the object parameter, emissivity, correctly. Therefore, calibration of the object emissivity is necessary. To find the emissivity of a sample, the reflected apparent temperature should be determined in advance. There are two methods, direct method and reflector method, as mentioned in the user manual of FLIR® R&D software.

Direct method straightforwardly measures the radiation intensity of reflection source by setting emissivity to 1.0 and distance from the object to zero. The latter one uses a large piece of aluminium foil to work as a reflector of the reflection source. And the reflected apparent temperature is measured by taking the temperature of the aluminium foil. In this research, the latter method was utilized for determination of the reflected apparent temperature.

The calibration of the emissivity of test samples was then carried out following the procedure suggested in FLIR® R&D software manual: (a) a piece of electrical tap with known high emissivity was put on a sample; (b) the sample was evenly heated to a temperature 20K above room temperature; (c) capture an infrared image of the sample; (d) adjust the emissivity to obtain equal temperatures of the tap surface and the sample surface. Figure 5.3 shows an image for the calibration of the emissivity of test samples. During calibration, a 3M type 88 black vinyl electrical tape with the emissivity of 0.96 was used and therefore the emissivity of test sample surface is calibrated as 0.340. Other parameters related are also calibrated and illustrated in Table 5.1

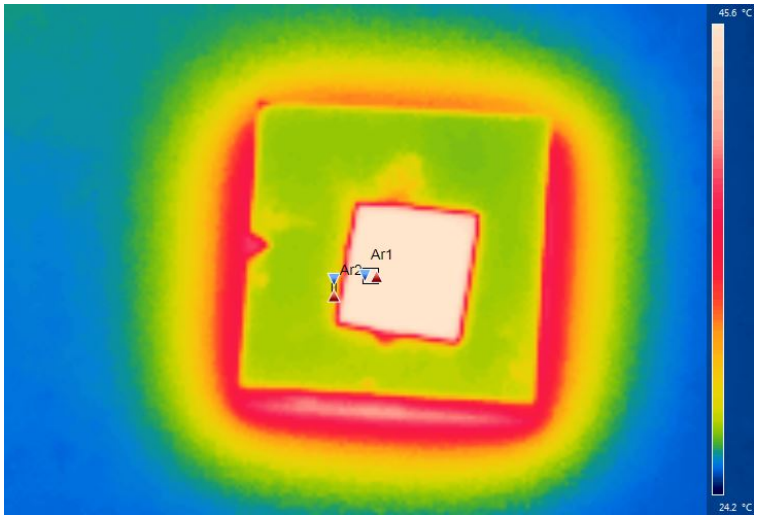

Figure. 5.3 Calibration of emissivity

Table 5.1 Parameters calibrated for the thermal infrared camera

Parameter	Value	Unit
Emissivity	0.34	1
Reflected apparent temperature	18	$^{\circ}C$
Atmosphere temperature	20	$^{\circ}C$
Relative humidity	0.5	1
Distance	0.4	m

5.2.4 Experimental arrangements and results

In order to establish the damage evolution model, a series of thermal fatigue tests are necessarily conducted to obtain a panorama view of the material behaviour. Generally, at least six series of strain controlled fatigue tests with three duplications. Such a test method is usually condemned time-consuming and it is even worse in the case of thermal fatigue. Uniform design offers efficient experimental arrays with acceptable accuracy kept. The experiment design method was adopted for the test and experimental runs were designed as illustrated in Table 5.2 and Table 5.3. The experimental plan takes three levels of each test variable into consideration.

Table 5.2 Experimental variables and levels for thermal fatigue testing

Variables/Levels	1	2	3
Frequency of induction current, F (Hz)	600	700	800
Heating Time, t_h (s)	1	2	3
Cooling Time, t_c (s)	1	1.5	2

Table 5.3 Experimental arrangement for thermal fatigue testing

No. of Sample	Factor A	Factor B	Factor C
N1	2	3	3
N2	1	3	2
N3	3	1	2
N4	3	2	1
N5	2	1	1
N6	1	2	3

Test specimens crack through the thickness and cracks of both sides were observed. With conservative concerns, the larger side is considered as the crack propagation data for the entire specimen. The crack growth data ($a - N$) of six experimental runs designed in the last section are depicted in Figure 5.4. From the figure, one can observe that six test conditions lead to a roughly three-area distributed $a - N$ curves. This in turn proves that the experimental array produced an uniform distribution of test points.

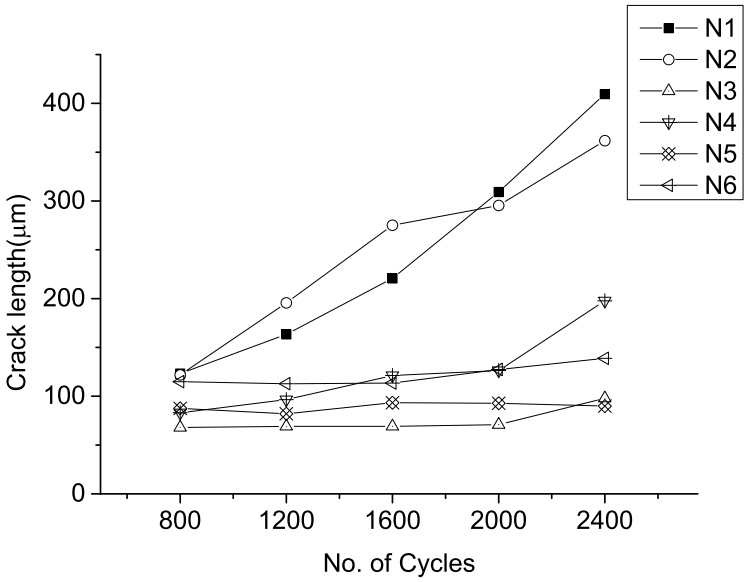

Figure. 5.4 Thermal fatigue crack growth under different testing conditions

Figure 5.5 illustrates an example of thermal cracking observed on sample N2. Following the procedure, the cracks are observed and measured using an optical microscope at 800, 1200, 1600, 2000 and 2400 cycles. From the figure, it is obvious that thermal cracks initiate from the vicinity of the tip. Because of the imperfection of the material and preparation of samples, there are usually more than one crack within the specimen, as shown in Figure 5.5a. But when specimens were tested for more number of cycles, one crack started to dominate the propagation until the failure of the structure, as illustrated in Figure 5.5b-5.5d.

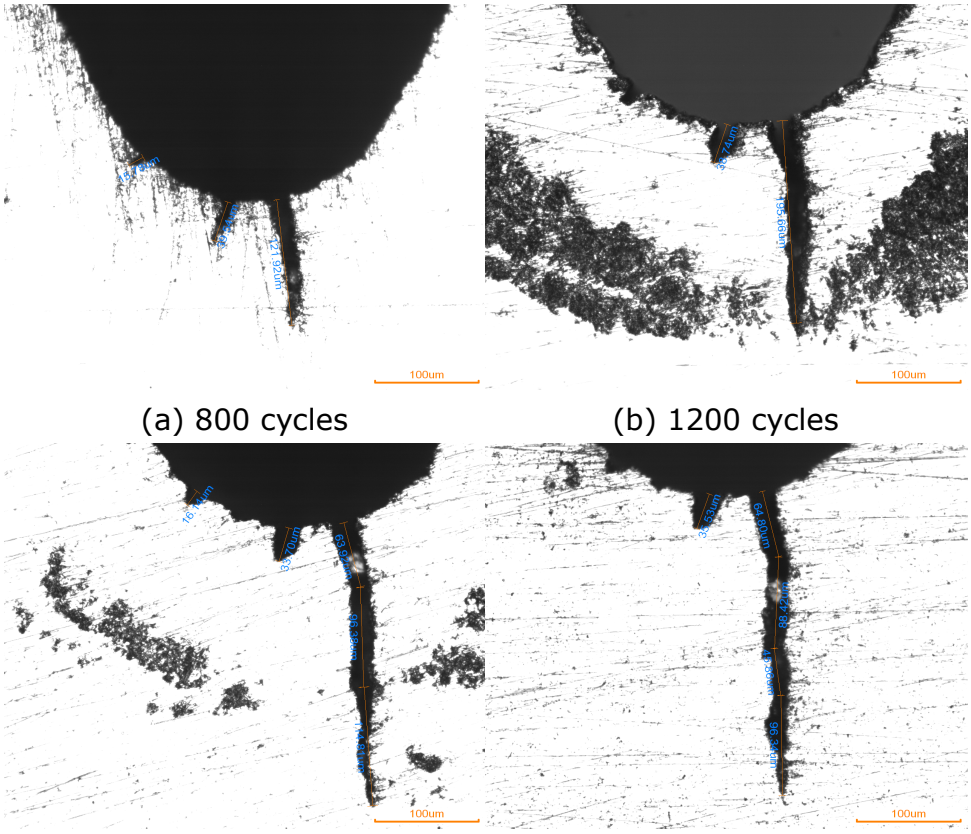

(a) 800 cycles (b) 1200 cycles

(c) 1600 cycles (d) 2000 cycles

Figure. 5.5 Thermal cracking observation on sample N2

Figure 5.6 shows temperature field of one sample during a thermal testing cycle using several frames. The same levels of temperature have been assumed for the figures so that thermal fatigue test cycle can be easily observed from the colour level. The water based lubricant is flushed down to the notch when the cooling starts. Therefore, the temperature is the lowest at the notch and gets higher towards the edge, as illustrated in Figure 5.6a. The hot area is getting smaller when cooling continues (see also Figure 5.6b). When heating begins, the specimen is heated the centre of both sides. The notch is then comparably cool within the sample (Figure 5.6c). And at the end of heating, the entire specimen gets heated up, as shown in Figure 5.6d

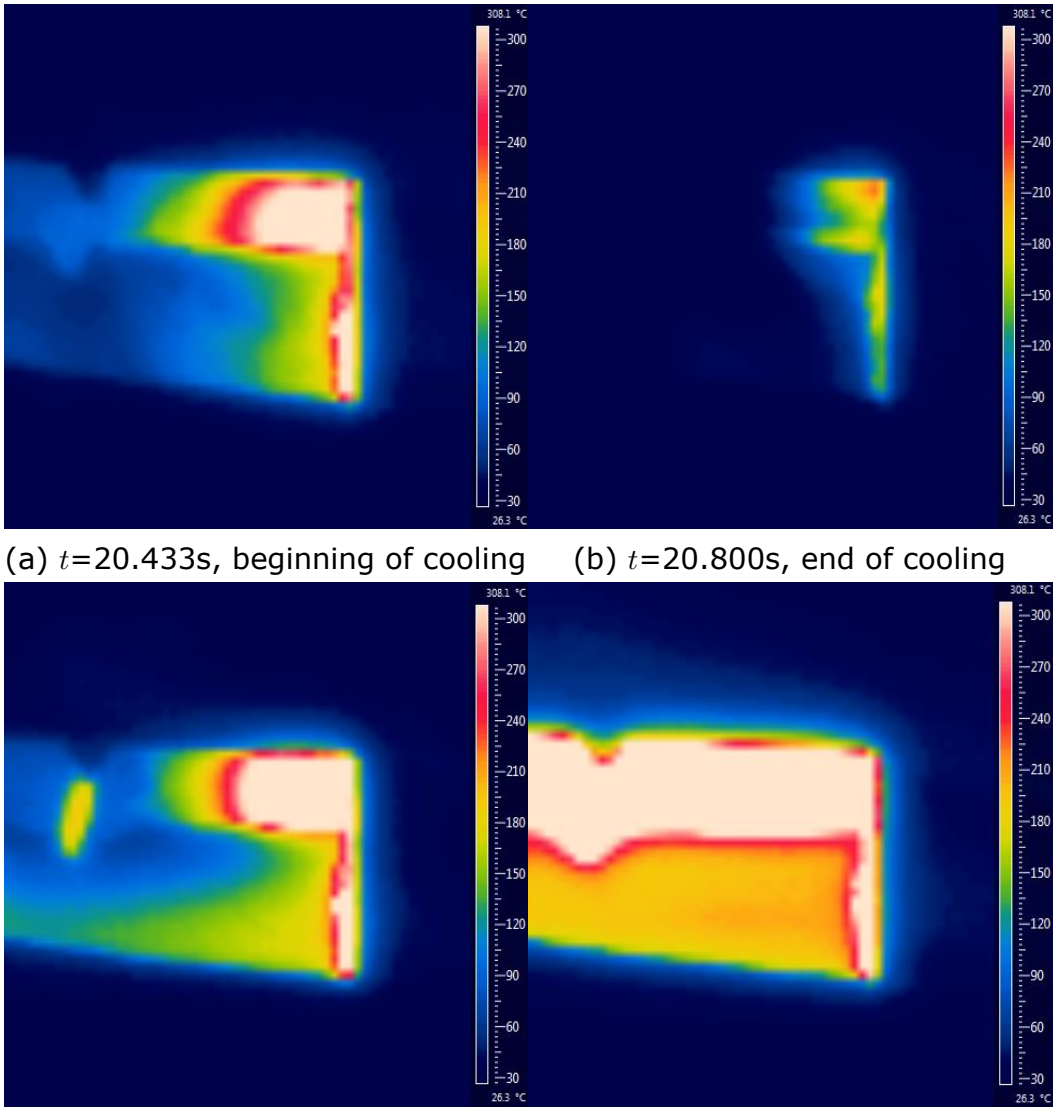

(a) t=20.433s, beginning of cooling (b) t=20.800s, end of cooling

(c) t=22.000s, beginning of heating (d) t=24.800s, end of heating

Figure. 5.6 Thermal infrared imaging on sample N2

Temperature profiles of every material point on the specimen surface can be extracted from the temperature field. Figure 5.7 illustrates the thermal profile of point P1 which is 1.5 mm below the notch tip. The temperature of point P1 varies between 430°C and 30°C. Great thermal gradients can be found right at the instants of heating and cooling. The reason is that thermal infrared cameras are only capable of capturing radiation of the material surface. Therefore, when the lubricant has not vaporised from the specimen,

the radiation obtained would be from the lubricant rather than the specimen surface.

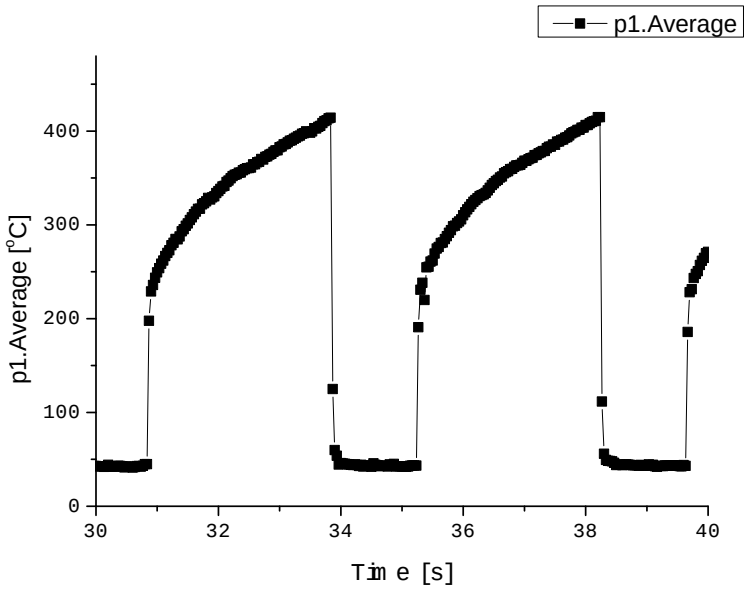

Figure. 5.7 Temperature profile of P1 under F600-h3-c1p5

5.3 Finite element modelling

Thermal fatigue crack evolution model is one of the important aspects with regard to evaluation of the service life of die casting dies. To understand thermal fatigue, it is necessary to know the thermal stresses experienced by the tool. The objective of the numerical simulation is to investigate stress-strain loops of test samples under different testing conditions. With the assumption of a weak coupling between the thermal and mechanical problem, the thermo-mechanical analysis is performed by the ABAQUS® FE package in sequentially coupled manner.

Due to the geometrical symmetry in two planes, i.e. XY plane and YZ plane, one quarter FE model of specimens is developed. This quarter model is analysed using eight-node linear hexahedron elements, as shown in Figure 5.8. The meshing is refined near the

notch tip and the outer surface of the sample to capture thermal gradients.

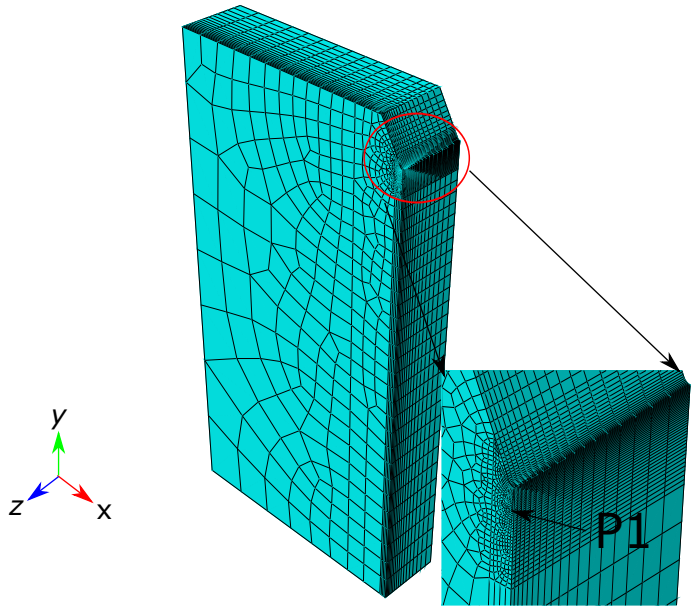

Figure. 5.8 Meshing of test specimens in FEM

5.3.1 Thermal analysis

The thermal fatigue cycle is comprised of two stages: induction heating and water cooling. The following boundary conditions during testing were considered in the finite element analysis:

- The symmetry planes indicated in Figure 5.9 are isolated.
- Surface heating introduced at heating stage. For better fitting with the experimental thermal cycles, a Gaussian distribution of heat flux density with respect to y axis is assumed on the heating surface.
- Acute convective exchange condition to account for water cooling. The heat transfer coefficient between the material and water is initially assumed as 0.028 W/mm^{2}K and then optimized through thermal calibration process depicted in Figure 5.10.

- Gentle convective heat transfer to account for the air cooling. A constant heat coefficient of 5 W/mm^{2}K is defined for all the surfaces.

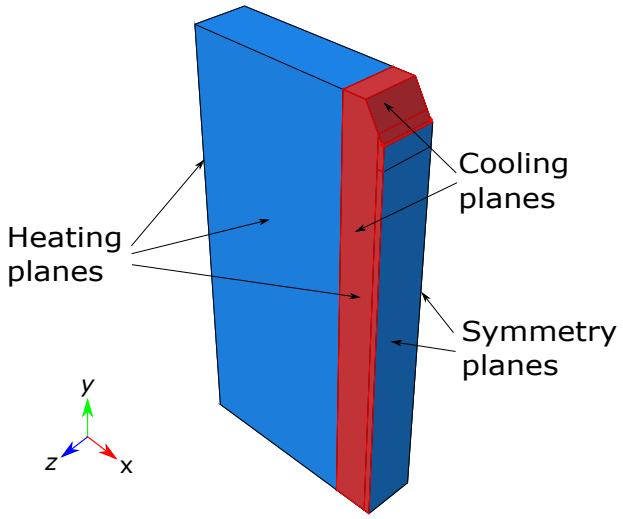

Figure. 5.9 Thermal analysis boundary conditions for thermal fatigue tested samples

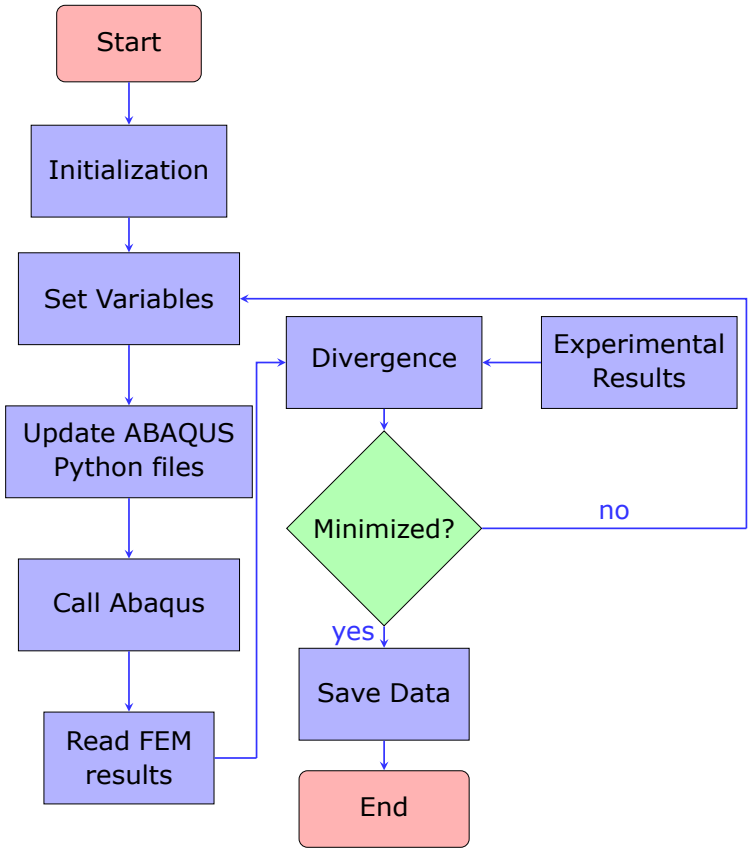

Figure. 5.10 Thermal calibration procedure using ABAQUS®-MATLAB® interaction

Figure 5.10 illustrates the procedure followed to calibrate heat flux due to induction heating and heat transfer coefficient between lubricant and specimen. MATLAB® is used to programme the main function which calls ABAQUS® executable during the whole analysis process. Several files are coded with Python language which is mainly used for ABAQUS® programming. These files facilitate with automatic running of finite element analysis and post-processing. The main function in MATLAB® modifies the variables and updates them in Python files accordingly. The Python files are then called in the MATLAB® environment to execute finite element analysis and postprocessing. The results from ABAQUS® analysis are compared with experimental data and the divergence is minimised to get optimal variables.

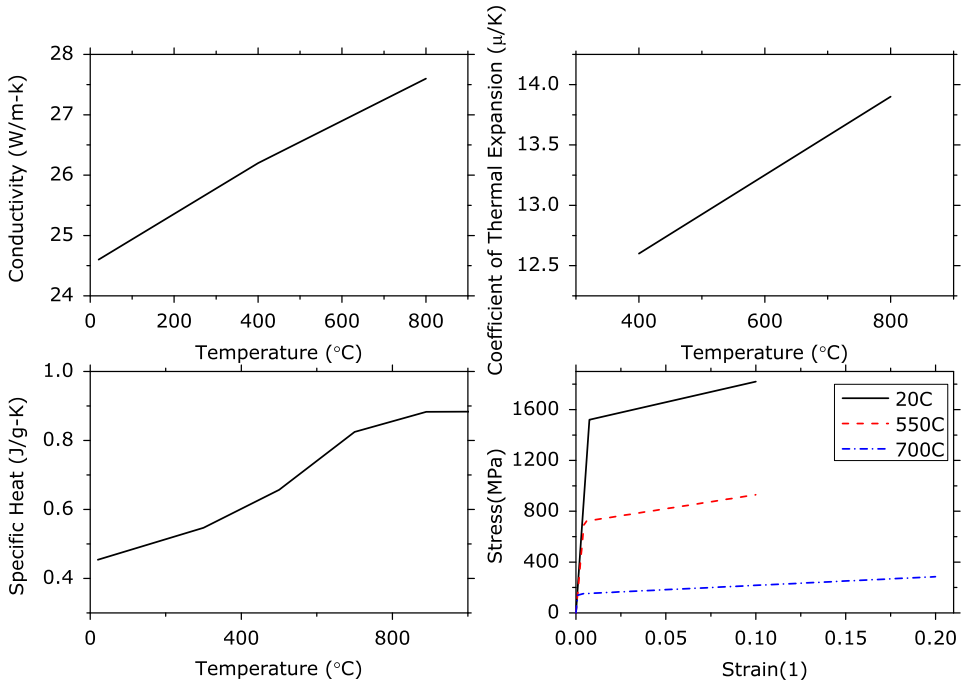

Figure. 5.11 Material properties of ASSAB 8407S mould steel

Other temperature-depended material properties of ASSAB 8407S (AISI H13 premium) tool steel are summarized in Figure 5.11 (ASSAB, 2012; Klobčar et al., 2004). In order to develop a quasi-steady-state heat transfer profile of the specimen, a series of twenty

thermal cycles were run. Each cycle is modelled as one heat transfer step in ABAQUS® with two amplitudes defined to stimulate two stages. The initial temperature of specimens is assumed equivalent to ambient temperature, i.e. 23°C.

Temperature profile of the point P1, 1.5 mm below the notch tip, was measured by the thermal infrared camera for comparison to data calculated by FEM. The divergence is minimized to optimize the non-uniform surface heat flux and the heat transfer coefficient between the sample and cooling water. In order to exclude the effects of cooling water, temperature data less than 100°C during heating are not considered in the optimisation. The optimised thermal analysis parameters enabled a close correlation between the measured and computed thermal fields, as illustrated in Figure 5.12.

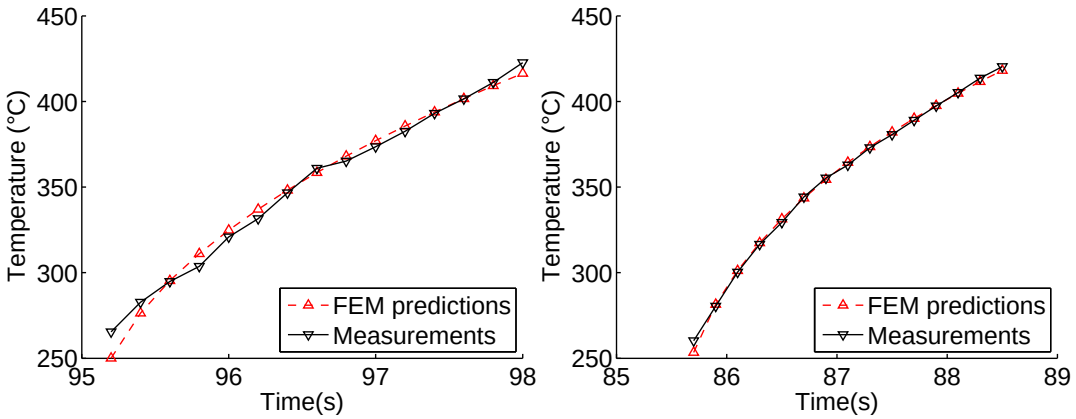

(a) $F = 700$, $t_h = 3.0$, $t_c = 2.0$ (b) $F = 600$, $t_h = 3.0$, $t_c = 1.5$

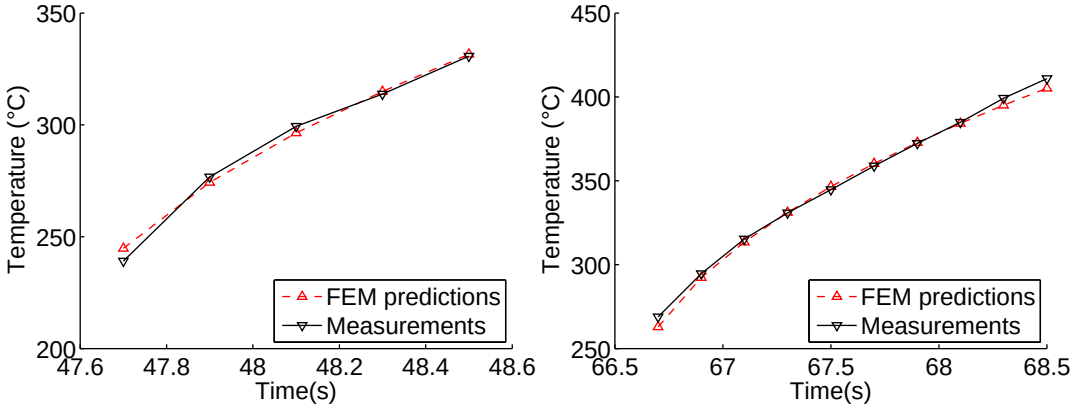

(c) $F = 800$, $t_h = 1.0$, $t_c = 1.5$ (d) $F = 700$, $t_h = 2.0$, $t_c = 1.5$

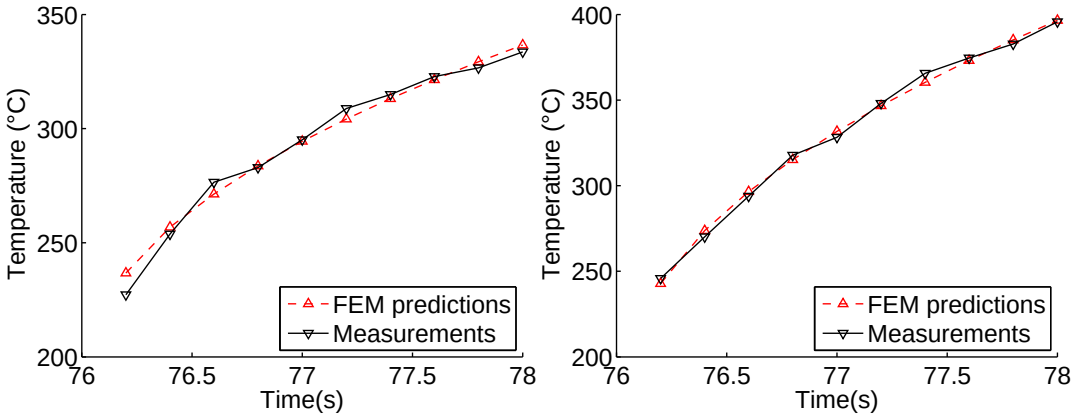

(e) $F = 600$, $t_h = 2.0$, $t_c = 2.0$ (f) $F = 800$, $t_h = 2.0$, $t_c = 2.0$

Figure. 5.12 Agreement between FEM calculated and measured thermal profiles under different conditions

5.3.2 Mechanical analysis

With the heat flux and the heat transfer coefficient calibrated, temperature history profiles of the sample can be computed via the thermal analysis as described in the previous section. The computed

thermal fields throughout the transient are then imported as the predefined field for the mechanical analysis. Since this analysis investigates the structural behaviour of test specimens after achieving quasi-steady-state thermal profile, only the thermal data of last step is introduced. The mechanical analysis also uses eight-node linear hexahedron elements. The elastic-plastic constitutive model is applied, with the yield stress, the ultimate stress, and elongation defining the work hardening properties of the material. A strain rate independent model with the Von Mises yield criterion, isotropic hardening, and Poisson's ratio of 0.3 is used in the analysis. Coefficient of thermal expansion of the material is considered temperature-dependent in the analysis.

Boundary conditions for the mechanical part are illustrated in Figure 5.13. The symmetrical XY plane and YZ plane of the specimen are restrained in z-axis and x-axis, respectively. Displacement in y-axis is fixed at the bottom plane, while engineering springs with stiffness of 0.5 N/mm are assumed on the top surface.

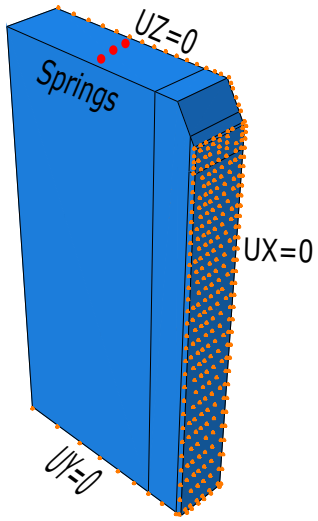

Figure. 5.13 Structural analysis boundary conditions for thermal fatigue tested samples

Figure 5.14 illustrates the transient 20-cycle temperature of the notch tip under designated six conditions. From the figures, one can find that test specimens accomplish the thermal equilibrium within around 20 cycles. Therefore, the temperature field of the 20^{th} cycle can be used for the study of structural behaviour.

The corresponding stress profiles of the notch tip under these six conditions are depicted in Figure 5.15. According to the stress profile, test samples experience great stresses at the notch tip in the x-direction due to the restraint of neighbouring elements. While in other directions, little stresses are produced since the notch tip is free to expand or contract. One can also observe that maximum compressive stress and maximum tensile stress were resulted at the notch tip at the beginning of heating and cooling, respectively. However, the magnitude of compressive stress is much smaller than that in tension. This is probably because the samples are heated from the centre rather than from the notch. Heat is firstly introduced to the central part and then to the top and bottom.

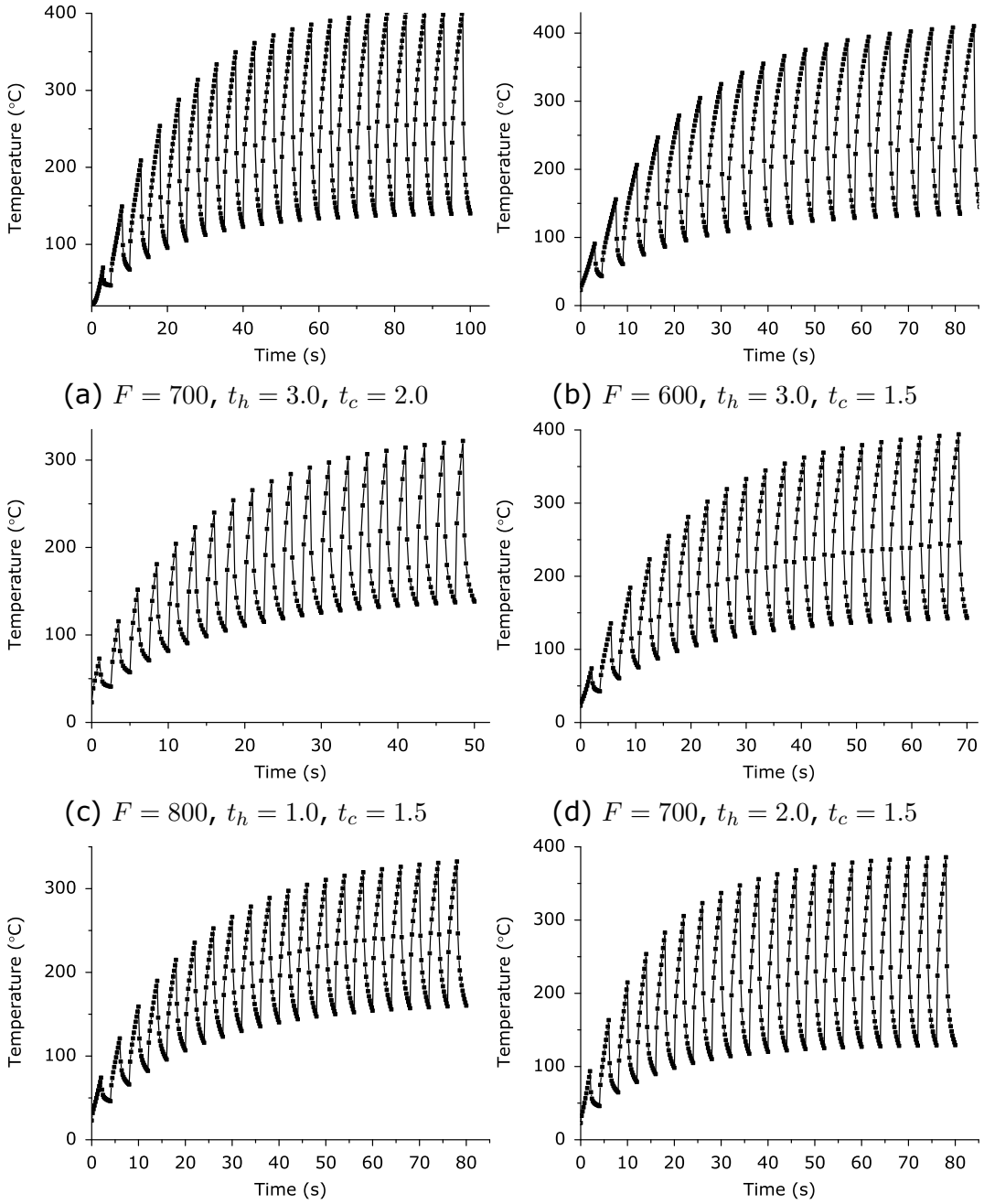

(a) $F = 700$, $t_h = 3.0$, $t_c = 2.0$

(b) $F = 600$, $t_h = 3.0$, $t_c = 1.5$

(c) $F = 800$, $t_h = 1.0$, $t_c = 1.5$

(d) $F = 700$, $t_h = 2.0$, $t_c = 1.5$

(e) $F = 600$, $t_h = 2.0$, $t_c = 2.0$

(f) $F = 800$, $t_h = 2.0$, $t_c = 2.0$

Figure. 5.14 Transient thermal profile of the notch tip under different conditions

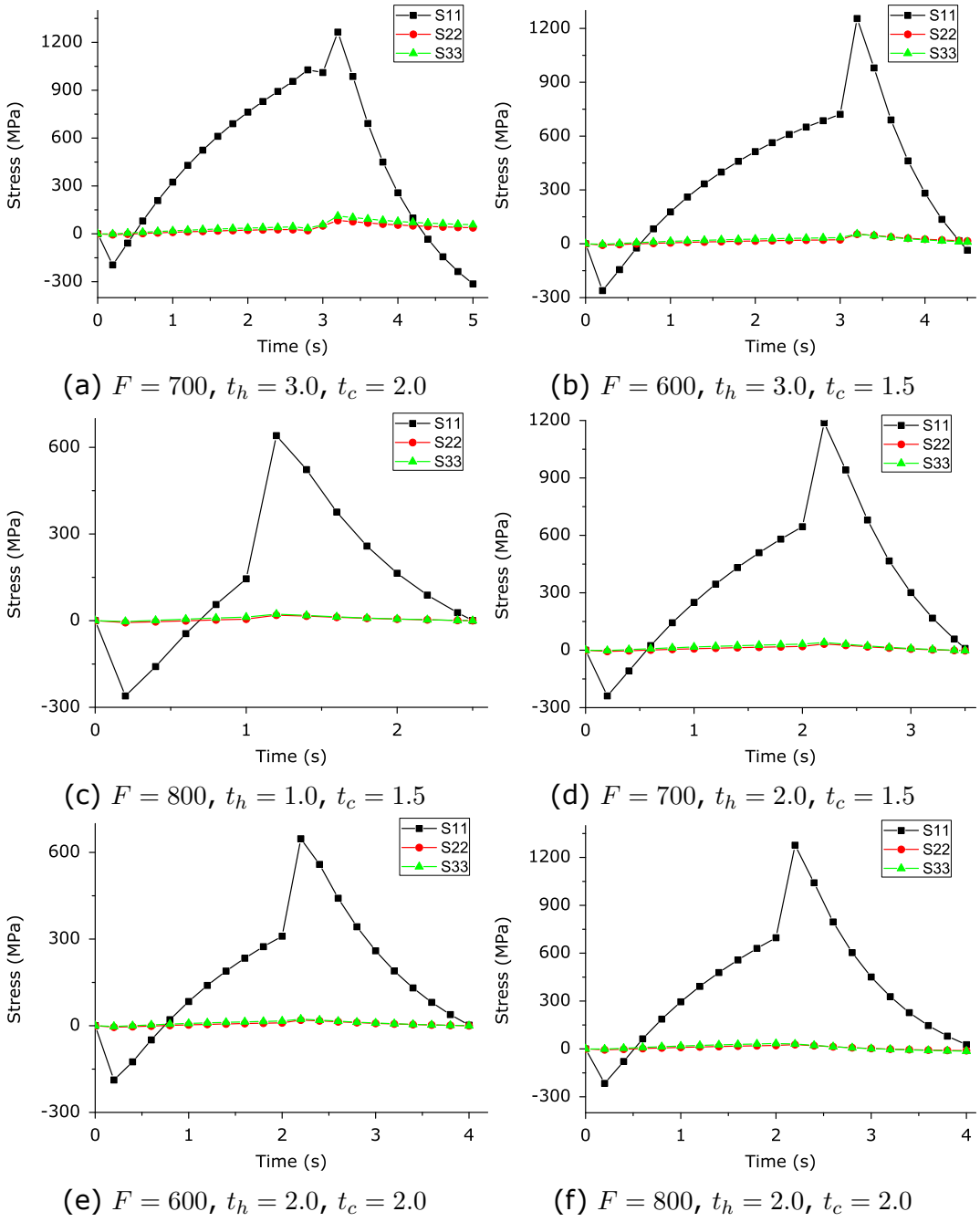

(a) $F = 700$, $t_h = 3.0$, $t_c = 2.0$ (b) $F = 600$, $t_h = 3.0$, $t_c = 1.5$

(c) $F = 800$, $t_h = 1.0$, $t_c = 1.5$ (d) $F = 700$, $t_h = 2.0$, $t_c = 1.5$

(e) $F = 600$, $t_h = 2.0$, $t_c = 2.0$ (f) $F = 800$, $t_h = 2.0$, $t_c = 2.0$

Figure. 5.15 Stress profiles of the notch tip under different conditions

5.3.3 Verification of modelling methodology

The modelling methodology adopted in this study is verified by conducting a benchmark study of published work in literature. Klobcar et al. (2008) studied the finite element computation of test specimens under thermal fatigue tests using immersion tests. The specimens are subjected to cyclic heating in bath of molten Alu-

minium Alloy 226 and cooling in bath of water-based lubricant. The specimens are also continuously cooled with cold water flowing through internal channels. In literature, they investigated the influence of immersion test parameters, material, specimen edge geometry, and thickness of maraging steel surfacing welds on thermal stresses.

The benchmark study only analyses the standard specimen shown in Figure 5.16. The results from the literature and the methodology utilized in this paper are compared, as illustrated in Figure 5.17 and Figure 5.18. The data are in general agreement with those from the literature. Transient thermal results are slightly greater than data from the benchmark methodology. The same case can be observed in the comparison of stresses except the last two stages where the data decrease more dramatically in benchmark analysis. From this benchmark comparison, it can be concluded that the methodology used in this work is viable.

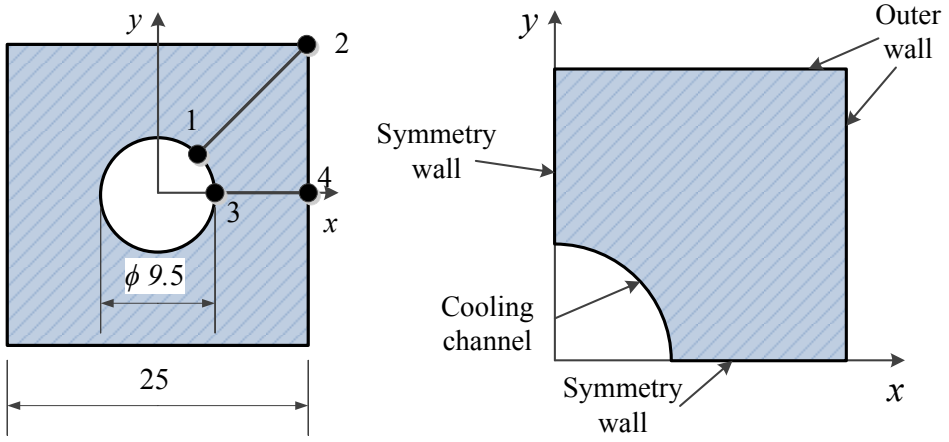

(a) complete (b) one-quarter model

Figure. 5.16 Cross section of test specimen in literature

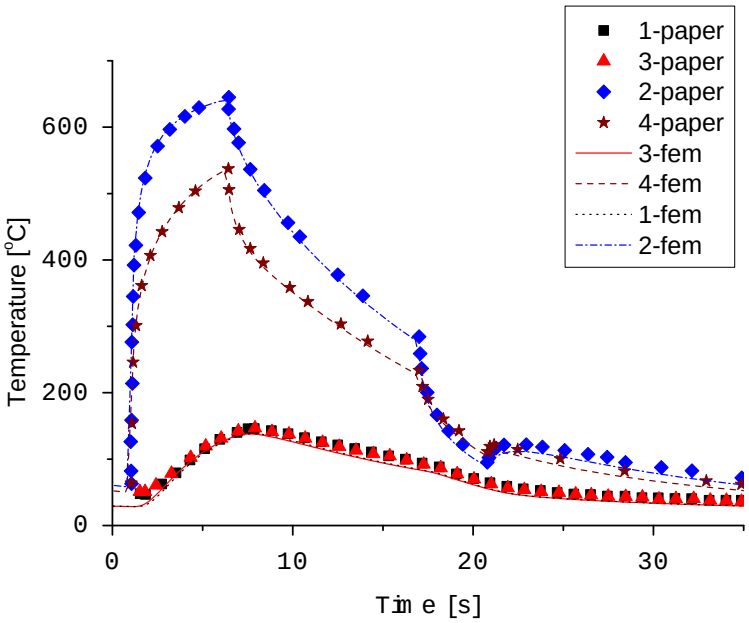

Figure. 5.17 Comparison of transient temperature from literature and FEM

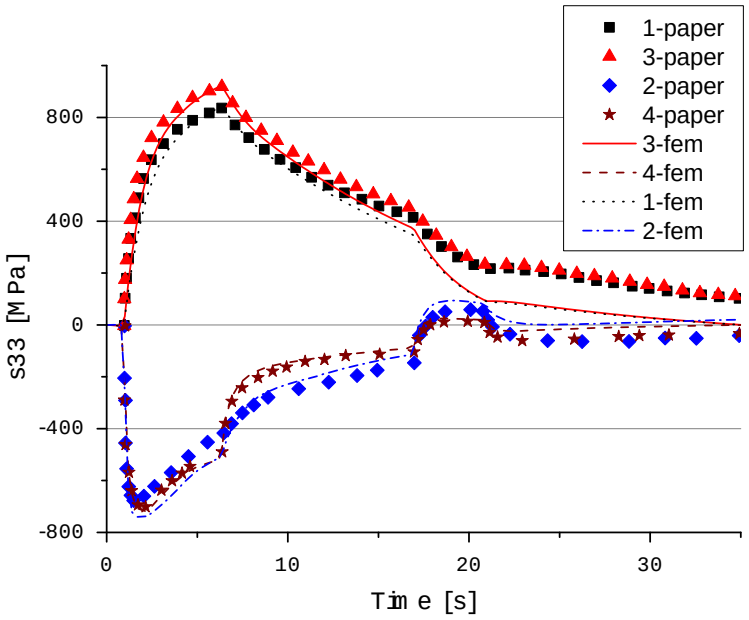

Figure. 5.18 Comparison of transient stress from literature and FEM

5.4 Thermal fatigue modelling

5.4.1 Fatigue criterion

Thermal fatigue failure in dies and moulds subject to thermal cycling tend to fall in the Low Cycle Fatigue (LCF) field where the fatigue

life to failure ranges between 100 and 10,000 cycles. The Coffin-Manson fatigue model, proposed independently by (Coffin, 1954; Manson, 1953), has been widely used for evaluation of low cycle fatigue failure(Sasaki and Takahasahi, 2005).

The total number of cycles to failure, N_f, is dependent on the plastic strain range, $\Delta\epsilon_p$, the fatigue ductility coefficient, ϵ'_f , and the fatigue ductility exponent, c, given in the expression below:

$$\frac{\Delta\epsilon_p}{2} = \epsilon'_f(2N_f)^c \tag{5.1}$$

The fatigue ductility coefficient, ϵ'_f , is approximately equal to the true fracture ductility, ϵ_f. The fatigue ductility exponent, c, varies between -0.5 and -0.7 (Kilinski et al., 1991), and experimental data are required to determine the constants. The constants in the Coffin-Manson model are dependent on temperature and cyclic frequency. This is a big difficulty for thermal fatigue situation where temperature fluctuates. Moreover, it is not able to account for crack propagation.

Energy-based fatigue criteria forms another group of models. The advantage of energy models is the capability of describing influences due to the interaction of stress and strain and allowing for a generalisation to multiaxial loading. Energy criteria are representative for the cyclic behaviour of materials and are linked to macroscopic crack initiation (Christiner et al., 2011).

An empirical plastic work model was developed by Darveaux (Darveaux, 2000; Lau, 1991) for solder joint subject to thermal cycling tests and is used to predict the crack initiation and crack growth behaviour using the equations given below:

$$N_0 = C_1\Delta W^{C_2} \tag{5.2}$$

$$\frac{da}{dN} = C_3 \Delta W^{C_4} \tag{5.3}$$

where ΔW is the plastic work, a is the area of the solder joint where a fatigue crack will grow till failure, $C_i, i = 1, ..., 4$ are constants fitted to the test data. This model must be used with a calibrated FEA model with a specific element size and volume.

In this research, the plastic work density per unit time was used as a parameter when evaluating thermal fatigue failure. Figure 5.19 shows the definitions of the plastic work density per unit time, the total strain amplitude $\Delta\epsilon$, plastic strain amplitude $\Delta\epsilon_p$, and stress amplitude $\Delta\sigma$ for the cyclic stress-strain curve. The plastic work density per unit time ΔP can be expressed by the plastic strain energy density ΔW, which is the area of the stress-strain loop of thermal stable cycles, and the cycle period Δt as follows:

$$\Delta P = \frac{\Delta W}{\Delta t} \tag{5.4}$$

Figure 5.20 plots the maximum principal stress and strain loops of the notch tip under proposed six different conditions. The stress-strain hysteresis curves indicate different stress-strain routes from those obtained by mechanical fatigues. The curve loops in the anti-clockwise direction instead of the clockwise direction as structures under mechanical fatigue.

By introducing the definition of the plastic work density per unit time, the fatigue criterion for this research is given as:

$$N_f = C_1 (\frac{\Delta W}{\Delta t})^{C_2} = C_1 \Delta P^{C_2} \tag{5.5}$$

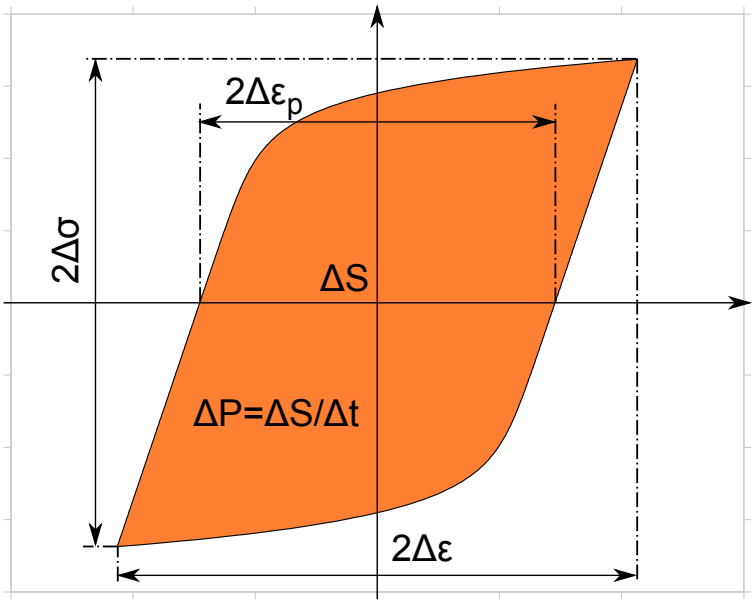

Figure. 5.19 Schematic representation of the plastic strain amplitude, stress amplitude, and plastic work density per unit time

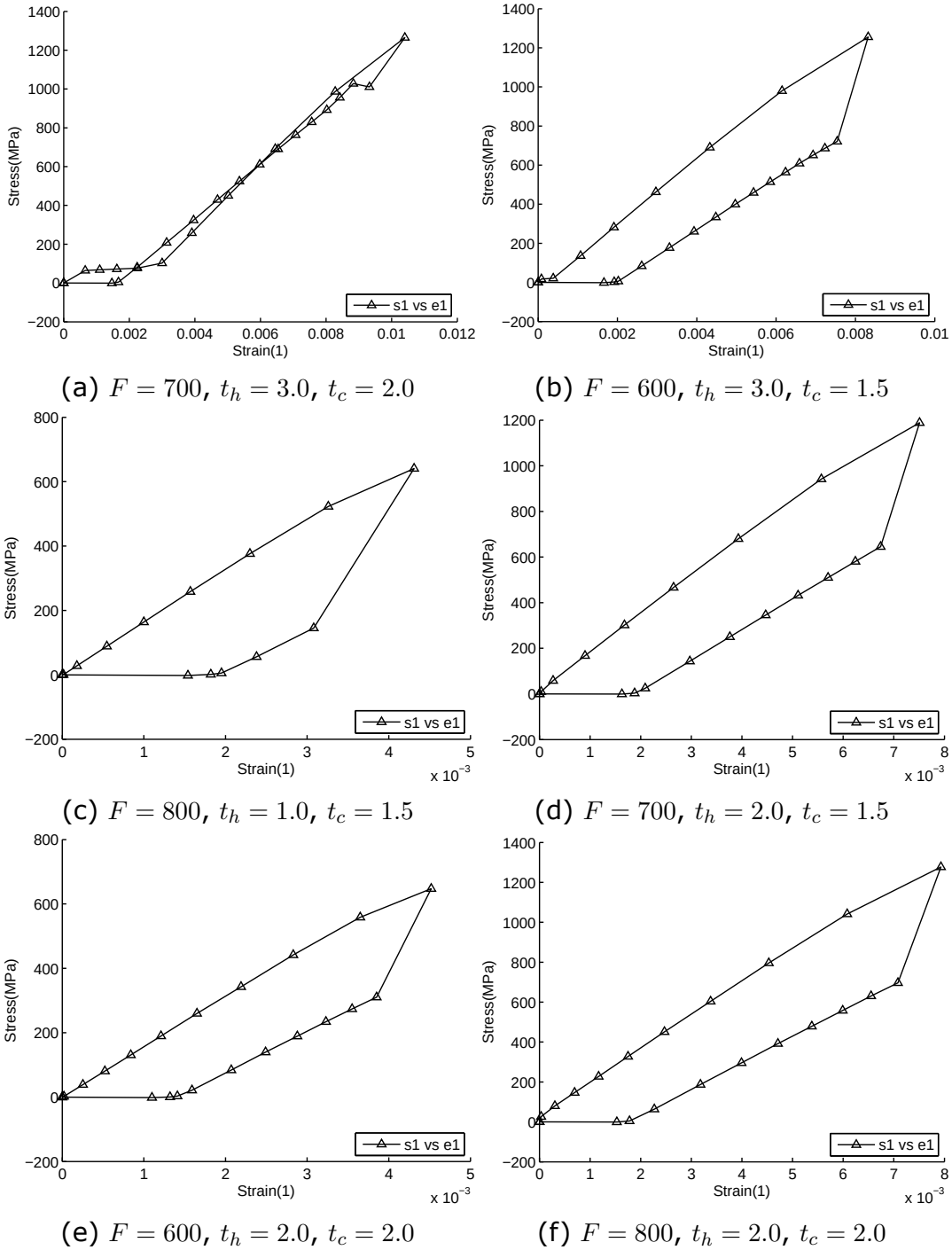

(a) $F = 700$, $t_h = 3.0$, $t_c = 2.0$

(b) $F = 600$, $t_h = 3.0$, $t_c = 1.5$

(c) $F = 800$, $t_h = 1.0$, $t_c = 1.5$

(d) $F = 700$, $t_h = 2.0$, $t_c = 1.5$

(e) $F = 600$, $t_h = 2.0$, $t_c = 2.0$

(f) $F = 800$, $t_h = 2.0$, $t_c = 2.0$

Figure. 5.20 Maximum principal stress and strain loops of different conditions

5.4.2 Criterion fitting

The constants of the fatigue model (Equation 5.5) need to be calibrated so that the criterion can be implemented for fatigue prediction.

For simplicity, the following assumptions were made to presented fatigue model:

- Crack initiates from the notch tip and propagates along the central line below the notch;
- Experimental crack data were observed on the central line of the specimen surface;
- A material point is damaged when the criterion applies;
- Loading variations due to crack evolution are ignored.

The constants of the fatigue model were calculated by undertaking the following steps:

(a) from the numerical part, stress-strain transients of material points along the central line were calculated by sequentially coupled thermo-mechanical analysis;

(b) the plastic work density was computed for every material point along the central line;

(c) from the experimental part, crack lengths were observed against number of cycles. The plastic work density of material points were interpolated in accordance with crack lengths, as illustrated in Figure 5.21;

(d) the plastic work density per unit time of material points observed by crack lengths were computed by dividing the plastic work density over test periods;

(e) the model constants were fitted by the plastic work per unit time vs number of cycles to failure data.

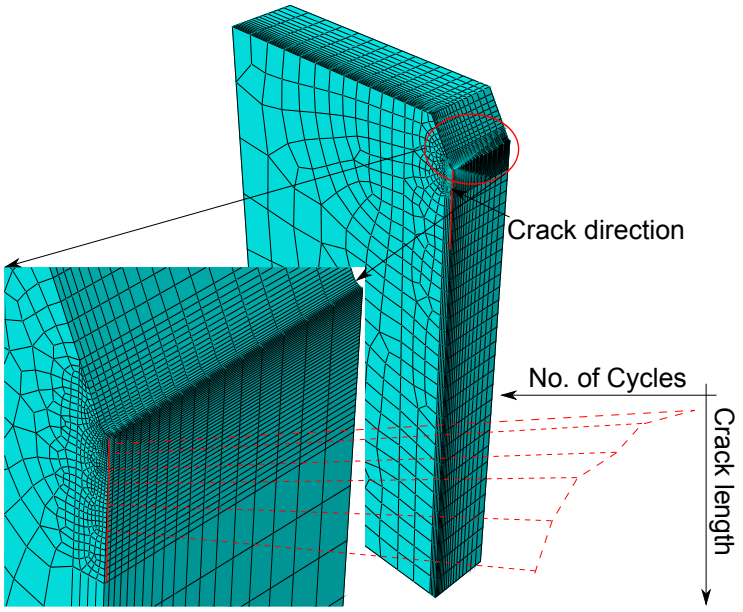

Figure. 5.21 Thermal fatigue crack evolution and mapping with FEM results

Figure 5.22 plots the mean plastic work per unit time of studied conditions with regard to each number of cycles to crack. The data was then used to fit the fatigue model proposed, as also depicted in Figure 5.22. The R squared value (0.9988) of coefficients indicates good fitting of the model. Therefore, the fatigue criterion is given by:

$$N_f = 61.38\Delta P^{-2.412} \tag{5.6}$$

By introducing

$$C_1 = C_3^{-C_2} \tag{5.7}$$

then the model can be rewritten as

$$N_f = (\frac{\Delta P}{C_3})^{C_2} \tag{5.8}$$

where $C_3 = \sqrt[-C_2]{C_1} = 5.512$ is the plastic work density per unit time due to one cycle fatigue.

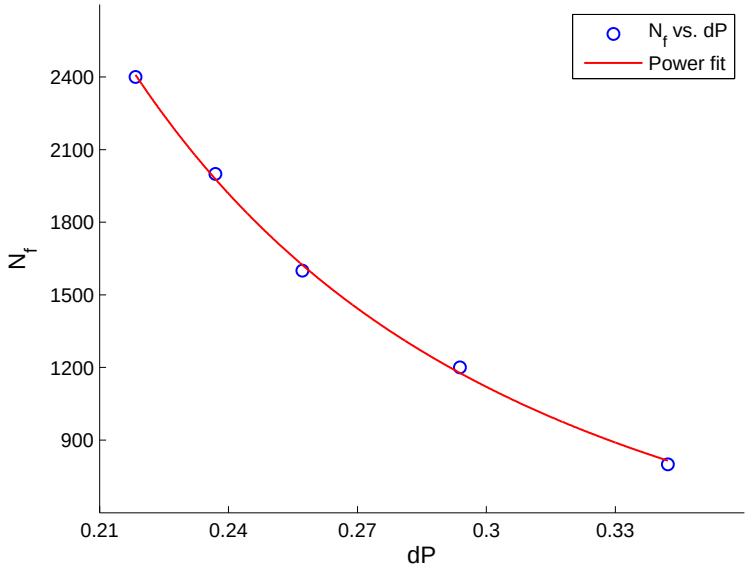

Figure. 5.22 $N_f - dP$ data and model fitting

The model can be validated by considering the worst case of fatigue loading known as fully-reversing load. One cycle of this type of fatigue loading occurs when a tensile stress of some value is applied to an unloaded part and then released, then a compressive stress of the same value is applied and released. Tensile test is a typical cycle of such cases. Assuming the sample fractures when strain reaches to 0.1, then the plastic work density might be approximated by the product of yield stress and the strain, i.e. $\Delta W = 1520 \times 0.1 = 152 J/m^3$. Thus, the period for a sample to failure in a tensile test is about 27.6 s which is a reasonable magnitude.

5.5 Summary

This chapter was to establish damage evolution model of the die material. An induction heating and water cooling method was used for thermal fatigue testing purpose. Uniform experimental runs was adopted to investigate the crack growth process of test samples. With thermal loadings worked out by finite element modelling, the selected damage model was fitted.

The coefficient of determination reaches to 0.9988. Together with the residual plot, it can be concluded that the damage model is well fitted.

Chapter 6

Optimization and calibration of laser welding

6.1 Introduction

This chapter is to establish the simulation method of laser welding so that residual stress due to laser welding can be calculated.

This chapter starts with the study of weld characteristics which is of great significance when carrying out welding remanufacture. It is followed by the calibration of laser source models which is an import part in computational welding mechanics. Then, laser welding simulations were conducted on the samples to calculate residual stresses introduced by the welding process.

6.2 Laser system setup

A pulsed Nd:YAG laser welder of 300W power (WF300, HAN'S) is utilised in this study. The wavelength of the Nd:YAG laser beam is only 1.064 μm, which indicates a more intensive energy would be achieved on the deposited zone compared to CO_2 laser beams with wavelength of 10.6 μm. Furthermore, the low beam energy

prevents the surface of the welding target from overheating and ensures that the heat-affected zone is small. Figure 6.1 depicts the configuration of the pulsed Nd:YAG laser beam welding device while the physical facility is shown in Figure 6.2. The energy per pulse generated by the laser system is correlated with current, as illustrated in Figure 6.3.

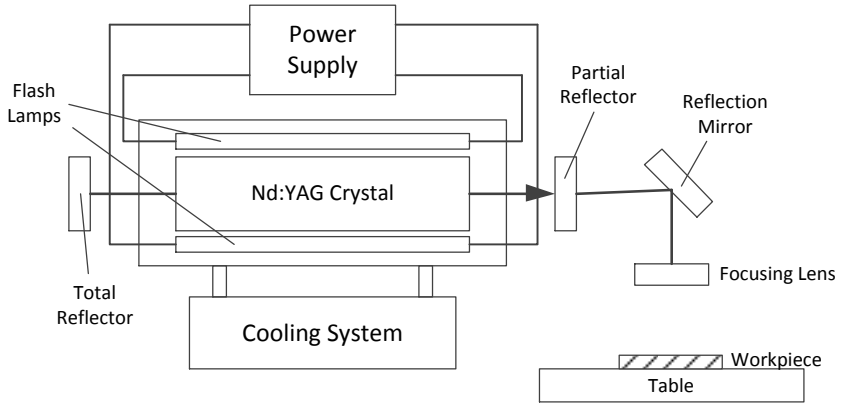

Figure. 6.1 Schematic representation of the pulsed Nd:YAG laser welding system

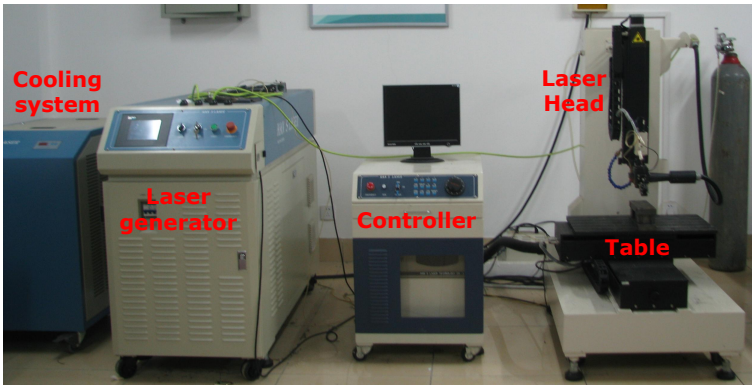

Figure. 6.2 Configuration of HAN's laser system - WF300

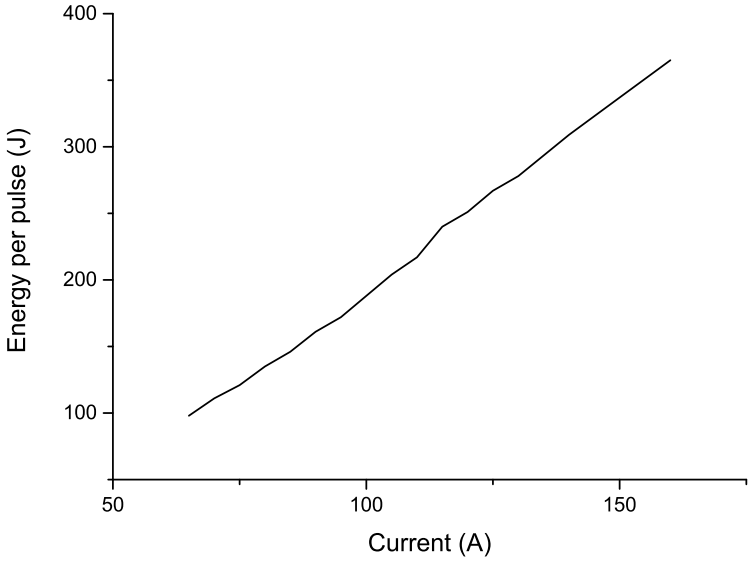

Figure. 6.3 Relationship between energy per pulse and current in Han's laser system

6.3 Experimental plans

For remanufacturing dies and moulds, it is of significance to obtain information about weld characteristics because it affects the mechanical strength of welded area. Once mathematical relationships between the process parameters and weld characteristics are constructed, it enables optimisation of the process parameters to control and obtain required shape and quality of weld beads.

The experimental programme aimed at investigating the weld characteristics of a typical hot-work tool steel. Main information about weld characteristics are given by the weld cross section in a stable area (Boboescu, 2011). The major dimensions of concern are the Depth of Penetration (DP), the Bead Width (BW), the Weld Area (WA) of molten zone and the Aspect Ratio (AR, or Depth to Width ratio), as defined in Figure 6.4. Since there are numerous parameters when laser welding materials, it is rather difficult to build the weld characteristic relationship with all the parameters taken into consideration. In this study, considered welding process

parameters include Current for creating laser power, Frequency, Depth of Focus (DoF), and Scanning Speed (SS).

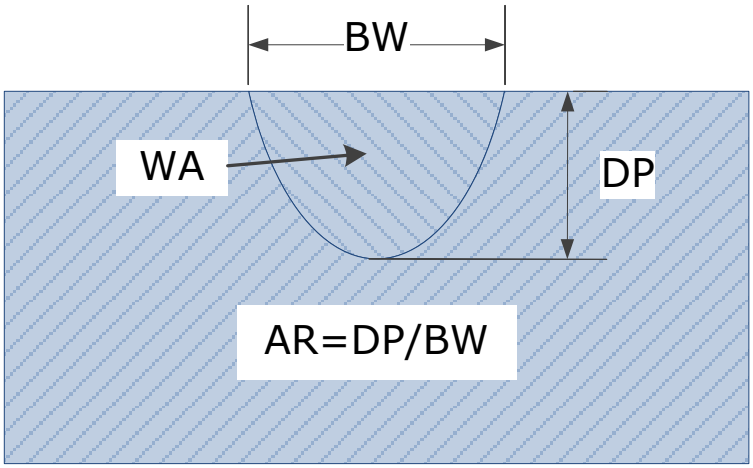

Figure. 6.4 Cross-section of a weld bead

Based on the measurements made on sections from failed dies, Parishram (2007) observed that cracks that cause noticeable heat checks for the die casting application had an average of 0.5 mm in length. Therefore, target depths of welds are determined to be around 0.5 mm in this research. To study the effects of laser welding parameters on weld profiles under this consideration, the experimentation follows three steps as below:

- Preliminary experiment, based on a Taguchi plan and aimed at identifying the significant factors and detecting curvatures of the responses;
- Uniform experimenting methodology, based on a Uniform Design (UD) scheme and aimed at full characterization of the factors that affect the weld profile, and;
- Validation runs, to assess the reliability of response models determined in the previous step.

The experimental procedures were carried out in sequential order. Results obtained in the previous step are fundamental information to the set-up of the next, as discussed below.

6.4 Experimental work and results

6.4.1 Preliminary experiment

Taguchi method, a systematic approach to design and analyses of experiments, is used for designing and improving product quality characteristic (Yousefieh et al., 2011). As a powerful tool for design of a high-quality system, it requires limited resources but still provides sufficient information for estimating effects of process variables (Hsiao et al., 2008; Pan et al., 2005). Furthermore, Taguchi method also features with its robustness of achieving optimal performance.

In this step, the four welding parameters, Current, Depth of Focus, Scanning Speed, and Laser Pulse Frequency are concerned altogether with three different levels of each parameter. Thus, a total of 81($3\times3\times3\times3$) different combinations need to be considered. However, according to Taguchi, the samples could be organized into only 9 groups and still yield results with the same confidence as if they were to be considered separately. Table 6.1 illustrates the concerned experimental variables and their levels. Depth of Penetration, Bead Width, Weld Area and Aspect Ratio are investigated for describing weld profiles, i.e. the dependent output variables. The experimental trials were carried out according to the groupings suggested by Taguchi method as depicted in Table 6.2. In Table 6.2, variables were arranged according to their difficulties to control during the experiment. Since this experimentation is to identify significant factors, no interactive effects were considered. The num-

bers in Table 6.2 indicate the various experimental layouts or levels of the different factors.

Taguchi method recommends the S/N ratio (signal-to-noise) as its performance characteristic, instead of the average value. The general trend is that the larger the S/N ratio, the better the performance. Optimum conditions could be determined by calculating the S/N ratio of experimental results. Generally, there are three categories of performance characteristics, i.e. the larger the better (LB), the smaller the better (SB) and the nominal the better (NB). After the selection of the performance feature, the mean S/N ratios at each level of various factors should be calculated. Contribution of studied factors to the response can also be ranked by sorting the S/N ratio difference between maximum and minimum for each factor. Moreover, the optimal level, i.e. the largest S/N ratio among all levels of the factors, can be determined, which leads to optimum working condition.

Preliminary experimental trials were conducted on a sheet specimen with dimensions of $100 \times 100 \times 5.5$ mm. A distance of about 10 mm was made between the welds and experimental runs were conducted in the order as illustrated in Figure 6.5 to rapidly exclude the effect of the previous weld. For preliminary study purpose, only one sample was laser surfaced. Argon gas with a pressure of 10 bar was used as shielding gas. The base material studied in this research is 8407 supreme hardened to 54 HRC. The chemical composition of the steel is depicted in Table 6.3.

Table 6.1 Experimental variables and levels for Taguchi method

Variables/Levels	1	2	3
Depth of Defocus, (mm)	-4	0	4
Current, (A)	65	75	85
Scanning Speed, (mm/s)	1	2	3
Frequency, (Hz)	3	6	9

Table 6.2 Standard orthogonal arrays of 9 different groups following Taguchi Method

No. of Sample	Factor A	Factor B	Factor C	Factor D
T1	1	1	1	1
T2	1	2	2	2
T3	1	3	3	3
T4	2	1	2	3
T5	2	2	3	1
T6	2	3	1	2
T7	3	1	3	2
T8	3	2	1	3
T9	3	3	2	1

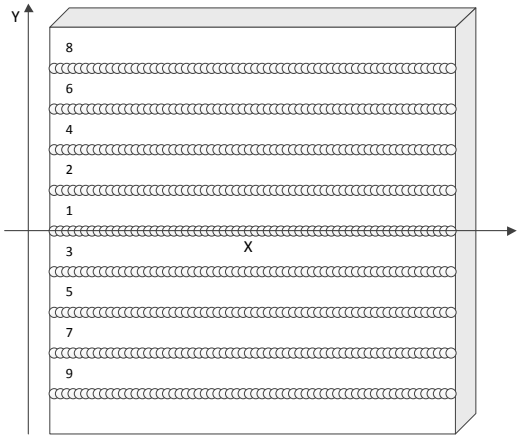

Figure. 6.5 Operating strategy for laser welds

After welding, the welded sample was wire Electrical Discharge Machining (EDM) machined into 18 sub-samples at a distance of 10 mm from both ends for microscope observation so that the error introduced during setting was minimized. The preparation of these samples, according to ASTM E3-11, consists of successive polishing with 400, 800 and 1200 grit silicon carbide emery sheets, disc polishing and chemical etching for the measurement of DP, BW, and WA. The data obtained from all the trials on the DP, BW and WA were recorded for analysis. AR data are computed via DP divided by BW.

Table 6.3 Chemical composition of the analysed mould steels (wt%)

Mould steel	C	Si	Mn	Cr	Mo	V
8407S (Premium AISI H13)	0.39	1.0	0.4	5.2	1.4	0.9

When repairing dies and moulds by welding, it is necessary to achieve the depth of mould defects with minimized heat-affected zone. Therefore, the performance of Depth of Penetration and Aspect Ratio are considered to be the larger the better (LB), while Bead Width and Weld Section Area are regarded to be the smaller the better (SB), as listed in Table 6.4. The measured performances and their computed S/N ratios are presented in Table 6.5. The response of each factor to its individual level was calculated by averaging the S/N ratios of all experiments at each level for each factor.

Table 6.4 Weld characteristics and their corresponding S/N ratios

Performance	Signal-to-Noise Ratio
Depth of Penetration	$S/N = -10\log(\frac{1}{n}\sum_{i=1}^{n}\frac{1}{Y_i^2})$
Bead Width	$S/N = -10\log(\frac{1}{n}\sum_{i=1}^{n}Y_i^2)$
Weld Section Area	$S/N = -10\log(\frac{1}{n}\sum_{i=1}^{n}Y_i^2)$
Aspect Ratio	$S/N = -10\log(\frac{1}{n}\sum_{i=1}^{n}\frac{1}{Y_i^2})$

Table 6.5 Performance characteristics with respect to experimental trials and their S/N ratios

Weld No.	DP_{avg} (μm)	BW_{avg} (μm)	WA_{avg} (μm^2)	AR	S/N ratio of DP	S/N ratio of BW	S/N ratio of WA	S/N ratio of AR
T1	287.0	1355.2	296313	0.21	49.2	-62.6	-109.4	-13.5
T2	311.4	989.4	228945	0.32	49.9	-59.9	-107.2	-10.0
T3	236.6	1260.7	206057	0.19	47.5	-62.0	-106.3	-14.5
T4	238.0	1305.6	227548	0.18	47.5	-62.3	-107.1	-14.8
T5	250.9	1014.6	179180	0.25	48.0	-60.1	-105.1	-12.1
T6	805.1	1112.5	533119	0.72	58.1	-60.9	-114.5	-2.8
T7	348.2	904.4	207247	0.39	50.8	-59.1	-106.3	-8.3
T8	279.5	1232.8	251131	0.23	48.9	-61.8	-108.0	-12.9
T9	300.6	1166.9	257240	0.26	49.6	-61.3	-108.2	-11.8

Main effects of each factor on the weld profile characteristics can also be observed from Figure 6.6-6.9. In general, the increase in heat input leads to a increase in the penetration, and a decrease in bead width and weld area. The results in Figure 6.6-6.9 are in good agreement with these tendencies. From the figures, we can see that four responses developed are determined by four

parameters in different ways. Most of the factors studied lead to non-linear responses. The nonlinear effects of current and frequency on the responses are mainly due to the overlapping between weld spots usually results in optimal performance at around 75% (Pan et al., 2005). The rankings of effects of four factors on all proposed responses can also be observed from Figure 6.6-6.9. It can be found that DP is correlated with BW because of their same ranks of studied factors. While the other two responses show great differences. The overall rank of effects on all responses could be summarized as frequency, scanning speed, current and depth of focus.

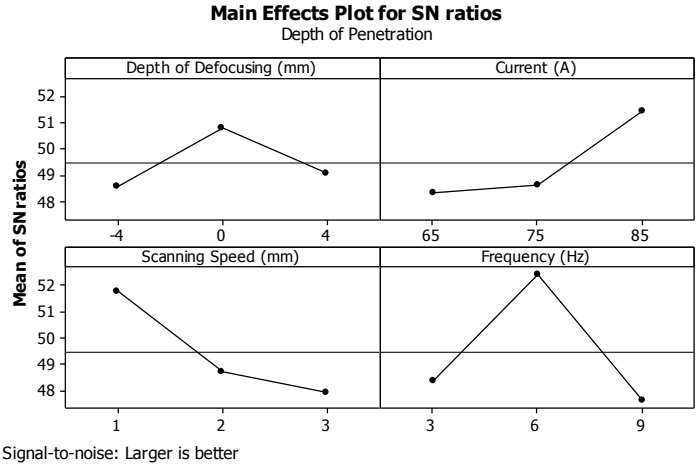

Figure. 6.6 Main Effects Plot for SN ratios-DP

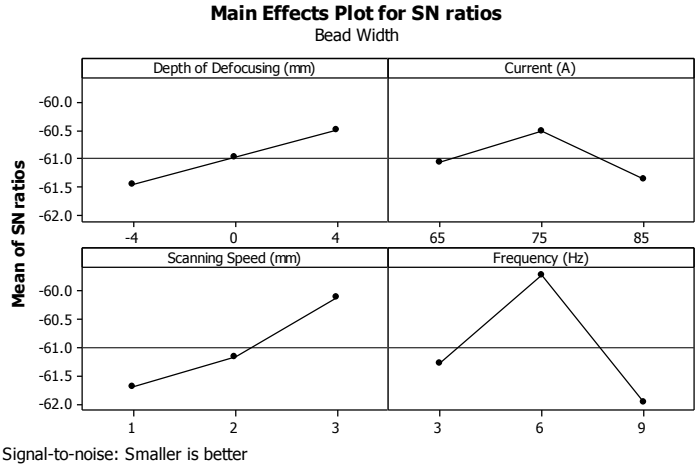

Figure. 6.7 Main Effects Plot for SN ratios-BW

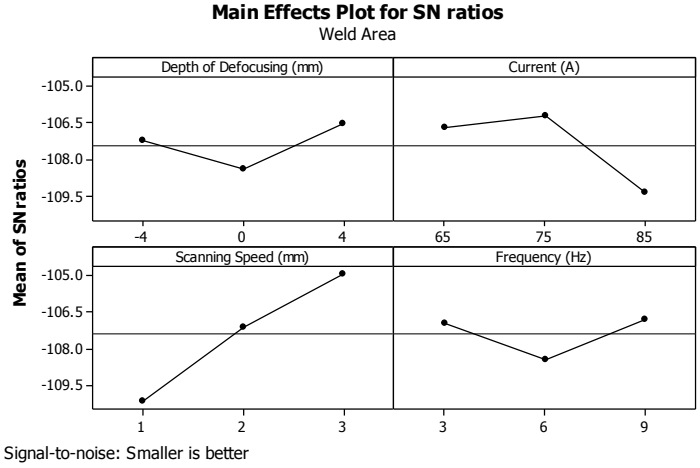

Figure. 6.8 Main Effects Plot for SN ratios-WA

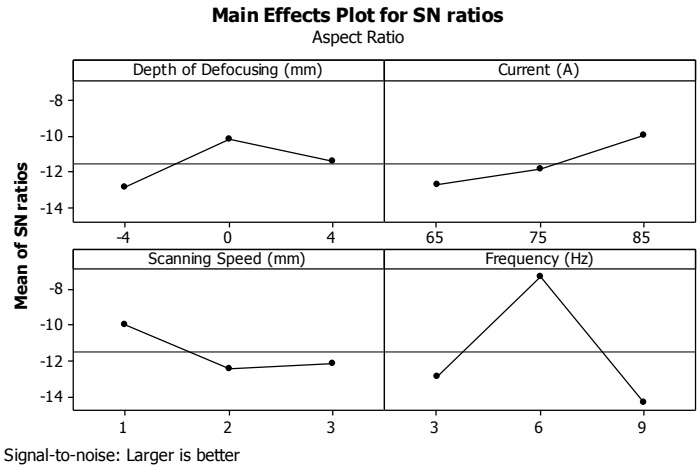

Figure. 6.9 Main Effects Plot for SN ratios-AR

Table 6.6 Effect rankings of four factors on all responses

	Depth of Penetration	Bead Width	Weld Area	Aspect Ratio
Depth of Defocus	4	4	4	2
Current	3	3	2	3
Scanning Speed	2	2	1	4
Frequency	1	1	3	1

Table 6.7 Optimal conditions for studied responses by Taguchi method (Numbers indicate the levels)

	Depth of Penetration	Bead Width	Weld Area	Aspect Ratio
Depth of Defocus	2	3	3	2
Current	3	2	2	3
Scanning Speed	1	3	3	1
Frequency	2	2	3	2

Table 6.7 summarizes the optimal levels of individual factors for all studied output variables. The optimum condition for all the responses is compromised as Level 2 of depth of focus, Level 3 of current, Level 3 of speed, and Level 2 of frequency, respectively. The Depth of Penetration for this set of parameters is predicted as 0.627 mm.

6.4.2 Uniform design

Classical experimental designs are mostly based on ANOVA-type models that typically involve main effects, interactions and random error. The preliminary experiment revealed main effects of laser welding process on weld profiles. When taking more factors and high-order effects into consideration, the number of parameters in the corresponding ANOVA-type model increases exponentially, as does the required number of experiments. In order to accurately predict the weld characteristics, numerical approximation models are required.

The uniform design (UD) concept, based on non-parametric regression models, significantly reduces the number of experiments by choosing experimental points of uniform scatter (Fang et al.,

2000). Experimental arrays in uniform designs are constructed by optimising the discrepancy of experimental points. Taking into consideration the average crack length in the die casting industry and the optimal condition concluded in the previous part, the ranges of experimental variables and arrangements were uniformly designed as shown in Table 6.8 and Table 6.9, respectively.

Table 6.8 Experimental variables and their ranges

Variables	Min Level	Max Level
Depth of Defocus, (mm)	-4	4
Current, (A)	80	120
Scanning Speed, (mm/s)	0.3	2.7
Frequency, (Hz)	2	10

Table 6.9 Experimental arrays of 9 different groups following uniform design method

No. of Sample	Factor A	Factor B	Factor C	Factor D
U1	7	8	9	7
U2	6	9	2	6
U3	7	1	3	3
U4	5	5	7	1
U5	8	3	8	5
U6	4	3	1	7
U7	1	6	8	8
U8	5	5	5	5
U9	2	1	5	6
U10	3	2	9	2
U11	6	2	6	9
U12	9	7	6	3
U13	3	7	3	9
U14	1	4	2	4
U15	4	9	7	4
U16	2	8	4	1
U17	8	6	1	2
U18	9	4	4	8

Experimental procedures leading to the measurements of weld profiles are identical to the previous step. The only difference is that this part considers a filler wire of 0.4 mm in diameter. The filler material is the same as 8407 supreme steel. The results regarding each uniform experimental trial were depicted in Table 10. The uniform design procedure then requires regression analysis to establish a regression model that fits the experimental data well.

Artificial Neural Network (ANN), a technique simulating the neural system of human beings, has the capability of modelling any given function. This advantage was taken in this paper to build regression models for weld profiles. Radial basis function (RBF) neural networks are feed-forward networks typically configured with a single hidden layer of units. They usually train much faster than back propagation networks and are less susceptible to problems with non-stationary inputs due to the behaviour of radial basis functions. RBF network based regression models for all the responses were established by MATLAB® R2013a m codes.

The generic structure of a RBF network involves three entirely different layers: the input layer, the hidden layer and the output layer. Radial basis functions relate the input layer to the hidden layer as follows:

$$y_j = \phi_j(\|X_i - C_j\|) \tag{6.1}$$

where X_i: the $i'th$ input vector on the input layer; $\phi_j(\cdot)$ is the selected radial basis function, such as the Gaussian function in this paper; y_j: the output of the j'th neuron on the hidden layer, $j = 0, 1, ..., m$, and $\phi_0 = 1$ (bias node); C_j: the centre vector of the j'th neuron on the hidden layer; and $\cdot$: the Euclidean distance. Then, the output of the mapping can be presented as linear combinations of these basis functions:

$$f(X_i) = \sum_{(} j = 0)^m w_j \phi_j(\|x_i - C_j\|) \tag{6.2}$$

where w_j denotes the connection weight between the hidden layer and the output layer.

RBF networks with 7 hidden neurons are selected to achieve good quality generalization while avoiding over-training. The parameters

of networks are optimized using Levenberg-Marquardt algorithm. After supervised learning, the weight and bias values of RBF network models for all responses are identified. The weld characteristics predicted by obtained RBF neural networks are also summarized in Table 6.10. According to the divergence of network model prediction from experimental measurements, established RBF neural network models have agreeable generalization of weld profiles.

Table 6.10 Performance characteristics and RBFNN predictions with respect to experimental trials

Weld No.	DP_{avg} (μm)	DP_{rbfnn} (μm)	BW_{avg} (μm)	BW_{rbfnn} (μm)	WA_{avg} (μm^2)	WA_{rbfnn} (μm^2)	AR_{avg}	AR_{rbfnn}
U1	135.5	142.2	1308.9	1290.5	315689	313740	0.103	0.102
U2	226.9	228.3	1062.5	1060.2	369770	359849	0.214	0.206
U3	109.3	102.7	651.4	654.6	240574	242013	0.168	0.176
U4	458.3	459.5	1187.3	1187.9	551587	558814	0.386	0.384
U5	293.2	288.6	1244.5	1254.9	375378	376043	0.236	0.244
U6	587.8	586.7	1473.3	1475.7	676466	664704	0.399	0.401
U7	504.5	500.4	1183.4	1205.4	582271	592817	0.426	0.425
U8	118.9	118.5	1066.5	1063.9	329706	328011	0.111	0.103
U9	55.0	56.8	201.8	201.7	7239	6706	0.273	0.274
U10	177.5	169.5	1388.6	1391.3	390837	384616	0.128	0.126
U11	277.5	276.8	1236.4	1239.7	416460	421732	0.224	0.225
U12	293.6	298.8	1029.7	1011.7	350308	348524	0.285	0.287
U13	238.1	245.8	1405.4	1407.8	434123	432642	0.169	0.170
U14	309.3	317.6	1010.5	1084.6	401101	418727	0.306	0.296
U15	485.0	484.2	1300.1	1286.4	630469	620544	0.373	0.374
U16	464.2	460.6	1132.2	1153.3	540078	538204	0.410	0.410
U17	328.4	337.4	1154.0	1123.9	463710	463014	0.285	0.284
U18	134.6	132.9	1204.2	1200.0	64834	62061	0.112	0.117

6.4.3 Validation runs

To verify whether the developed models are acceptable for prediction, extra experimental runs are necessary to compare the estimated responses and the observed ones. Table 6.11 lists the welding process parameters adopted for the validation runs. And the obtained experimental results and their corresponding predictions by RBF neural network models are depicted in Table 6.12. From the table, one can observe that the prediction errors (δ) of RBF networks at validation runs are relatively small. Table 6.11

Table 6.11 Parameter set for validation runs

Weld No.	Current (A)	Frequency (Hz)	Scanning Speed (mm)	Depth of Defocus (mm)
U19	80	10	2.1	-2
U20	85	9	1.2	1
U21	90	8	0.3	4
U22	95	7	2.4	-3
U23	100	6	1.5	0
U24	105	5	0.6	3
U25	110	4	2.7	-4
U26	115	3	1.8	-1
U27	120	2	0.9	2

Table 6.12 Experimental results of validation runs and their model predictions

Weld No.	DP_{avg} (μm)	DP_{rbfnn} (μm)	δ_{DP}	BW_{avg} (μm)	BW_{rbfnn} (μm)	δ_{BW}	WA_{avg} (μm^2)	WA_{rbfnn} (μm^2)	δ_{WA}	AR_{avg}	AR_{rbfnn}	δ_{AR}
U19	239.8	232.3	3.13%	1330.7	1351.5	1.57%	416270	413034	0.78%	0.180	0.184	2.05%
U20	262.9	262.0	0.34%	1324.2	1286.1	2.88%	431994	429169	0.65%	0.199	0.200	0.96%
U21	547.0	546.0	0.18%	1246.7	1239.3	0.59%	438552	435624	0.67%	0.439	0.439	0.00%
U22	143.9	148.5	3.16%	1480.1	1487.9	0.52%	351636	359915	2.35%	0.097	0.103	5.67%
U23	329.9	317.6	3.73%	1115.0	1084.6	2.73%	450701	418727	7.09%	0.296	0.296	0.22%
U24	403.0	408.8	1.42%	1134.5	1125.5	0.80%	490613	493092	0.51%	0.355	0.352	0.88%
U25	172.2	177.1	2.86%	1515.9	1513.6	0.15%	376740	383164	1.71%	0.114	0.104	8.05%
U26	134.8	127.3	5.58%	1382.9	1378.3	0.34%	346257	342787	1.00%	0.097	0.098	0.89%
U27	397.9	395.8	0.52%	1267.7	1278.1	0.82%	496069	493966	0.42%	0.314	0.316	0.78%

6.5 Heat source calibration

Heat input model is one important part when carrying out welding simulations. The interaction of a heat source (arc, electron beam or laser beam) with a weld pool remains a complex physical phenomenon due to the arc digging and stirring, thus still cannot be modelled rigorously. Welding analysts have been devoted much of their effort to developing different heat source models that could describe the shape of the weld and the temperature field in the workpiece.

It is significant to accurately define the parameters associated with the mathematical description of the heat source because all simulations in Computational Welding Mechanics (CWM) consider only thermo-mechanical phenomena in the weld and incorporate all the physics of the welding processes into empirical heat input models (Deshpande et al., 2011; Lindgren, 2007). Thus the heat source model must be calibrated so that the simulations yield results closely correlating with the experimental data. After calibration, the

parameters of the heat source can be used for transient analysis (Deshpande et al., 2011).

6.5.1 Heat source model for laser welding

The proposed heat input models in literature range from point source model, disc model, Gaussian heat source model to ellipsoidal power density distribution (Goldak and Akhlaghi, 2005; Klobčar et al., 2004; Lindgren, 2007). For laser and electron beam welding processes which have a comparatively concentrated energy distribution and deep penetration, a conical heat source with uniform heat flux as some Gaussian distribution may yield more accurate results (Goldak and Akhlaghi, 2005; Lindgren, 2007). The heat flux with a Gaussian distribution was represented as

$$q(r) = q(0)\exp(-cr^2) \tag{6.3}$$

where $q(0)$ is the maximum heat flux, c is the concentration coefficient and r the radial distance of a point from the symmetric heat source axis.

The major problem then becomes the determination of heat flux distribution along the thickness. Analyses suggest that the laser beam power decreases with increasing penetration depth. Different shapes along the depth are considered in laser beam heat source models to account for this effect. In this study, Goldak ellipsoidal power density distribution is considered for laser welding modelling (Figure 6.10 and Figure 6.11):

$$q(r,z) = \frac{6\sqrt{3}\eta Q}{\pi\sqrt{\pi}r_0^2 H}\exp\left(-\frac{3r^2}{r_0^2} - \frac{3z^2}{H^2}\right) \tag{6.4}$$

where η is the energy absorption efficiency, Q the laser power, r_0 the radius of the heat source, and H the depth of the heat source, respectively.

6.5.2 Calibration process

The calibration of heat source is performed by comparing fusion zone temperature contour plots from simulation with the corresponding weld macrographs. Experimental tests were carried out to remelt workpieces with 100×100×7.5mm in size, made of 8407 supreme hot work steel, under the experimental conditions listed in Table 6.13. Weld profiles were then prepared by sectioning the weld trajectory in transverse direction. While in the simulation, weld macrographs were defined by the contour of material melting temperature, i.e. 1447$^{\circ}C$.

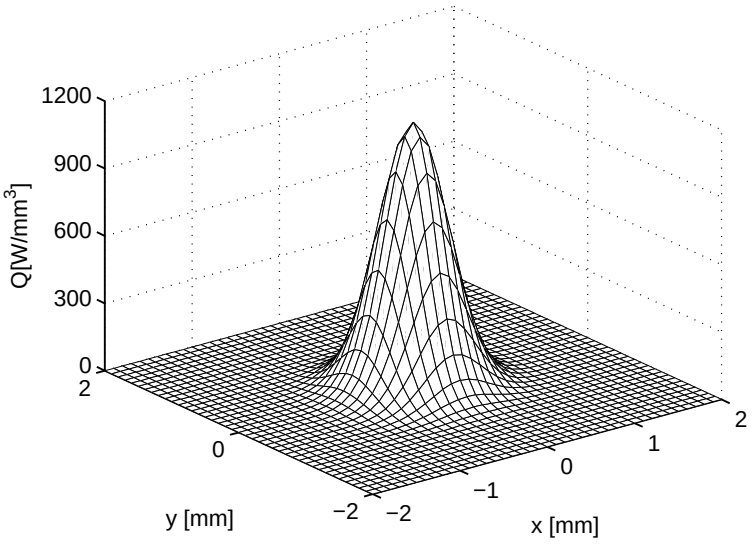

Figure. 6.10 Heat source power distribution at the top surface

An interaction between MATLAB® and ABQUS® was built to calibrate the laser heat source model, as the flow chart indicates in Figure 6.12. Figure 6.13 shows the analysis model and moving direction of the pulsed laser beam. Due to geometric symmetry, only half the plate was used to reduce the simulation computation

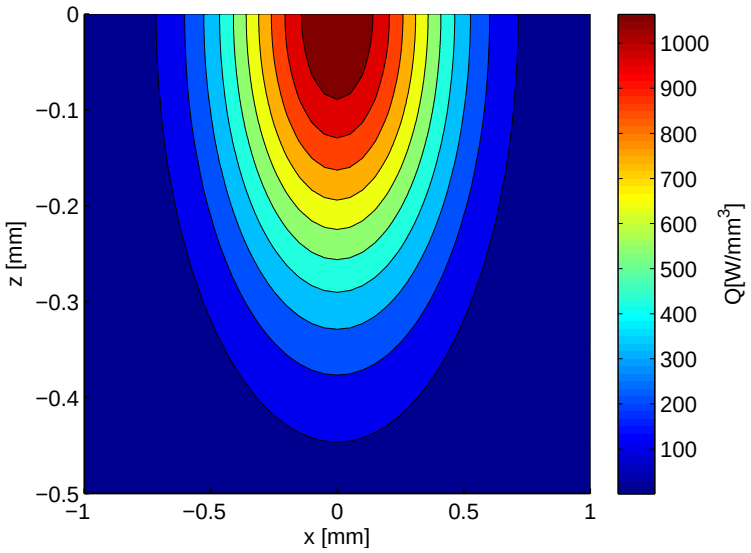

Figure. 6.11 Heat source power distribution in cross section

time. A fine mesh was used for areas in contact with the laser beam since they experienced a complicated thermal sequence of momentary heating and cooling. A subroutine was created to define the shape and motion of laser beam heat source. And the the laser pulse was simulated with fixed average beam power of the welding condition.

The boundary conditions for the simulation include the heat input condition of the laser beam, and convection and radiation of surfaces exposed to the air. The thermal properties in this simulation were also considered temperature-dependent. Some properties of hight temperatures in literature were used.

Table 6.14 shows the calibration result of the laser heat source model. An obvious comparison can be made through the weld profiles obtained by the simulation and experimentation, as depicted in Figure 6.14. The final parameters of the heat source model for studied welding conditions are summarised in tab:Parameters calibrated for laser heat source models in welding.

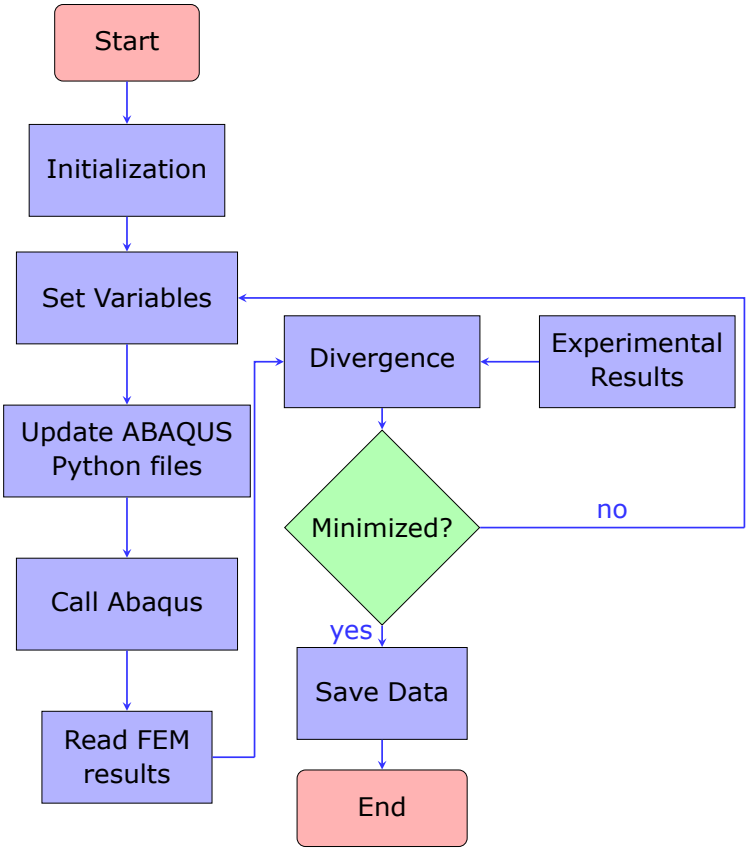

Figure. 6.12 Heat source calibration flow chart

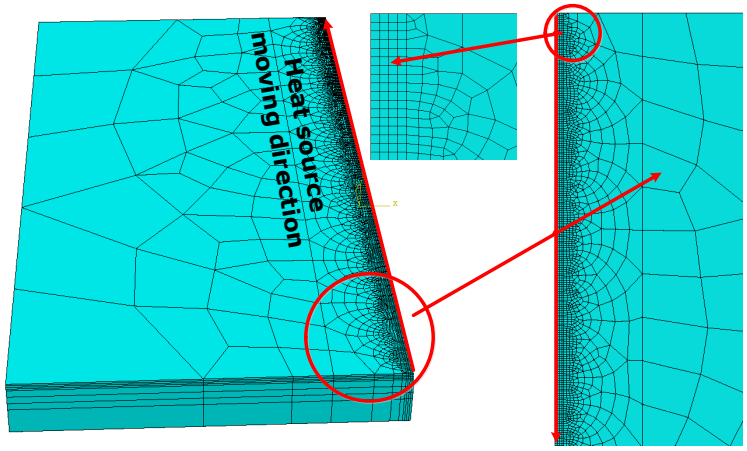

Figure. 6.13 Half model of the plate for heat source calibration

Table 6.13 Process parameters used for heat source calibration of laser welding

Weld No.	Current (A)	Depth of Defocus (mm)	Scanning Speed (mm/s)	Frequency (Hz)
1	80	-2	0.9	10
2	95	-3	0.6	7
3	110	-4	0.3	4
4	125	-1	0.3	10

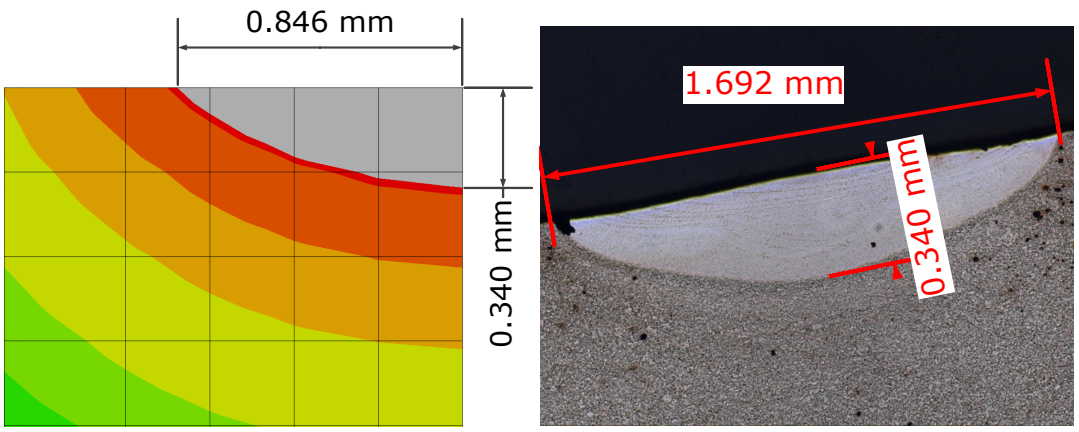

(a) Simulated (b) Measured

Figure. 6.14 Weld macrograph simulated for parameters (80A, -2mm, 0.9mm/s, 10Hz)

Table 6.14 Results for heat source calibration of laser welding

Weld No.	Measured weld width (mm)	Measured weld depth (mm)	Simulated weld width (mm)	Simulated weld depth (mm)
1	1.6928	0.3403	1.6920	0.3401
2	1.8034	0.3315	1.8032	0.3315
3	1.9320	0.2776	1.9319	0.2771
4	1.8842	0.6884	1.8833	0.6877

Table 6.15 Parameters calibrated for laser heat source models in welding

Weld No.	Current (A)	Depth of Defocus (mm)	Scanning Speed (mm/s)	Frequency (Hz)	η	r_0	H
1	80	-2.0	0.9	10	0.1292	1.879	0.1925
2	95	-3.0	0.6	7	0.1490	2.143	0.1876
3	110	-4.0	0.3	4	0.1980	2.962	0.1490
4	125	-1.0	0.3	10	0.0935	1.697	0.8255

6.5.3 Mathematical models for Goldak parameters

To simulate laser welding of conditions outside studied sets, it is necessary to build mathematical models correlating heat source model parameters and laser welding conditions. Since the scanning speed and frequency were already considered in the simulation, the task of mathematical modelling is to create maps between the other two variables i.e. laser beam power and depth of defocus, and three heat source parameters (efficiency, radius and depth).

A correlation matrix was proposed using IBM SPSS Statistics 22, as shown in Table 6.16, to investigate the correlations among these variables. From Table 6.16, one can find that efficiency and depth are correlated with both depth of defocus and laser beam power, while the laser source radius is further relevant to depth of focus rather than beam power. For simplicity, the parameters of heat source model were assumed to be one-variable dependent. The mathematical models were constructed using the curve estimation in IBM SPSS Statistics 22 environment.

Table 6.16 Pearson correlation of heat source model variables

	D_f	P_a	η	r_0	H
D_f	1.000	0.903	-0.987*	-0.938	0.808
P_a	0.903	1.000	-0.891	-0.755	0.981*
η	-0.987*	-0.891	1.000	0.969*	-0.786
r_0	-0.938	-0.755	0.969*	1.000	-0.613
H	0.808	0.981*	-0.786	-0.613	1.000

*. Correlation is significant at the 0.05 level (2-tailed).

η **vs** D_f

The absorption efficiency of laser beam, η, is considered dependent on the depth of defocus, D_f, because they are statistically significantly correlated. Figure 6.15 shows the estimated curves for the relationship between the efficiency η and depth of focus D_f and the fitted models are summarised in Table 6.17. To obtain a model statistically confident while avoiding overfitting, the relationship between η and D_f is best built up by an exponential function:

$$\eta = b_0 \times \exp(b_1 \times D_f) \tag{6.5}$$

where $b_0 = 0.075528$ and $b_1 = -0.239350$.

Table 6.17 Model summary of curve estimations for η vs D_f

Equation	R Square	F Value	Significance
Linear	.974	76.128	.013
Quadratic	.982	27.525	.134
Cubic	1.000		
Exponential	.981	102.598	.010

r_0 **vs** D_f

The heat source radius of laser beam, r_0, is considered dependent on the depth of defocus, D_f as well. Figure 6.16 shows the estimated curves for the relationship between the radius r_0 and depth of focus D_f and the fitted models are summarised in Table 6.18. The relationship between r_0 and D_f is then modelled by a quadratic function:

$$r_0 = b_0 + b_1 \times D_f + b_2 \times D_f^2 \tag{6.6}$$

where the constants $b_0 = 1.9513$, $b_1 = 0.390$ and $b_2 = 0.1592$.

Table 6.18 Model summary of curve estimations for r_0 vs D_f

Equation	R Square	F Value	Significance
Quadratic	.988	41.327	.109
Cubic	1.000		

H **vs** P_a

According to the correlation matrix, the heat source depth of laser beam, H, is considered dependent on the average laser power, P_a. Figure 6.17 shows the estimated curves for the relationship between the radius H and depth of focus P_a and the fitted models are summarised in Table 6.19. The relationship between H and P_a is determined by an exponential function:

$$H = b_0 \times \exp(b_1 \times P_a) \tag{6.7}$$

where $b_0 = 0.056454$ and $b_1 = 0.001$.

Table 6.19 model summary of curve estimations for H vs P_a.

Equation	R Square	F Value	Significance
Cubic	1.000	1775.345	0.017
Exponential	0.987	157.631	0.006

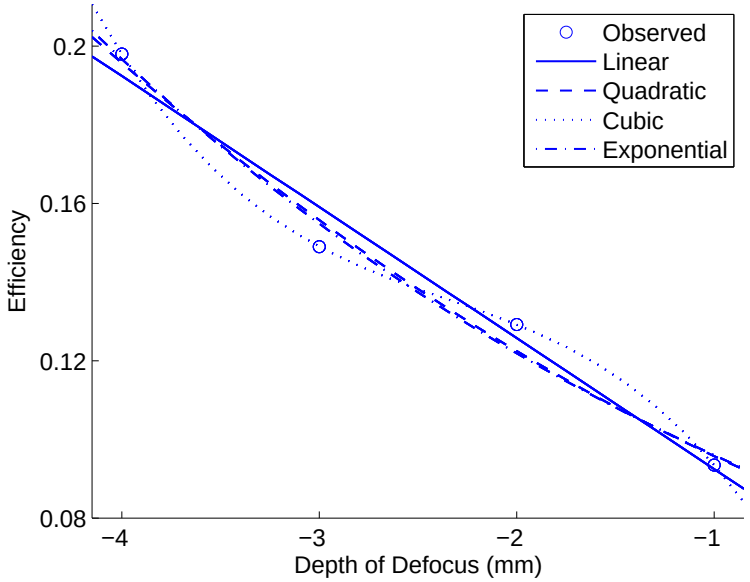

Figure. 6.15 Curve estimation of the relationship between η and D_f.

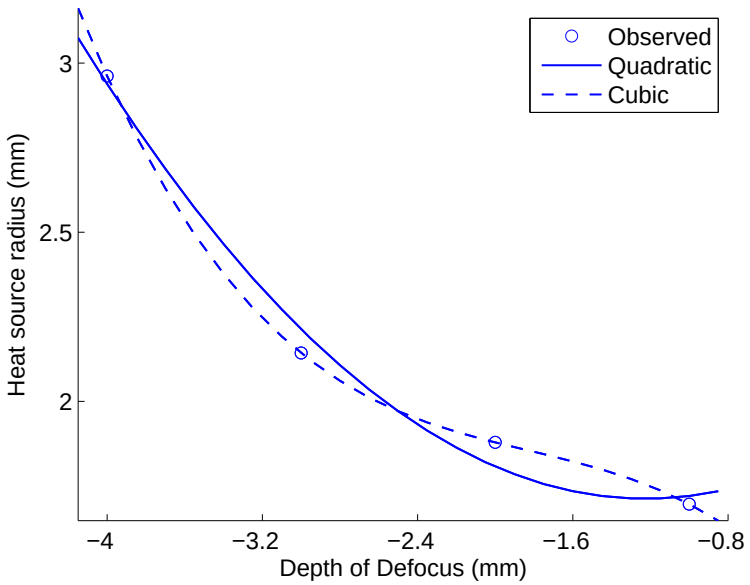

Figure. 6.16 Curve estimation of the relationship between r_0 and D_f.

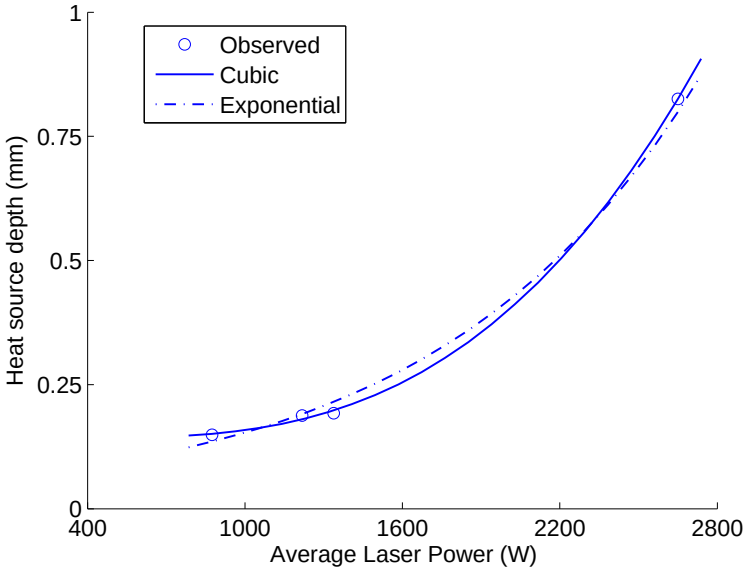

Figure. 6.17 Curve estimation of the relationship between H and P_a.

6.6 Summary

Weld profile characteristics are important information because they are strongly related to the mechanical strength of welded areas. This chapter firstly studied this significant point by designing a sequential set of experiments using Taguchi method and Uniform Design. Weld profiles, characterised by depth of penetration, bead width, weld area and aspect ratio, were modelled utilising Radial Basis Function Neural Networks.

With the weld characteristics models, it is convenient for remanufacturer to identify an optimal set of welding parameters for remanufacturing. To predict the effect of the process on the service life of remanufactured dies and moulds, it is necessary to conduct a numerical simulation to take residual stresses due to remanufacturing activities into consideration.

Heat source model is one of important parts regarding laser welding simulation. In this chapter, the heat source model is calibrated by comparing finite element simulated weld profiles with

measured experimental counterparts. Three parameters dominating the popular Goldak Ellipsoidal model were modelled using mathematical expressions, respectively. This then enables the calculation of residual stress introduced by laser welding process.

Chapter 7

Residual life assessment

7.1 Introduction

Remanufacturing process such as laser welding introduces new variation to the prediction of thermal fatigue life. Therefore, the effect of remanufacturing processes must be identified, thereby resulting in an corrected thermal fatigue model for life assessment of dies and moulds after remanufacturing process. This chapter regards residual stresses as the effect of laser welding process and updates thermal fatigue life model of die material correspondingly.

The first part of this chapter describes the experimental detail, followed by the numerical part which was used to calculate residual stresses of test specimens after laser welding. Thermal fatigue life model proposed in Chapter 5 was then corrected by considering the effect of residual stress. And lastly, the updated model was verified by extra simulation and experiment.

7.2 Experimental testing

Test specimens were also heat treated to achieve 54HRC as in the Chapter 5, with the dimensions of 20×20×5mm. The notch free

samples were then laser welded at centre lines of both sides. Laser welding processing was carried out when the sample was totally cooled down to ambient temperature so that the interaction between two laser welding procedures can be neglected. Extra material above two side surfaces were eliminated by mechanical polishing using a semi-automatic grinding and polishing machine BUEHLER AutoMet™. Notches were EDM cut to achieve same geometries as re-shown in Figure 7.1.

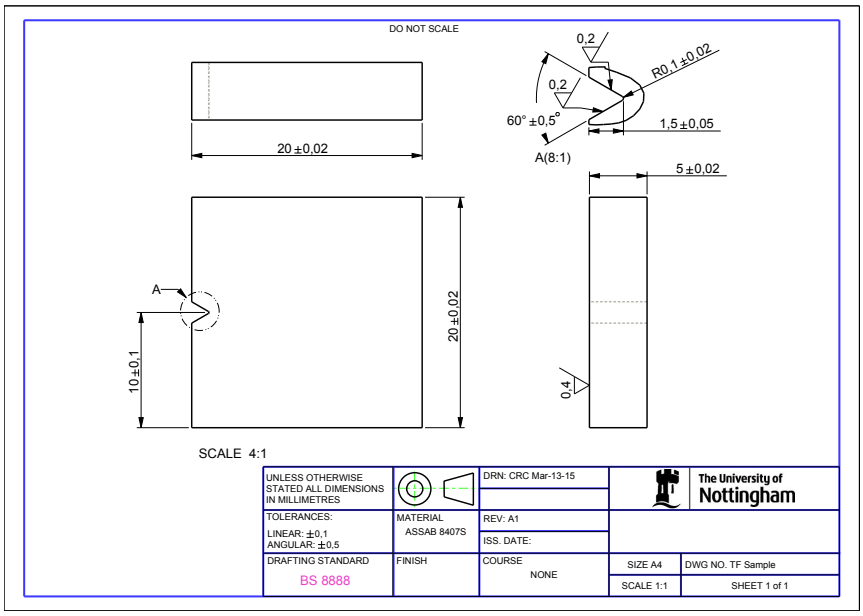

Figure. 7.1 Schematic diagram of thermal fatigue testing sample

The procedures of thermal fatigue tests were kept in consistence with the previous investigation. Same experimental runs i.e. six test conditions, were arranged for this part as in the thermal fatigue assessment section. The arrangement is re-illustrated here in Table 5.2 and Table 5.3. The process parameters for laser welding centre lines of samples are tabulated in Table 7.1.

Table 7.1 Laser welding parameters for thermal fatigue samples

Parameters/Set	1	2	3	4
Current, (A)	160	130	105	120
Depth of focus, (mm)	-2	-1	-1	-2
Scanning speed, (mm/s)	0.9	0.6	0.6	0.6
Frequency, (Hz)	2	5	9	2

7.3 Calculation of residual stresses

With heat source model calibrated in the previous chapter and the material properties of die material ASSAB 8407 Supreme, it is ready to establish finite element models to simulate laser beam welding and calculate residual stresses.

7.3.1 Modelling methodology

Calculation of residual stresses of laser welded samples was conducted by sequentially coupled thermo-mechanical simulations using FE package ABAQUS®. Calculation processes should be carried out according to the experimental processing of samples. Therefore, laser welding simulations were conducted twice. And the results from first simulation were imported into the next one if necessary. Each calculation consists of two analyses, i.e. thermal analysis and structural analysis. Temperature profiles were firstly computed in the thermal analysis and then exported into the mechanical counterpart for calculation of stresses afterwards. And for the second simulation, residual stresses obtained from the first simulation were also used as initial state of second analysis.

Thermal analysis is divided into two steps: heating and cooling. The former step models the application of laser heat source to the sample while the latter one simulates cooling process after the sample is heated up. The laser is assumed to heat the sample along the centre line from the top edge till the position 5 mm from the bottom. To facilitate computation, only highlighted area, as shown in Figure 7.2, are taken as laser heated region. Goldak heat source model was implemented to calculate volumetric heat flux due to the laser. It is finite elementally accomplished by developing the User Subroutine DFLUX. Cooling, mainly due to convection between sample and ambient air, was assigned until no variation in sample temperature was observed. The temperature transients of thermal model was finally output for the structural analysis.

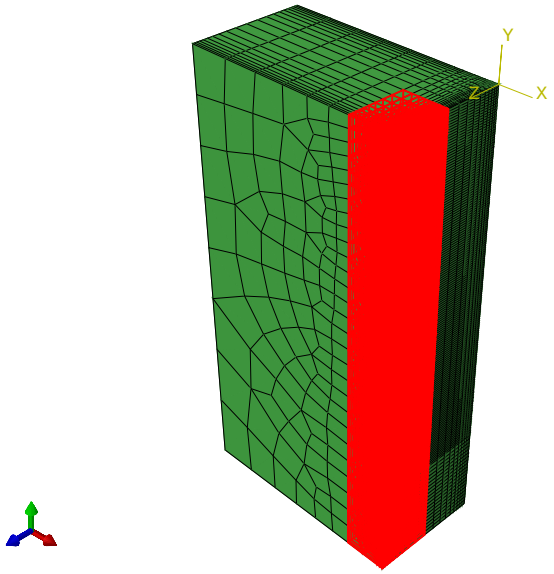

Figure. 7.2 Heat source region considered in laser welding process

In mechanical analysis, only one step was used to calculate the residual stress. The sample is assumed to be of ambient temperature initially. Temperature transients obtained from thermal analysis was then defined as predefined field. Boundary conditions in the symmetrical planes and positions with constant displacement need

be defined. Thermal and mechanical properties of die material ASSAB 8407S were considered here, respectively.

7.3.2 Meshing

Test samples were half modelled by 36,300 hexahedral elements, as shown in Figure 7.3a. The meshing was refined in the laser heating region as well as the outer surfaces in order to capture thermal gradients. The smallest element used is of dimension $0.1 \times 0.1 \times 0.1$ mm. Detail of the refinery is illustrated in Figure 7.3b and Figure 7.3c.

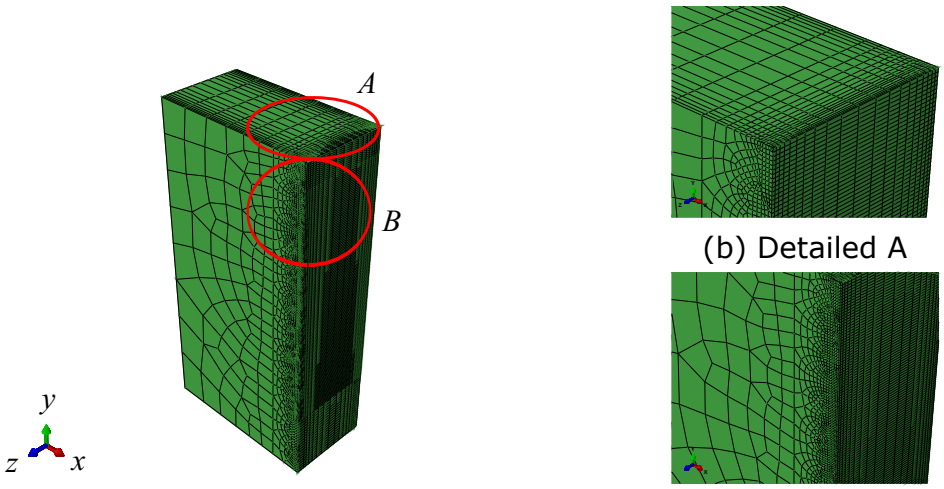

(a) Meshing (b) Detailed A (c) Detailed B

Figure. 7.3 Mesh of half test sample for laser welding

7.3.3 Boundary conditions

Boundary conditions were specified for thermal and mechanical analysis, respectively. For thermal analysis, the symmetrical YZ plane of the specimen was considered free from heat flux. Convection was defined by temperature-dependent heat transfer coefficient to model the heat transfer between the sample and ambient air. All the surfaces except the symmetrical plane were considered as illustrated in Figure 7.4.

For the structural analysis, since the sample was free to deform on the work table when being laser welded, only fundamental constraints were considered. Specifically, the symmetrical YZ plane was restrained in x axis. Displacement in the y axis was fixed at the top back point while in the z-axis, the displacement was constrained at both the top back point and the bottom back point, as depicted in Figure 7.5. For the second welding process, i.e. welding the rear side, the constraints in the y and z axes were applied to the top front and bottom front points correspondingly.

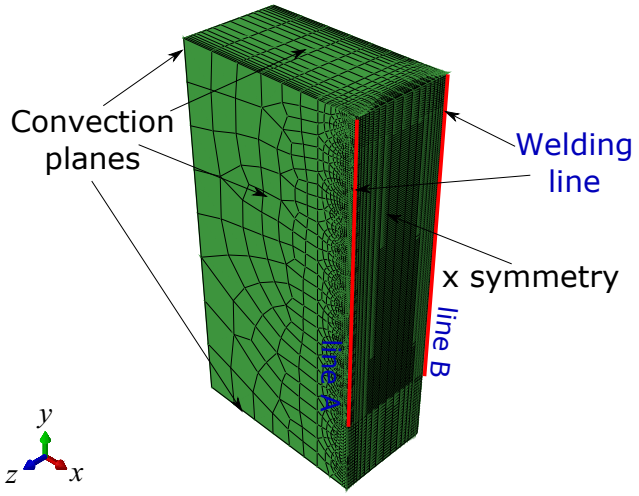

Figure. 7.4 Boundary conditions for thermal analysis of laser welding

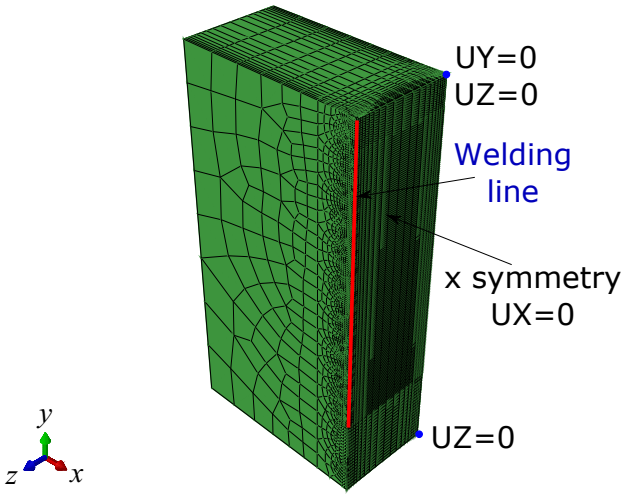

Figure. 7.5 Boundary conditions for structural analysis of laser welding

7.4 Correction of thermal fatigue model

This section is to take into consideration the effect of laser welding on thermal fatigue model established in the previous chapter. Since the preparation of both welded and non-welded specimens is similar. The variation of the fatigue strength observed in the repaired specimens must be due to other factors such as filler material mechanical properties, residual stresses or welding defects. However, the repaired specimens, tested at , present a similar fatigue resistance to the correspondent non-welded specimens tested at the same condition. Therefore, residual stresses are probably the main factor affecting the fatigue behaviour (Borrego et al., 2009).

7.4.1 Residual stress

Residual stresses were calculated from the FEM of laser welding process. For simplicity, von Mises stress was used for revealing the effect of residual stress. The von Mises stress or equivalent stress, σ_v, is defined as follows:

$$\sigma_v = \sqrt{(\frac{\sigma_{11}-\sigma_{22})^2+(\sigma_{22}-\sigma_{33})^2+(\sigma_{33}-\sigma_{11})^2+6(\sigma_{12}^2+\sigma_{23}^2+\sigma_{31}^2)}{2}}$$
$$= \sqrt{\frac{(\sigma_1-\sigma_2)^2+(\sigma_2-\sigma_3)^2+(\sigma_3-\sigma_1)^2}{2}}$$

where $\sigma_{ij}, i, j = 1, 2, 3$ are stress components, and $\sigma_k, k = 1, 2, 3$ are three principal stresses.

Also, stress relaxation due to EDM cutting of notch and polishing is considered negligible compared to the retained residual stress.

Figure 7.6 and Figure 7.7 plot the von Mises stresses retained in the sample (both Line A and Line B) after laser welding. From two figures, we can find that residual stresses along Line A are comparably small to those along Line B. Therefore, for correction

of thermal fatigue life model. The retained stresses at the back surface (Line A) could be neglected. From Figure 7.7, it can be found that residual stresses increase from zero at the starting and ending points of welding and peak at around the centre of welding trajectory. This is in good agreement with general distribution of welding residual stresses. Therefore, the calculation of residual stresses could be assumed viable.

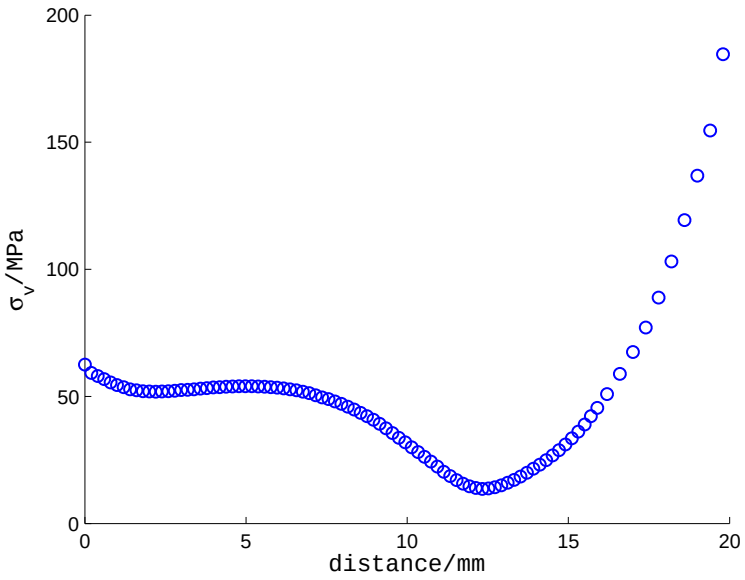

Figure. 7.6 FEM von Mises stress along line A after 2nd welding

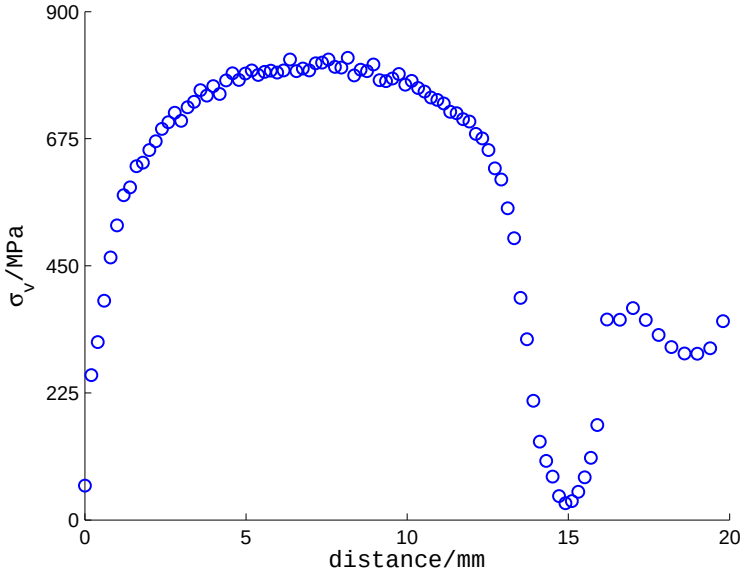

Figure. 7.7 FEM von Mises stress along line B after 2nd welding

Residual stresses of material points where crack propagation was observed were linearly interpolated. The plastic energy density was calculated using the same method as in Chapter 5. The final data for correcting thermal fatigue model is tabulated in Table 7.2. Figure 7.8 shows the N_f vs ΔP curves for two sides under the same test condition of N1. From the plot, it is obvious that crack propagation of two sides are different. Cracks were observed at material points experiencing higher plastic energy density per cycle. This again suggests the loss of fatigue strength in welded samples.

Table 7.2 Thermal fatigue data for life model correction

No	σ_v	ΔP	N_f
1	52.62	0.5650	800
2	52.52	0.4560	1200
3	52.28	0.3083	1600
4	52.10	0.2383	2000
5	52.00	0.2159	2400
6	637.53	0.4688	800
7	635.43	0.2854	1200
8	634.10	0.2420	1600
9	633.95	0.2241	2000
10	650.98	0.2022	2400

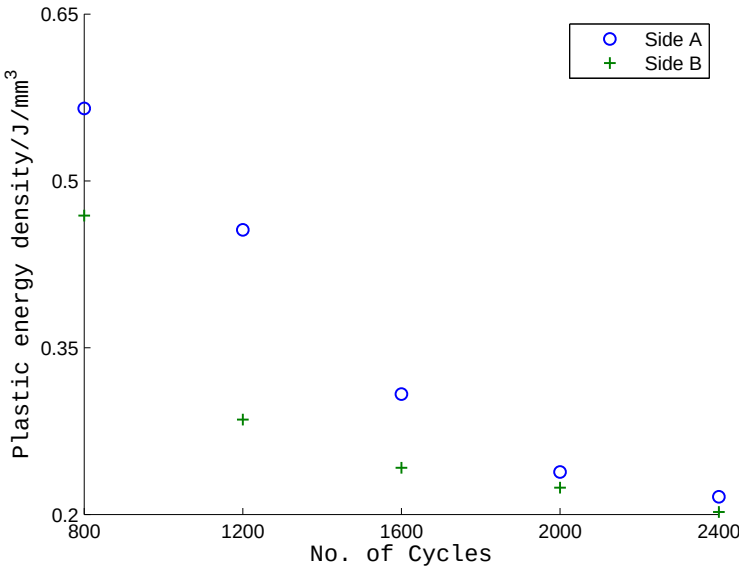

Figure. 7.8 Comparison of $N_f - \Delta P$ curves for two sides

7.4.2 Fitting of thermal fatigue model regarding weld

The correction of thermal fatigue life model was conducted via MATLAB® computing program. From Figure 7.8, it can be concluded that the function of $N_f(\sigma_v, dP)$ should still keep a power relation. And since the only variation in new model should be due to the induction of residual stress, the power function should be similar to that in the uncorrected model. Therefore, the life model without consideration of weld was corrected in the fashion as shown in Equation 7.1.

$$N_f = a + b \cdot \sigma_v + 61.38 \cdot (\Delta P)^c \tag{7.1}$$

where a, b and c are coefficients need be fitted. The constant 61.38, is taken from Equation 5.6 to retain a similar power relation. Equation 7.1 can be re-written in the following way for comparison to Equation 5.6.

$$N_f = a + b \cdot \sigma_v + 61.38 \cdot (dP)^{-2.412+d} \tag{7.2}$$

with

$$d = c + 2.412$$

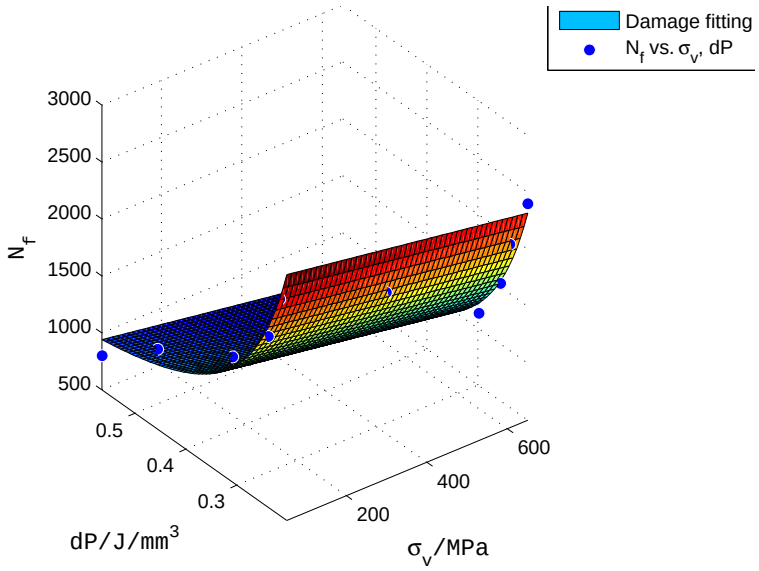

Figure. 7.9 Fitting of thermal fatigue damage with weld

The coefficients fitted are tabulated in Table 7.3 and the comparison of model surface and experimental data is made in Figure 7.9. From the figure, it can be observed that the fitted model is in small divergence from the experimental data. The R-square value of the fitting is 0.9698 and adjusted R-square value is 0.9612, which indicate fairly good fitting of experimental data. The coefficient $d = c + 2.412 = 0.256$ is close to zero. This proves that the major variation results from the von Mises residual stress.

Table 7.3 Thermal fatigue model correction results

Coefficient	Value	95% confidence bounds
a	760.5	(591.5, 929.5)
b	-0.566	(-0.8788, -0.2532)
c	-2.156	(-2.247, -2.064)

7.5 Verification of thermal fatigue model

The verification of corrected damage model was accomplished by conducting another fitting using another set of experimental data. The data for model fitting, as illustrated in Table 7.4, were calculated from the test condition N2. The difference in test conditions results in different crack propagation data, thereby different plastic energy densities.

The R-square value for the verification is 0.9661 and adjusted R-square is 0.9564. This suggests that the fitted model is a good explanation of experimental data. Comparison of fitted model and experimental data is shown in Figure 7.10. The coefficients of verification fitting were depicted in Table 7.5.

Comparing with the correction results, it can be found that the verification coefficients all lie in the 95% confidence bounds of correction coefficients. This demonstrates a good generalization of the corrected fatigue life model.

Table 7.4 Thermal fatigue data for verification

No	σ_v (MPa)	ΔP	N_f
1	52.68	0.7003	800
2	52.52	0.4570	1200
3	52.36	0.3673	1600
4	52.19	0.2805	2000
5	52.09	0.2564	2400
6	643.45	0.6492	800
7	626.74	0.3445	1200
8	637.45	0.2844	1600
9	633.03	0.2565	2000
10	633.90	0.2447	2400

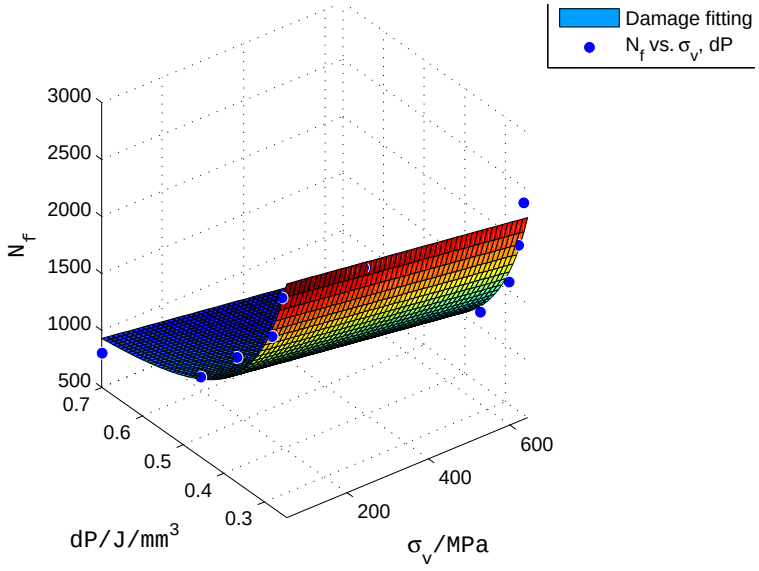

Figure. 7.10 Verification of corrected thermal fatigue damage model with weld

Table 7.5 Thermal fatigue model verification fitting results

Coefficient	Value	95% confidence bounds
a	812.2	(635.4, 988.9)
b	-0.5016	(-0.8326, -0.1707)
c	-2.387	(-2.498, -2.276)

7.6 Summary

This chapter investigates the effect of residual stress due to laser welding on the thermal fatigue behaviour of die material. The experiment detail was firstly introduced, followed by the numerical part used for calculation of residual stresses retained in test specimens after laser welding processing. The variation of thermal fatigue strength was then explained by correcting the fatigue life model previously established. Lastly, verification fitting was carried out to understand the generalization of corrected model. The verification fitting has a similar R-square(0.9661) and all coefficients fall in the

bounds of 95% confidence of corrected coefficients. Therefore, it can be concluded that the correction model has good generalization and is flexible for thermal fatigue life prediction.

Chapter 8

Conclusions and future work

8.1 Introduction

Increased pressure from the legislation and environmental challenges has forced manufacturers to implement sustainable measures. To make a step change in practice, the entire life cycle of a product from extraction of raw materials, through manufacturing, product use and final disposal need be considered. Remanufacture, due to its economic and ecological benefits, has been applied in a number of industries.

The conventional life cycle of dies and moulds is not eco-efficient, which shows great potential for the application of remanufacture. The essence of remanufacturing activity is to ensure the quality of remanufactured products. Therefore, development of life evaluation technology has become a fundamental part for carrying out remanufacture of dies and moulds.

A numerical based methodology was proposed for assessing thermal fatigue life of dies and moulds after remanufacturing processing, such as laser welding. Optimization of remanufacturing process was also conducted as well as numerical methodology for predicting residual stresses. The predictions made by the methodology were in relatively good agreement with experimental measurements.

The assessment method presented represents a starting point towards developing accurate models for the life prediction of dies and moulds with resepct to thermal cracking. Die makers and operators may benefit from this method for obtaining useful life data for their die operations.

8.2 Research contributions

A computational method has been developed for evaluating remaining useful life of thermal fatigued dies and moulds after remanufacturing by laser welding. In the developed approach, an energy based life model is proposed and established for the mould material with consideration of cycling period. The effect of residual stresses due to laser welding is also identified in the developed approach.

Potential benefits can be rendered for die designers and users in following manners.

- The energy based life approach enables die designers to predict thermal life of both crack initiation and propagation. Conventional methods frequently only consider thermal cracking life at a subjectively defined length, which is not in accordance with industrial observations. The incorporation of two stages of cracking in the energy based life enhances life evaluations without any initiation length assumptions.

- Remanufacturers are capable of predicting remaining useful life of dies and moulds after remanufacturing process. The evaluation of remaining useful life would facilitate management of remanufactured dies and moulds. Based on the results, remanufacturers are able to make decisions on the warranty of their products.

- The life approach can also be used for optimization of remanufacturing process. The computational life evaluation approach could also play a key role in optimization laser welding process to obtain the most appropriate parameters for designated life. The optimization process will also be cost and labour saving.

8.3 Extension to industrial applications

The life assessing methodology developed in this thesis has investigated two major aspects, residual stress due to remanufacturing process and thermal fatigue life model. Both are established based on the designed die sample. Even though that the die sample is representative of real die casting dies, they are naturally simple compared to real complex die geometries. Furthermore, loading conditions of real dies and moulds have also been simplified for experimenting purpose. To extend the approach to real dies and moulds, sources of inaccuracies during the life evaluation procedure should be stringently controlled. The following section discusses the differences between the results obtained from the research and real applications.

The first step is to calculate residual stresses of failed die halves due to remanufacturing process. In the research, simulations were conducted on the test sample which is not difficult to obtain extreme fine meshing at the vicinity of laser heat source. Laser welding repair was also conducted along the central lines. Furthermore, laser surfacing was assumed for the process of welding repair to ignore the effect due to re-machining. This only applies to the case that extreme fine polishing process is applied for removing extra materials.

However, complex die geometries would require more devotion to finite element meshing of fine geometry features. In addition, the real three dimensional geometries are also different from the line welding case in the research. And the machining process after laser welding should also be identified to account for its effect on residual stress distribution. Extra effort need be paid to avoiding computation divergence and obtaining acceptable accuracy. Therefore, inaccuracies of real life evaluations may occur due to the insufficient refining of meshing in critical features of die halves, simple processing of machining and inappropriate configuration of computations.

Then, loading conditions of die halves are to be modelled. In the thesis, only thermal loads are considered because they are the most critical factor that causes thermal cracks in die casting dies. During a typical die casting cycle, there are a certain set of mechanical loads that undoubtedly affect the performance of die halves. The clamping is applied on the toggle location to keep die halves in contact during the injection and dwell stages. For well adjusted die halves, the clamping pressure is small and constant, but non-uniform. After the filling of die cavity is completed, another mechanical load-intensification pressure is exerted on the molten metal to guarantee filling of intricate regions in the cavity and avoid porosity in castings. The dynamic effect of the pressure has been identified as the cause of flashing problems. It is the combined effect of all these loads that leads to various die failures. To accurately model the work loadings experienced by the die halves, it is preferable taking all these loads into account. Fluid-structure interaction (FSI) is necessarily implemented to investigate the effect of metal flow on the die halves. Furthermore, the solidification process of casting molten metal need also be modelled to capture

varying temperature profiles of casting. Any simplifications of the die casting process and loadings will cause a compromise in computation accuracies.

The last step is to predict remaining useful life using established life model. Functioning as one property, the life model obtained in the thesis is also applicable for the assessment of real dies and moulds. However, the models should be identified specifically for other mould steels. Numerical errors in computing stress-strain fields for establishing the life model are the major source of inaccuracies.

8.4 Conclusions

In the thesis, a numerical life evaluation technique has been established to assess thermal fatigued dies and moulds after remanufacturing by laser welding. The advantage of this assessing method is its numerical feature. Because dies and moulds are usually product specific and one off, numerical method is advantageous over experimenting methods which usually needs specific configurations for different products and die geometries. Another advantage of this approach is that crack initiation and propagation are integrated as a unified form in the developed method. Therefore, it offers straightforward evaluations without conducting computing intensive cracking simulations. Based on all the results obtained in previous sections, the following conclusions can be drawn:

- By investigating thermal equilibrium, representative geometry is presented for real dies and moulds. It is found that thermal equilibrium of die half is correlated to the ratio of cavity

dimension to die dimension. The critical ratio can be used as reference for design of general die halves.

- Thermal fatigue life of die material was modelled by an energy based life approach with consideration of test period. Compared to conventional strain life approach, the energy life approach has enabled prediction of crack initiation and propagation within a unified expression.

- Residual stresses due to laser welding were explained as a linear effect in the established life model. The corrected life model has extended conventional life approaches to being capable of accounting for residual stresses after laser welding.

8.5 Future work

The following works should be considered in the future for further investigation:

(a) In the calculation of residual stresses retained in test samples were assumed to be not significantly affected by the machining of notch and polishing. This assumption is actually conservative. And therefore, residual stresses in test samples are overestimated. More accurate calculation should be carried out to investigate the relaxation of residual stresses due to cutting and polishing.

(b) In this work, life assessment was undertaken to the designed test samples rather than real dies and moulds. The variations in structures, working conditions and surroundings may affect the application of proposed models. Therefore, further study of the feasibility should be considered.

References

Abachi, S., Akkök, M., and Gökler, M. I. (2010). Wear analysis of hot forging dies. *Tribology International*, 43(1-2):467–473.

Alblas, A. D. K. J. B. (1969). *Thermoelasticity: basic theory and applications*. Groningen: Wolters-Noordhoff.

Allwood, J. and Cullen, J. (2011). *Sustainable Materials - with Both Eyes Open: Future Buildings, Vehicles, Products and Equipment - Made Efficiently and Made with Less New Material*. UIT Cambridge, London.

Altan, T., Lilly, B., and Yen, Y. C. (2001). Manufacturing of dies and molds. *CIRP Annals - Manufacturing Technology*, 50(2):404–422.

Amaya, J., Zwolinski, P., and Brissaud, D. (2010). Environmental benefits of parts remanufacturing: the truck injector case. In *17th CIRP International Conference on Life Cycle Engineering*.

Amelia, L., Wahab, D. A., Che Haron, C. H., Muhamad, N., and Azhari, C. H. (2009). Initiating automotive component reuse in malaysia. *Journal of Cleaner Production*, 17(17):1572–1579.

Aoshima, S. (1999). Electro-spark process for repair and maintenance of die-casting dies. Report, TechnoCoat International.

Archard, J. F. (1953). Contact and rubbing of flat surfaces. *Journal of Applied Physics*, 24(8):981–988.

ASSAB (2012). *ASSAB 8407 Supreme*. UDDEHOLM.

Banjevic, D. (2009). Remaining useful life in theory and practice. *Metrika*, 69(2-3):337–349. Times Cited: 0 8th German Open Conference on Probability and Statistics Mar, 2008 RWTH Aachen Univ, Aachen, GERMANY.

Bannantine, J., Comer, J., and Handrock, J. (1990). *Fundamentals of metal fatigue analysis*. Prentice Hall, New Jersey, USA, 1 edition.

Barrau, O., Boher, C., Gras, R., and Rezai-Aria, F. (2003). Analysis of the friction and wear behaviour of hot work tool steel for forging. *Wear*, 255(7-12):1444–1454.

Behrens, B. A. (2008). Finite element analysis of die wear in hot forging processes. *CIRP Annals - Manufacturing Technology*, 57(1):305–308.

Behrens, B. A. and Schaefer, F. (2005). Prediction of wear in hot forging tools by means of finite-element-analysis. *Journal of Materials Processing Technology*, 167(2-3):309–315.

Biswas, W. and Rosano, M. (2011). A life cycle greenhouse gas assessment of remanufactured refrigeration and air conditioning compressors. *International Journal of Sustainable Manufacturing*, 2(2/3):222–236.

Boboescu, R. (2011). Applications of full factorial design experiments for laser welding. In *TEHNOMUS XVI - New Technologies and Products in Machine Manufacturing Technologies*, pages 215–222.

Borrego, L. P., Pires, J. T. B., Costa, J. M., and Ferreira, J. M. (2009). Mould steels repaired by laser welding. *Engineering Failure Analysis*, 16(2):596–607. Sp. Iss. SI 399QA Times Cited:3 Cited References Count:12.

Carden, A. (1963). Thermal fatigue — an analysis of the experimental method. Technical report, Oak Ridge National Laboratory.

Christiner, T., Eichlseder, W., Gódor, I., and Reiser, J. (2011). Fretting fatigue and wear: Experimental investigations and numerical simulation. *SAE Technical Paper*.

Coffin, L. (1954). A study of the effects of cyclic thermal stresses on a ductile metal. *Transactions of the American Society of Mechanical Engineering*, 76:931–951.

Darveaux, R. (2000). Effect of simulation methodology on solder joint crack growth correlation. In *Electronic Components amp; Technology Conference, 2000. 2000 Proceedings. 50th*, pages 1048–1058.

Deshpande, A. A., Tanner, D. W. J., Sun, W., Hyde, T. H., and McCartney, G. (2011). Combined butt joint welding and post weld heat treatment simulation using sysweld and abaqus. *Proceedings of the Institution of Mechanical Engineers Part L-Journal of Materials-Design and Applications*, 225(L1):1–10.

Esterman, M., Gerst, P., DeBartolo, E., and Haselkorn, M. H. (2006). Reliability prediction of remanufactured product: A welding repair process case study. *ASME Conference Proceedings*, 2006(47675):279–289.

Fang, K.-T., Lin, D. K. J., Winker, P., and Zhang, Y. (2000). Uniform design: Theory and application. *Technometrics*, 42(3):237–248.

Farahmand, B., Bockrath, G., and Glassco, J. (1997). *Fatigue and fracture mechanics of high risk parts: application of LEFM & FMDM theory*. Springer London, Ltd, London, UK.

FLIR (2012). *Flir R&D Software 3.3 User's manual*.

Garza-Delgado, A. (2007). *A STUDY OF CASTING DISTORTION AND RESIDUAL STRESSES IN DIE CASTING*. PhD thesis, The Ohio State University.

Giuntini, R. and Gaudette, K. (2003). Remanufacturing: The next great opportunity for boosting us productivity. *Business Horizons*, 46(6):41–48.

Goldak, J. A. and Akhlaghi, M. (2005). Computational welding mechanics.

Goldey, C. L., Kuester, E.-U., Mummert, R., Okrasinski, T. A., Olson, D., and Schaeffer, W. J. (2010). Lifecycle assessment of the environmental benefits of remanufactured telecommunications product within a "green" supply chain. In *2010 IEEE International Symposium on Sustainable Systems and Technology (ISSST)*, pages 1–6. Times Cited: 0 Issst 2010 IEEE International Symposium on Sustainable Systems and Technology May 17-19, 2010 Arlington, VA Ieee.

Grum, J. and Slabe, J. M. (2004). Possibility of introducing laser surfacing into maintenance service of die-casting dies. *Surface & Coatings Technology*, 180-81:596–602. 813EH Times Cited:8 Cited References Count:9.

Hammond, R., Amezquita, T., and Bras, B. (1998). Issues in the automotive parts remanufacturing industry a discussion of results from surveys performed among remanufacturers. *International Journal of Engineering Design and Automation - Special Issue on Environmentally Conscious Design and Manufacturing*, 4(1):27–46.

Hatcher, G. D., Ijomah, W. L., and Windmill, J. F. C. (2011). Design for remanufacture: a literature review and future research needs. *Journal of Cleaner Production*, 19(17-18):2004–2014.

Hauser, W. and Lund, R. T. (2003). Remanufacturing-an american resource. Report, Boston University.

Hsiao, Y. F., Tarng, Y. S., and Huang, W. J. (2008). Optimization of plasma arc welding parameters by using the taguchi method with the grey relational analysis. *Materials and Manufacturing Processes*, 23(1):51–58.

ICER (2000). Uk status report on waste from electrical and electronic equipment. Technical report, Industry Council for Electrical and Electronic Equipment Recycling (ICER).

Ijomah, W. L. (2002). *A Model-Based Definition of the Generic Remanufacturing Business Process*. Doctorate, University of Plymouth.

Ijomah, W. L., McMahon, C. A., Hammond, G. P., and Newman, S. T. (2007). Development of design for remanufacturing guidelines to support sustainable manufacturing. *Robotics and Computer-Integrated Manufacturing*, 23(6):712–719.

Jiang, W. and Molian, P. (2001). Nanocrystalline tic powder alloying and glazing of h13 steel using a co2 laser for improved life of die-casting dies. *Surface & Coatings Technology*, 135(2-3):139–149.

Kang, J. H., Park, I. W., Jae, I. S., and Kang, S. S. (1999a). A study on a die wear model considering thermal softening: (i) construction of the wear model. *Journal of Materials Processing Technology*, 96(1-3):53–58. 259FN Times Cited:23 Cited References Count:7.

Kang, J. H., Park, I. W., Jae, J. S., and Kang, S. S. (1999b). A study on die wear model considering thermal softening (ii): Application of the suggested wear model. *Journal of Materials Processing Technology*, 94(2-3):183–188.

Kilinski, T., Lesniak, J., and Sandor, B. (1991). Modern approaches to fatigue life prediction of smt solder joints. In Lau, J., editor, *Solder Joint Reliability*, pages 384–405. Springer US.

Kim, D. H., Lee, H. C., Kim, B. M., and Kim, K. H. (2005). Estimation of die service life against plastic deformation and wear during hot forging processes. *Journal of Materials Processing Technology*, 166(3):372–380.

Kim, Y. J. and Choi, C. H. (2009). A study on life estimation of hot forging die. *International Journal of Precision Engineering and Manufacturing*, 10(3):105–113. 470VM Times Cited:1 Cited References Count:14.

King, A. M., Burgess, S. C., Ijomah, W., and McMahon, C. A. (2006). Reducing waste: Repair, recondition, remanufacture or recycle? *Sustainable Development*, 14(4):257–267. 100ZP Times Cited:17 Cited References Count:37.

Klobcar, D. and Tusek, J. (2008). Thermal stresses in aluminium alloy die casting dies. *Computational Materials Science*, 43(4):1147–1154. 372QR Times Cited:2 Cited References Count:20.

Klobcar, D., Tusek, J., and Taliat, B. (2008). Thermal fatigue of materials for die-casting tooling. *Materials Science and Engineering a-Structural Materials Properties Microstructure and Processing*, 472(1-2):198–207. 255HP Times Cited:10 Cited References Count:24.

Klobčar, D., Tušek, J., and Taljat, B. (2004). Finite element modeling of gta weld surfacing applied to hot-work tooling. *Computational Materials Science*, 31(3-4):368–378.

Lau, J. (1991). *Solder Joint Reliability: Theory and Application*. Van Nostrand Reinhold.

Lavtar, L., Muhic, T., Kugler, G., and Tercelj, M. (2011). Analysis of the main types of damage on a pair of industrial dies for hot forging car steering mechanisms. *Engineering Failure Analysis*, 18(4):1143–1152.

Lee, J. C., Kang, H. J., Chu, W. S., Ahn, S. H., and Oh, S. I. (2007). Repair of damaged mold surface by cold-spray method. *Cirp Annals-Manufacturing Technology*, 56(1):577–580. 194ZU Times Cited:4 Cited References Count:17.

Lee, J.-H., Jang, J.-H., Joo, B.-D., Yim, H.-S., and Moon, Y.-H. (2009). Application of direct laser metal tooling for aisi h13 tool steel. *Transactions of Nonferrous Metals Society of China*, 19(Supplement 1):s284–s287.

Lee, R. S. and Jou, J. L. (2003). Application of numerical simulation for wear analysis of warm forging die. *Journal of Materials Processing Technology*, 140:43–48. Sp. Iss. SI 724LU Times Cited:9 Cited References Count:9.

Lee, Y.-C. and Chen, F.-K. (2001). Fatigue life of cold-forging dies with various values of hardness. *Journal of Materials Processing Technology*, 113(1-3):539–543.

Lemaitre, J. (1992). *A course on Damage Mechanics*. Springer-Verlag, Berlin.

Li, S.-X., Yu, S.-R., Zeng, H.-L., Li, J.-H., and Liang, R. (2009). Predicting corrosion remaining life of underground pipelines with a mechanically-based probabilistic model. *Journal of Petroleum Science and Engineering*, 65(3-4):162–166.

Lindgren, L.-E. (2006). Numerical modelling of welding. *Computer Methods in Applied Mechanics and Engineering*, 195(48-49):6710–6736.

Lindgren, L. E. (2007). *Computational welding mechanics : thermomechanical and microstructural simulations*. Woodhead : Maney Pub. ; CRC Press, Cambridge, England; Boca Raton.

Lund, R. T. (1984). *Remanufacturing : the experience of the United States and implications for developing countries*. World Bank technical paper ; no. 31. World Bank, Washington, D.C., U.S.A. :. Bibliography: p. 103.

Luo, J. H., Namburu, M., Pattipati, K., Qiao, L., Kawamoto, M., and Chigusa, S. (2003). Model-based prognostic techniques. In *AUTOTESTCON 2003. IEEE Systems Readiness Technology Conference. Proceedings*, pages 330–340. Bx81d Times Cited:4 Cited References Count:30.

Manson, S. (1953). Behavior of materials under condition of thermal stress. Technical report, University of Michigan Engineering Research Institute.

Mazhar, M. I., Kara, S., and Kaebernick, H. (2007). Remaining life estimation of used components in consumer products: Life cycle data analysis by weibull and artificial neural networks. *Journal of Operations Management*, 25(6):1184–1193.

Mazumder, J., Choi, J., Nagarathnam, K., Koch, J., and Hetzner, D. (1997). The direct metal deposition of h13 tool steel for 3-d components. *JOM Journal of the Minerals, Metals and Materials Society*, 49(5):55–60.

Morrow, W. R., Qi, H., Kim, I., Mazumder, J., and Skerlos, S. J. (2007). Environmental aspects of laser-based and conventional tool and die manufacturing. *Journal of Cleaner Production*, 15(10):932–943.

Ortegon, K., Nies, L. F., and Sutherland, J. W. (2013). Preparing for end of service life of wind turbines. *Journal of Cleaner Production*, 39(0):191–199.

Pan, L. K., Wang, C. C., Hsiao, Y. C., and Ho, K. C. (2005). Optimization of nd:yag laser welding onto magnesium alloy via taguchi analysis. *Optics & Laser Technology*, 37(1):33–42.

Parishram, P. (2007). Laser assisted repair welding of h13 tool steel for die casting. Thesis, Mechanical Engineering.

Parishram, P., Malshe, A. P., and Fulton, A. (2006). Laser melt processing of h13 tool steel. *ASME Conference Proceedings*, 2006(47748):87–90.

Pecas, P., Henriques, E., Pereira, B., Lino, M., and Silva, M. (2006). Fostering the use of welding technology in the mould repair. In *RPD 2006-Building the future by innovation*.

Persson, A. (2004). Strain-based approach to crack growth and thermal fatigue life of hot work tool steels. *Scandinavian Journal of Metallurgy*, 33(1):53–64. 761FL Times Cited:2 Cited References Count:17.

Persson, A., Hogmark, S., and Bergstrom, J. (2005). Thermal fatigue cracking of surface engineered hot work tool steels. *Surface & Coatings Technology*, 191(2-3):216–227. 885WV Times Cited:41 Cited References Count:30.

Pigosso, D. C. A., Zanette, E. T., Filho, A. G., Ometto, A. R., and Rozenfeld, H. (2010). Ecodesign methods focused on remanufacturing. *Journal of Cleaner Production*, 18(1):21–31.

Pleterski, M., Tusek, J., Kosec, L., Klobcar, D., Muhic, M., and Muhic, T. (2008). Laser repair welding of thermal cracks on aluminium die casting dies. *Materiali in Tehnologije*, 42(5):211–214. 368DT Times Cited:0 Cited References Count:6.

Qamar, S. Z., Sheikh, A. K., Arif, A. F. M., Younas, M., and Pervez, T. (2008). Monte carlo simulation of extrusion die life. *Journal of Materials Processing Technology*, 202(1-3):96–106. 318MF Times Cited:1 Cited References Count:26.

Rosbrook, C. (1992). *Analysis of thermal fatigue and heat checking in die-casting dies: a finite element approach*. Thesis, Mechanical Engineering.

Sakai, S.-i., Yoshida, H., Hiratsuka, J., Vandecasteele, C., Kohlmeyer, R., Rotter, V., Passarini, F., Santini, A., Peeler, M., Li, J., Oh, G.-J., Chi, N., Bastian, L., Moore, S., Kajiwara, N., Takigami, H., Itai, T., Takahashi, S., Tanabe, S., Tomoda, K., Hirakawa, T., Hirai, Y.,

Asari, M., and Yano, J. (2014). An international comparative study of end-of-life vehicle (elv) recycling systems. *Journal of Material Cycles and Waste Management*, 16(1):1–20.

Sakhuja, A. and Brevick, J. R. (2004). Prediction of thermal fatigue in tooling for die-casting copper via finite element analysis. *Materials Processing and Design: Modeling, Simulation and Applications, Pts 1 and 2*, 712:1881–1886+2298. Baj45 Times Cited:6 Cited References Count:6 Aip Conference Proceedings.

Sasaki, K. and Takahasahi, T. (2005). Low cycle thermal fatigue and microstructural change of ac2b-t6 aluminum alloy. *International Journal of Fatigue*, 28(3):203–210.

Shah, S. V. and Dahotre, N. B. (2002). Laser surface-engineered vanadium carbide coating for extended die life. *Journal of Materials Processing Technology*, 124(1-2):105–112.

Shannon, B. E., Jaske, C. E., and Smith, M. C. (2010). Optimizing reformer tube life through advanced inspection and remaining life assessment. *Process Safety Progress*, 29(4):299–304. Times Cited: 0.

Sherwood, M., Shu, L. H., and Fenton, R. G. (2000). Supporting design for remanufacture through waste-stream analysis of automotive remanufacturers. *CIRP Annals - Manufacturing Technology*, 49(1):87–90.

Si, X.-S., Wang, W., Hu, C.-H., and Zhou, D.-H. (2011). Remaining useful life estimation - a review on the statistical data driven approaches. *European Journal of Operational Research*, 213(1):1–14.

Sikorska, J. Z., Hodkiewicz, M., and Ma, L. (2011). Prognostic modelling options for remaining useful life estimation by industry. *Mechanical Systems and Signal Processing*, 25(5):1803–1836.

Silva, B., Pires, I., and Quintino, L. (2008). Welding technologies for repairing plastic injection moulds. *Advanced Materials Forum IV*, 587-588:936–940+1040. Bii83 Times Cited:0 Cited References Count:6 Materials Science Forum.

SIMULIA (2012). *Abaqus 6.12 Analysis User's Manual Volume II: Analysis*.

Skov-Hansen, P., Bay, N., Grønbæk, J., and Brøndsted, P. (1999). Fatigue in cold-forging dies: tool life analysis. *Journal of Materials Processing Technology*, 95(1-3):40–48.

Smith, V. M. and Keoleian, G. A. (2004). The value of remanufactured engines - life-cycle environmental and economic perspectives. *Journal of Industrial Ecology*, 8(1-2):193–221. Times Cited: 26.

Song, R., Hanaki, S., Yamashita, M., and Uchida, H. (2008). Reliability evaluation of a laser repaired die-casting die. *Materials Science and Engineering a-Structural Materials Properties Microstructure and Processing*, 483-484:343–345. doi: DOI: 10.1016/j.msea.2006.10.207.

Stahlberg, U. and Hallstrom, J. (1999). A comparison between two wear models. *Journal of Materials Processing Technology*, 87(1-3):223–229. 167RM Times Cited:5 Cited References Count:8.

Starling, C. M. D. and Branco, J. R. T. (1997). Thermal fatigue of hot work tool steel with hard coatings. *Thin Solid Films*, 308-309:436–442.

Subramoniam, R., Huisingh, D., and Chinnam, R. B. (2009). Remanufacturing for the automotive aftermarket-strategic factors: literature review and future research needs. *Journal of Cleaner Production*, 17(13):1163–1174.

Sun, B. and Guo, Y. (2004). High-cycle fatigue damage measurement based on electrical resistance change considering variable electrical resistivity and uneven damage. *International Journal of Fatigue*, 26(5):457–462.

Sun, Y. H., Hanaki, S., Uchida, H., Sunada, H., and Tsujii, N. (2003). Repair effect of hot work tool steel by laser-melting process. *Journal of Materials Science & Technology*, 19:91–93. Suppl. 1 813HS Times Cited:1 Cited References Count:6.

Sun, Y. H., Sunada, H., and Tsujii, N. (2001). Crack repair of hot work tool steel by laser melt processing. *ISIJ International*, 41(9):1006–1009. 473ZY Times Cited:10 Cited References Count:4.

Teunter, R. H. and Flapper, S. D. P. (2011). Optimal core acquisition and remanufacturing policies under uncertain core quality fractions. *European Journal of Operational Research*, 210(2):241–248.

Thompson, S. (1999). *Handbook of mold, tool and die repair welding*. William Andrew Publishing, Cambridge, UK.

Tian, Z., Wong, L., and Safaei, N. (2010). A neural network approach for remaining useful life prediction utilizing both failure and suspension histories. *Mechanical Systems and Signal Processing*, 24(5):1542–1555.

Tong, X., Zhou, H., Liu, M., and Dai, M.-j. (2011). Effects of striated laser tracks on thermal fatigue resistance of cast iron samples with biomimetic non-smooth surface. *Materials & Design*, 32(2):796–802.

Turk, R., Perus, I., and Tercelj, M. (2004). New starting points for the prediction of tool wear in hot forging. *International Journal of Machine Tools and Manufacture*, 44(12-13):1319–1331.

Tusek, J., Taljat, B., and Klobcar, D. (2007). How to extend the life of die-casting tools. *Metalurgija*, 46(1):67–71. 116XV Times Cited:0 Cited References Count:11.

Vedani, M., Previtali, B., Vimercati, G. M., Sanvito, A., and Somaschini, G. (2007). Problems in laser repair-welding a surface-treated tool steel. *Surface & Coatings Technology*, 201(8):4518–4525. 128KF Times Cited:6 Cited References Count:24.

Velay, V., Persson, A., Bernhart, G., Penazzi, L., and Bergström, J. (2002). Thermal fatigue of a tool steel: experiment and numerical simulation. In *Proceedings of the 6th international tooling conference : The use of tool steels: experience and research*, pages 667–685.

Vinarcik, E. J. (2003). *High Integrity Die Casting Processes*. John Wiley & Sons.

Watson, M., Byington, C., Edwards, D., and Amin, S. (2005). Dynamic modeling and wear-based remaining useful life prediction of high power clutch systems. *Tribology Transactions*, 48(2):208–217. Times Cited: 6 STLE/ASME Tribology Conference Oct 24-27, 2004 Long Beach, CA.

Yousefieh, M., Shamanian, M., and Saatchi, A. (2011). Optimization of the pulsed current gas tungsten arc welding (pcgtaw) parameters for corrosion resistance of super duplex stainless steel (uns s32760) welds using the taguchi method. *Journal of Alloys and Compounds*, 509(3):782–788.

Zhu, Y. L., Schwam, D., Wallace, J. F., and Birceanu, S. (2004). Evaluation of soldering, washout and thermal fatigue resistance of advanced metal materials for aluminum die-casting dies. *Materials Science and Engineering a-Structural Materials Properties Microstructure and Processing*, 379(1-2):420–431. 846QG Times Cited:7 Cited References Count:35.

Zio, E. and Di Maio, F. (2010). A data-driven fuzzy approach for predicting the remaining useful life in dynamic failure scenarios of a nuclear system. *Reliability Engineering & System Safety*, 95(1):49–57. Times Cited: 2.